# ESTIMATION OF REACTOR POWER FROM CORE TEMPERATURE SIGNAL OF FAST REACTOR

*By*
**PAAWAN SHARMA**
(ENGG02201004003)

**Indira Gandhi Centre for Atomic Research, Kalpakkam**

***A thesis submitted to the***
***Board of studies in engineering sciences***
***In partial fulfillment of requirements***

***For the degree of***

**Doctor of philosophy**

***Of***

**HOMI BHABHA NATIONAL INSTITUTE**

**MAY, 2013**

# Homi Bhabha National Institute

## Recommendations of the viva voce board

As members of the viva voce board, we certify that we have read the dissertation prepared by Paawan Sharma entitled “Estimation of Reactor Power from Core Temperature Signal of Fast Reactor” and recommend that it may be accepted as fulfilling the dissertation requirement for the degree of doctor of philosophy.

**Date:**

Chairman – Dr. B.K. Panigrahi

**Date:**

Convener – Dr. T. Jayakumar

**Date:**

Member 1 – Dr. R.S. Keshavamurthy

**Date:**

Member 2 – Dr. K. Devan

**Date:**

Technology Advisor – Shri N. Murali

Final approval and acceptance of this dissertation is contingent upon the candidate’s submission of the final copies of the dissertation to HBNI.

I hereby certify that I have read this dissertation prepared under my direction and recommend that it may be accepted as fulfilling the dissertation requirement.

**Date:**

Guide – Dr. T. Jayakumar

# Certificate

I hereby certify that I have read this dissertation prepared under my direction and recommend that it may be accepted as fulfilling the dissertation requirement.

________________________________________ **Date:**

**Guide: Dr. T. Jayakumar**

**Place:**

# Statement by Author

This dissertation has been submitted in partial fulfillment of requirements for an advanced degree at Homi Bhabha National Institute (HBNI) and is deposited in the library to be made available to borrowers under rules of the HBNI.



(Paawan Sharma)

# Declaration

I, hereby declare that the investigation presented in the thesis has been carried out by me. The work is original and has not been submitted earlier as a whole or in part for a degree / diploma at this or any other institution / university.

(Paawan Sharma)

# Abstract

## 1. Context

Nuclear reactors must follow stringent norms for their reliable and safe operation. To meet such requirements, all safety critical systems in Nuclear Power Plants (NPPs) must be validated using diverse methods.

Presently in NPPs, measurement of generated thermal power is performed through neutronic channels, which also require validation. The neutronic readings are calibrated using absolute/steady state value of the core temperature at regular time intervals. Hence, there is a need for a diverse method to complement the existing power measurement. Also, presence of alternative method may help in facing complex and unforeseen situations such as unavailability of other monitoring systems. Hence, a new method for power measurement must be investigated to meet safety requirements.

## 2. Objectives

(i) To investigate the feasibility of using temperature fluctuations in coolant at the outlet of subassemblies to estimate reactor power.

(ii) To study the properties of associated temperature fluctuations at various reactor thermal power levels.

(iii) To propose a method to derive generated thermal power information from temperature fluctuations.

(iv) To estimate the resource utilization for a signal processing implementation on a FPGA-based reference platform.

## 3. Methods

To study the feasibility of using temperature fluctuations for reactor power estimation; time, frequency, time-frequency, and statistical tests were performed on the data collected from the Fast Breeder Test Reactor (FBTR), at every discrete power level for both constant as well as during reactor power increase.

A hybrid approach was developed to derive a parameter proportional to core thermal power after utilizing information from various domain analyses. Standard deviation (time domain), Fourier analysis (frequency domain), various time-frequency distributions (TFDs) (time-frequency domain), and many stationarity tests were performed on the data for in-depth analysis of temperature fluctuations. As part of statistical tests, KPSS (Kwiatkowski-Phillips-Schmidt-Shin) test, Reverse Arrangement test (RAT) and Runs test were performed. NULL hypothesis ($H_o$) for KPSS test was that the data is stationary. $H_o$ for RAT and runs test was that the data is from a random source. Approximate Entropy and Recurrence plots were utilized as a measure to quantify the amount of regularity and the unpredictability of fluctuations over time-series. The signal processing model was proposed on the basis of above test results. The proposed model was simulated with simulated data and validated with actual reactor data. Signal processing blocks were coded in verilog and tested for resource utilization for implementation on Altera FPGA, and to check for functionality and timing constraints.

## 4. Results

The calculated parameter (CP) from such approach was found to be in close correlation with actual thermal power as well as neutronic calculation-based thermal power. Standard deviation ($\sigma$) was observed to increase with thermal power, but with a few major exceptions. It was observed that the trend was highly dependent on the number of data points taken to calculate $\sigma$. Also, a few $\sigma$ values were observed to be out of trend with thermal power. Using Fourier analysis, temperature fluctuations were found to be in the frequency range of 0.001 Hz to 5 Hz. The scale factor obtained in case of scalogram technique was found to increase with thermal power. $H_o$ was passed in KPSS test and rejected in RAT and runs test.

## 5. Conclusions

It is concluded that:

- The overall degree of fluctuation increases with thermal power.
- These fluctuations are non-linearly localized in time.
- Scalogram technique best suits for fluctuation analysis.
- Recurrence analysis helps in good understanding of the dynamic system evolution with time.

## List of Figures

## List of Tables

## List of Acronyms

| | |
|---|---|
| **ApEn** | Approximate Entropy |
| **CP** | Calculated parameter |
| **CSA** | Central subassembly |
| **FBTR** | Fast Breeder Test Reactor |
| **FPGA** | Field programmable gate array |
| **LE** | Logic elements |
| **MOX** | Metal oxide |
| **NPP** | Nuclear power plant |
| **PFBR** | Prototype Fast Breeder Reactor |
| **PuC** | Plutonium Carbide |
| **RAT** | Reverse Arrangement Test |
| **RMS** | Root mean square |
| **RP** | Recurrence plot |
| **STFT** | Short time Fourier transform |
| **UC** | Uranium Carbide |
| **UO2** | Uranium oxide |
| **VRA** | Visual recurrence analysis |

## List of Publications

Journals:

(1) Sharma, P., Murali, N., & Jayakumar, T. (2014). Effect of thermocouple time constant on sensing of temperature fluctuations in a fast reactor subassembly. Journal of Sensors and Sensor Systems, 3, 55-60.

(2) Sharma, P., Murali, N., & Jayakumar, T. (2013). Statistical testing of temperature fluctuations for estimating thermal power in central subassembly of fast reactor. Annals of Nuclear Energy, 60, 406-411.

(3) Sharma, P., Nagarajan, M., Mohanakrishnan, P., & Iyer Swaminathan, P. (2012). Signal Processing Analysis of Temperature Fluctuations for a Fuel Subassembly using SCILAB. International Journal of Modelling and Simulation, 32(3), 171.

(4) Sharma, P., Murali, N., Mohanakrishnan, P., & Swaminathan, P. (2011). An Intuitive Signal Processing Approach for Temperature Fluctuations in Fuel Subassemblies. International Journal of Computer Applications, 33(10), 22-27.

Conference Proceedings:

(1) Sharma, P., Murali, N., & Jayakumar, T. (2012, October). A time-frequency analysis of temperature fluctuations in a fast reactor. In Image and Signal Processing (CISP), 2012 5th International Congress on (pp. 1546-1550). IEEE.

(2) Bhattacharyya, A., Sharma, P., Murali, N., & Murty, S. S. (2011, December). Development of FPGA based IIR Filter implementation of 2-degree of Freedom PID controller. In India Conference (INDICON), 2011 Annual IEEE (pp. 1-8). IEEE.

# Acknowledgements

I would like to express my gratitude towards my guide Dr T. Jayakumar (Director, MMG, IGCAR) and co-guide Dr. R. S. Keshavamurthy (Head, RSDD, IGCAR) for their valuable guidance and encouragement.

I am extremely grateful to my doctoral committee members Dr B. K. Panigrahi and Dr K. Devan for their constant encouragement and fruitful discussions during the work.

My sincere thanks to Dr. P. Swaminathan (Former Group Director, EIG, IGCAR), and Dr. P. Mohanakrishnan (Former Head, RPD, IGCAR) for introducing and motivating me for the research topic.

I am indebted to my technology advisor Shri N. Murali (Associate Director, ICG, EIRSG, IGCAR) for his constant support and detailed discussions on various aspects of the project, which significantly improved my work.

My special thanks to Shri S.A.V. Satyamurty (Director, EIRSG, IGCAR) for his motivation and support.

I would like to thank Dr. G. Srinivasan (Director, ROMG) for allowing me; and K. Vinolia and Gowri Lakshmanan for helping me in collecting crucial FBTR data at various power levels.

I am thankful to Dr. M. Sai Baba (Associate Director, RMG, IGCAR) for all his support and encouragement during the tenure.

Many thanks to former Director, IGCAR, Shri S. C. Chetal for his support and recommendation for attending the International conference at Chongqing, China.

I would like to thank Shri M. Sivaramakrishna, Anindya Bhattacharya, M. Chandramouli Sharma, A. Santhana Raj, Aditya Gour, R.P. Behra, Venkat Kishore, Satish, and other EIRSG staff members for their encouragement and suggestions.

I am thankful to the EIRSG administrative staff for their help at numerous occasions.

I am grateful to my father Mr. Baijnath Sharma, mother Mrs. Sudha Sharma, brother Mr. Puneet Sharma and family, relatives-in-law, and family for their moral support and numerous blessings.

Most importantly, I thank my wife Mrs. Swati Sharma and son Aarav for always being there with me and being a constant source of inspiration.

I am thankful to my friends Anil, Ashutosh, Bubathi, Deepak, Govindha, Hari Babu, Naveen, Arun Babu, Ravikirna, Saptarishi, Sharath, Srihari, and others for all their help and socio-interactions at various occasions.

I am thankful to Department of Atomic Energy, Government of India for providing me with D.G.F.S. Ph.D. fellowship to pursue my research at IGCAR.

Paawan Sharma
May, 2013

# Contents

# 1

# INTRODUCTION

## 1.1 Problem Statement

All safety critical systems in Nuclear Power Plants (NPPs) must be validated using diverse methods. Measurement of thermal power in NPPs is very important. It is done through neutronic method, which also has to be validated.

Fluctuations present in the thermocouple output of Central Subassembly (CSA) changes with reactor thermal power. This thesis is intended to provide detailed analysis of temperature fluctuations in CSA to derive a parameter proportional to reactor thermal power. This includes statistical and multi domain testing, model development, and validation of model.

## 1.2 Objective of thesis

The major objectives of the thesis are

- To analyze the feasibility of using temperature fluctuations in fuel subassemblies to estimate thermal power in the core.
- To propose a model to establish correlation between thermal power and temperature fluctuations.
- To use data driven model based design approach to achieve the correlation.
- To estimate resource utilization and performance optimization for practical implementation of such approach.
- To analyze main factors affecting the formation of temperature fluctuations in subassemblies.

## 1.3 Background information

### 1.3.1 Core Structure of a Fast Reactor

Fig. 1.1 shows a pool type fast breeder reactor setup. Heat energy released during fission process in core is transported to steam generator by liquid sodium as coolant in various steps. There are two loops for coolant flow, viz. primary and secondary loop. The flow in these loops is maintained by pumps. Heat energy is first transferred to secondary sodium loop through intermediate heat exchanger (IHX). Then, this energy is used to convert water into steam in steam generator (SG). The core, primary sodium pump, and intermediate heat exchanger (IHX) are present submerged in liquid sodium inside main vessel in case of a pool type reactor.

Fast Breeder Test Reactor (FBTR) is another type of fast reactor known as loop type reactor where pump and IHX are outside the main vessel [1]. Fuel is arranged in closely packed manner inside cylindrical metallic pins known as fuel pins. This closely packed arrangement of fuel pins known as subassembly, which has a hexagonal sheath. Many subassemblies are placed together in a structure to form reactor core. A typical arrangement of core with subassemblies and fuel pins is shown in Fig. 1.2. There are 65 fuel pins per subassembly and 55 subassemblies in total. When coolant flows through each subassembly, it takes heat energy from the surface of fuel pins to the pool of sodium where coolant streams from other subassemblies get mixed and give rise to an average coolant temperature. The whole heat transport phenomenon in this process is convection type and since the flow is maintained by pump, it is known as forced convection. The temperature of each subassembly is monitored by individual pair of thermocouples located just above the subassembly outlet. The central subassembly lies at the center of the core and exhibits maximum temperature due to highest flux levels.

### 1.3.2 Power Calculation in a Fast Reactor

Thermal power ( $P_{th}$ ) in a fast reactor is proportional to the fast neutron flux ( $\phi_{th}$ ) [2].

$$P_{th} \propto \phi_{th} \tag{1}$$

$P_{th}$ is measured in a fast reactor by processing the neutronic signals over a wide range. The complete range is divided in several decades categorized into three regions: pulse ($10^0 - 10^5 n/cm^2.\sec$), MSV (mean square value)/Campbell ($10^4 - 10^{10} n/cm^2.\sec$) and power region ($10^6 - 10^{12} n/cm^2.\sec$) [3]. In pulse region, as the neutron flux is low, the output of the neutron detector is a series of pulses proportional to neutron flux. The detector used in this region is capable of discriminating gamma induced signals. In Campbell region, fluctuations in neutron detector signal are processed.

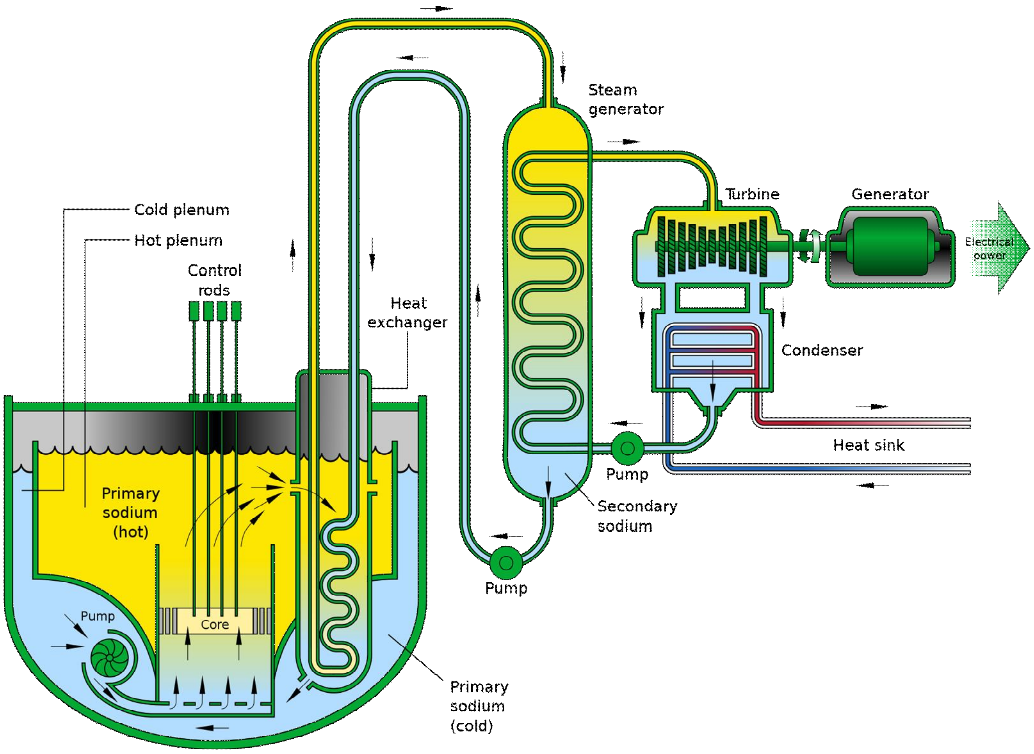


Fig. 1.1: Pool type reactor.

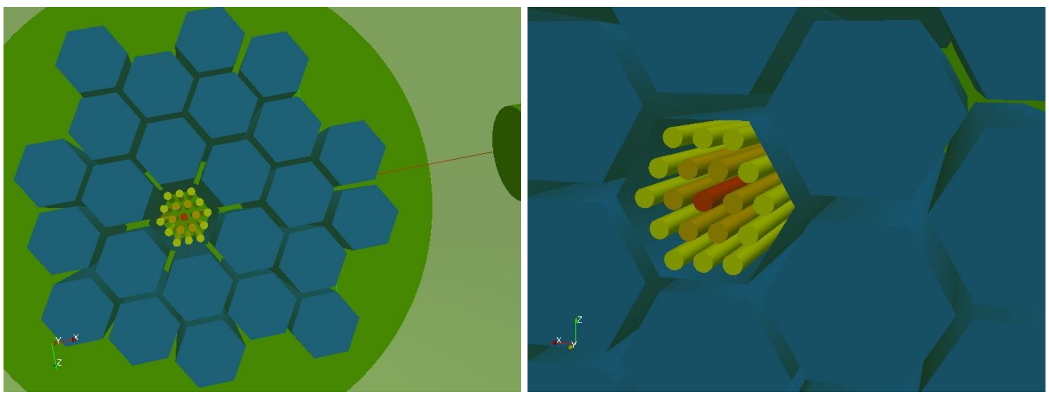

Fig. 1.2: Typical Subassembly arrangement inside a fast reactor.

This method is based on the fact that variance is a direct measure of mean for signals which follow Poisson distribution [4].

$$\sigma^2 = \overline{n} \tag{2}$$

where $\overline{n}$ is the mean no. of counts indicated by sensor in a given time interval. This technique offers better discrimination against high gamma background [5].

Equation (3) and (4) represents discrimination ratios for standard method of measuring direct current of ionization chamber, and Campbell's method respectively.

$$D_{dc} = \frac{s_n \overline{q_n} \phi}{s_\gamma \overline{q_\gamma} X(\phi)} \tag{3}$$

$$D_{rms} = \frac{s_n \overline{q_n^2} \phi}{s_\gamma \overline{q_\gamma^2} X(\phi)} \tag{4}$$

where, $s_n \overline{q_n}$ ($s_n \overline{q_n^2}$) and $s_\gamma \overline{q_\gamma}$ ($s_\gamma \overline{q_\gamma^2}$)are detector susceptibilities for neutron and gamma flux respectively, $X(\phi)$ is dosage.

The discrimination ratio for MSV method to d-c method is,

$$\frac{D_{rms}}{D_{dc}} = \frac{\overline{q_n^2} / \overline{q_\gamma^2}}{\overline{q_n} / \overline{q_\gamma}} = \left[ \frac{\overline{q_n^2}}{\overline{q_n}^2} \cdot \frac{\overline{q_\gamma}^2}{\overline{q_\gamma^2}} \right] \cdot \frac{\overline{q_n}}{q_\gamma} \approx 1000 \tag{5}$$

In power region, where the reactor operates near or at full power; a dc (direct current) component derived from sensor reading gives power measurement.

## 1.4 **Related Work**

Most of the previous temperature fluctuation related analysis focused on study of thermal stripping, blockage and other thermodynamic studies (figure 1.3), which are discussed below.

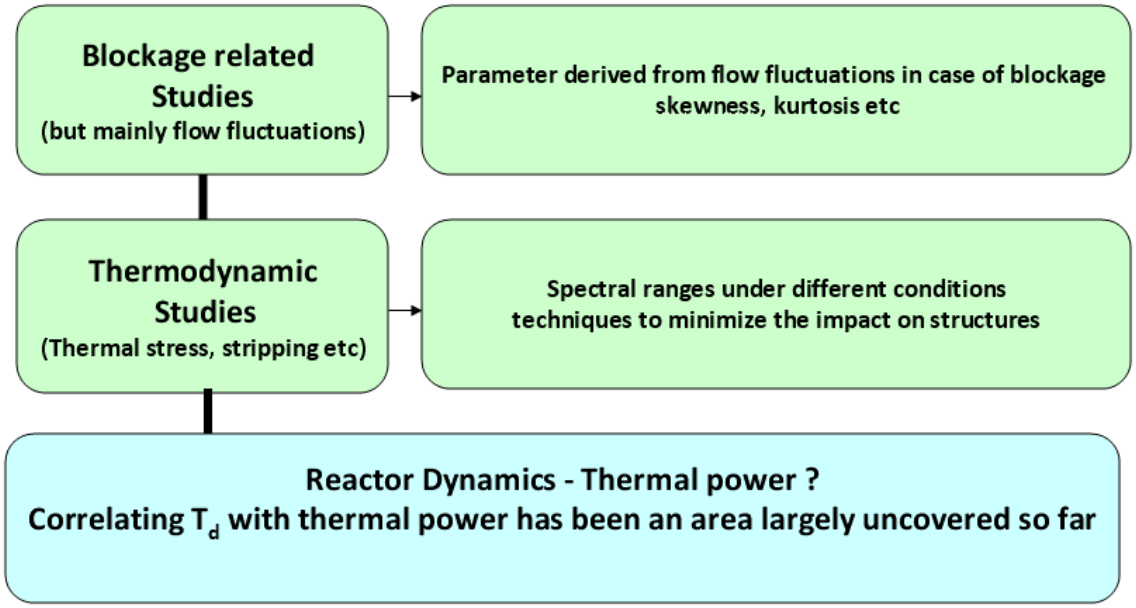


Fig. 1.3: Analysis history.

Tsunoda [6] performed temperature fluctuation experiments with water and strongly recommended the idea of using the temperature fluctuations in aid to detect flow blockages or local hot-spot. It was assumed that the turbulent mixing in subassembly gives rises to random temperature fields which follow a flat (constant) power spectral density (white noise).

Miyazaki et al. [7] performed forced sodium circulation experiment in an annular channel and simulated blockage and concluded that the detector (thermocouple) location should be near to the outlet of reactor core in order to get a high level of fluctuation signal, and the root mean square (RMS) value of such fluctuations are proportional to clad material and fluid temperature difference. Presence of Vortex Street due to blockage under the presence of temperature gradient was suggested as the main reason for temperature fluctuation generation, and that temperature gradient depends strongly on the turbulence factor. One important conclusion made by the authors was that the temperature gradient overtook the turbulence effect on fluctuation level.

Greef [8] established a technique for local blockage detection in a fast reactor subassembly using temperature fluctuations and proposed a theoretical model of noise production and dissipation in subassembly. The temperature noise technique was proposed covering In-cluster attenuation, peak wake temperatures, downstream flow recovery, generation and dissipation of temperature fluctuations downstream of the pin cluster, background noise sources, effects of reactor geometry, and its implications for the fast reactor.

Krebs and Weinkotz and [9] took different blockage sizes into consideration in their experimental work and proposed the concept of bundle coefficient to indicate the coolant channel disturbances. Authors concluded that significant boiling detection is possible by the use of statistical analysis of temperature fluctuations at the outlet of a subassembly.

Inujima et al. [10] suggested a good technique to detect a local sodium boiling accident using temperature and flow fluctuations. The whiteness test method (WTM) of fluctuation signals was suggested as a sensitive and reliable way for detecting local accidents in a subassembly, provided the boiling intensity becomes fairly large. However, the correlation between temperature fluctuations at different positions at the outlet of the subassembly was not clarified.

Analysis done by Wey et al. [11] proved that central blockages as small as 2–3% could be detected by RMS values of temperature. Modeled axial variation of turbulence field was analyzed along with temperature profile with the help of STATEN (STatistical Analysis of TEmperature Noise) code. Authors suggested that for larger size blockages, skewness or kurtosis could be used for detection.

Krebs and Weinkotz [12] performed experiments for analysis of mean and fluctuating temperature profiles downstream of a simulated reactor subassembly. They suggested use of a faster SS–Na (stainless steel-Sodium) junction thermocouple for enhanced detection of temperature fluctuations, thereby improving reactor instrumentation.

However, Ogino and Inujima [13] supported the idea of using flow fluctuations over temperature as the variation of former was considerably higher. With the help of a series of tests conducted using simulated pin bundle tests, authors insisted that a local blockage can be detected with the help of temperature fluctuation at the outlet of subassembly only when there is significant reduction in flow and a large variation in radial temperature distribution at the end of the subassembly.

Nomoto et al. [14] summarized observation of subassembly outlet coolant temperature distributions obtained at various power levels, different coolant flowrates, and unequal reactor inlet temperatures. Authors observed that the subassembly outlet temperature increases proportionally with power increase, and that the individual subassemblies flowrates vary slightly with changes in total system flowrate, which resulted in variations in axisymmetric temperature distribution across the core.

Takeda et al. [15] proposed a 3D model for root mean square (RMS) of fluctuation distribution for fuel subassemblies with blockages. Authors concluded that RMS values of temperature fluctuations depend on transverse eddy diffusivity of enthalpy and Taylor's microscale, with latter having large effect on RMS value.

Takeda et al. [16] in another experiment analyzed RMS for fuel subassemblies with bundle and upper plenum region. The authors found out that RMS ratios for blockage to that without blockage increases with power, and temperature noise can be used efficiently for detection of local flow blockages.

Takeshi et al. [17] observed that the RMS values of temperature noise increases fourteen times at the subassembly outlet in case half of edge cells blocked. Also, it was found out that edge blockages are easily detectable than central blockages, and that increase in no. of pins in a subassembly results into less attenuation of temperature noise downstream to the outlet.

A method for detecting vibrations in absorber rod using reactivity noise was proposed by Lord et al. [18] and concluded that dominant source of noise is subassembly vibration.

Edelmann et al. [19] analyzed different techniques for calculating thermal hydraulic parameters using noise and concluded that noise analysis and reactivity perturbation techniques are applicable under normal reactor operating conditions.

Edelmann et al. in another analysis [20] suggested that heat transfer parameters of fuel elements can be possibly determined by analyzing reactor power transients, and early fuel failure detection could be possible if the thermocouples are placed nearer to the subassembly outlet.

Seong et al. [21] developed and recommended a neural network model for detection of partial blockage in an assembly by using simulated temperature profiles obtained from Large Eddy Simulation (LES) turbulence model.

Velusamy et al. [22] developed a suitable model for numerically simulating thermal stripping, which is caused by mixing of different temperature streams and results into a random component. These fluctuations are responsible for high cycle fatigue to mechanical structures. The oscillations in temperature become more periodic under forced convection, and tend to become random when free convection also occurs.

Velusamy et al in another study [23] highlighted thermal hydraulics of a fast breeder reactor, design constraints and other investigations related to thermal stratification, thermal stripping, and gas entrainment. A quick detection of 6-8% flow reduction by absolute temperature readings has been reported. For different interfaces, the frequency of temperature oscillations has been reported to be in the range 2-40 Hz. Low frequency (0·01–2 Hz) temperature oscillations of large amplitude were reported in case of thermal stratification.

Chapuliot et al. [24] investigated cracking of piping due to thermal loading in flow mixing zone, such as residual heat removal system mixing tee. Authors found out that strong temperature fluctuations in the region results into high thermal load, and that the high frequency random fluctuations lead to large scale instability.

Kasahara et al. [25], in a bid to analyze innovative reactor structural designs which can withstand high cycle thermal fatigue, discussed presence of fluid temperature fluctuations at junctions where mixing of different temperature streams takes place.

Krishna Chandran et al. [26] performed a numerical analysis of thermal stripping phenomenon for Prototype Fast Breeder Test Reactor (PFBR) using ten jet water model. It was suggested that the temperature fluctuations reduces as the velocity ratio for hot and cold jets increases. The main conclusion of the study was that the effects of high temperature fluctuations can be reduced by maintaining a proper hot to cold jet velocity. In a recent work by Mesquita et al [27], new processes for reactor power measurement by thermal means were proposed; out of which thermal balance method was decided to be chosen as standard for IPR-R1 TRIGA reactor.

## 1.5 Thesis Structure

The thesis is organized as follows.

*Chapter 2* explains various methods and techniques used in analyzing experimental data. The probability distribution of fluctuations is investigated by the use of various test statistics. Statistical tests; time, frequency and time-frequency domain methods and visual recurrence analysis are employed to understand the system's evolution with power. The experimental data used for analysis is reviewed for coverage of complete power range.

*Chapter 3* is devoted to detailed analysis of reactor data and subsequent conclusions from those tests. A signal processing model is proposed in *Chapter 4* based on the findings of the tests. This model is validated by a different set of data for FBTR. Also, a method to simulate various power level temperature fluctuations is devised. This helps in obtaining abundant data sets for their possible use in other analysis. Also, the effect of various other parameters such as sensor time-constant, flow rate etc., on fluctuations is also discussed, which is necessary for a proper correlation.

*Chapter 5* encompasses the resource utilization details of block level implementation on a FPGA based hardware platform.

*Chapter 6* summarizes the work, contributions and highlights future directions for the present work.

## 1.6 **Conclusions**

The motivation and objectives for the research topic were presented. Literature survey in the related area/domain was also discussed. It is found that there always has been an interest in the analysis of dynamic signal variations such as temperature fluctuations, in order to obtain meaningful information. But exploration of temperature fluctuation data for a possible correlation with thermal power has been an area largely uncovered so far. The exploration of vast amount of information present in coolant outlet temperature fluctuations is the prime focus of the thesis.

# 2

# RESEARCH METHODOLOGY

This chapter discusses the use and applicability of various techniques for developing a system model from temperature fluctuation data of a fast reactor. A data driven grey box model based design concept is adopted for the model development. The method involves detailed testing of temperature fluctuation data for determinism/stochasticity, stationarity, multi domain analysis and various other statistical analysis namely approximate entropy (ApEn) and recurrence plots (RPs).

## 2.1 Data driven model based design

System identification involves development of mathematical models from measured data [28]. The model so developed comes under model based design methodology. Model based design simplifies problems associated with low complex to highly complex systems in the areas of signal processing, control theory, instrumentation, embedded systems etc. Model based design approach has several benefits such as fast prototyping, testing and verification. Such designs can be based on either first principles (FP) or data driven (DD) [29]. Models based on former are termed as white box models and black (or grey) for the latter. First principles involve mathematical equations associated with the physical process of the system. But, it becomes difficult to build models from FP when the system complexity is higher. Data driven approach involves establishing mathematical relations between several observed input-output parameters of the system. No information regarding the internals of the system is available in a black box model. In grey box models, however, a little insight of the system is utilized during the process of model development. In present work, a grey box model approach is adopted towards model design. Central subassembly outlet temperature, reactor outlet temperature, primary sodium flow, inlet temperature, neutronic measurements are considered for the analysis. The various types of analysis are as shown in figure 2.1. The system data is univariate since temperature readings from thermocouple would yield steady state value and parameters such as standard deviation, mean etc. can be calculated with the help of recorded data. The need for the usage of several tests arises due to complexity of a nuclear reactor system, as their use in analysis gives confidence in the model building process.

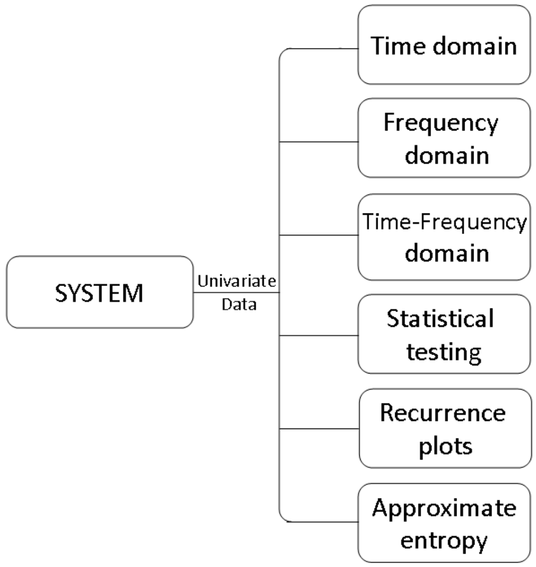


Figure 2.1: Analysis tree.

## 2.2 Domain based Analysis Techniques

The concept of unique parameters in different domains acts as a powerful indicator of information contained in the observed data. Study of these parameters leads to the different time series analysis techniques [30]. Many such related works can be found in [31], [32], [33], where useful information was extracted from the time-series.

In *time domain*, it is necessary to explore the nature of the signal under study. The signal can be classified as deterministic, stochastic, stationary and non-stationary [34]. Figure 2.2 shows deterministic and stochastic signals. There are many ways to test a time series for stochasticity which are discussed in section 2.5. Histograms are useful in differentiating between stationary and non-stationary signals, since probability distribution of non-stationary signals shifts with time. Figure 2.3 shows such signals along with their amplitude histograms at different time instants.

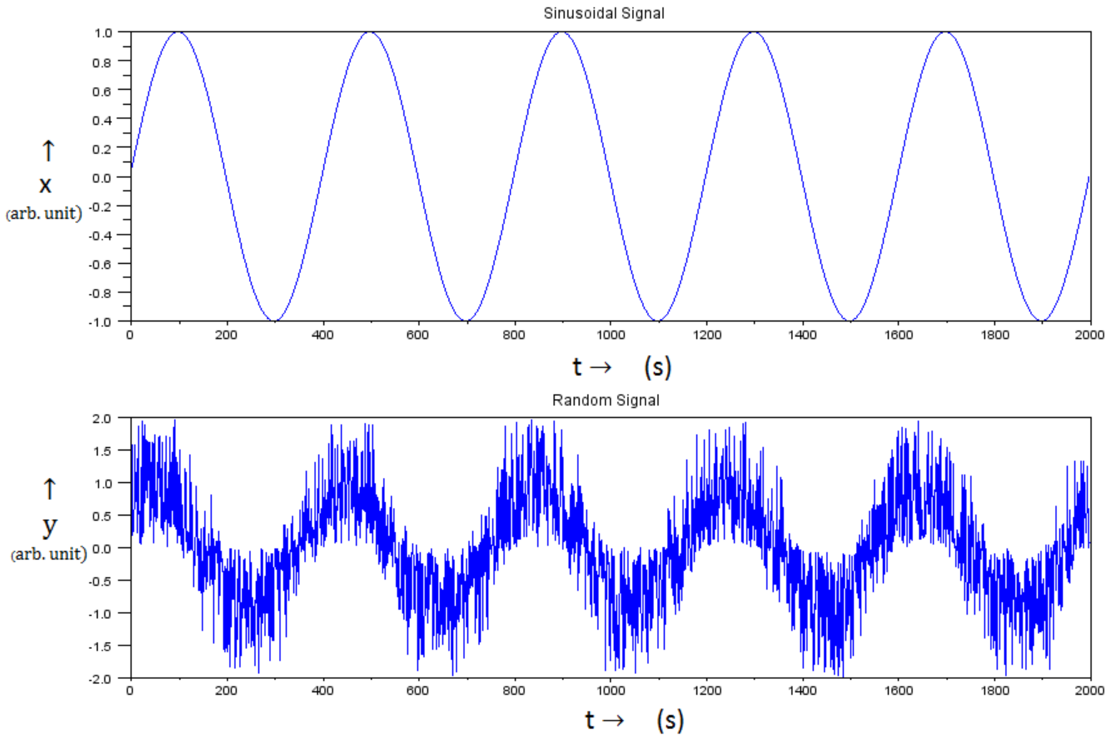


Figure 2.2: Deterministic vs. Stochastic signal.

Corresponding equations for waveforms shown in figure 2.2 are as follows.

$x = \sin(\omega t)$,
$A = rand() : A \in R(0,2)$,
$\phi = rand() : \phi \in R(0, \pi/2)$,
$y = A.*\sin(\omega t + \phi)$ (SCILAB command), where $\omega$ is angular frequency in radian/sec.

In time domain, autocorrelation function (ACF) plays an important role in understanding general features of a time series. Figure 2.4 shows the ACF plots for sine, (sine + noise) and white noise. ACF and partial ACF (PACF) plots reveals information about possible use of autoregressive (AR) and/or moving average (MA) components for a time series.

If the PACF of the differenced series displays a sharp cutoff and/or autocorrelation is positive at the origin, then the model contains an AR term. Similarly, if the ACF of the differenced series displays a sharp cutoff and/or autocorrelation is negative at the origin, then a MA component is present in the model. However, an AR(1) term is equivalent to first order difference operation [35].

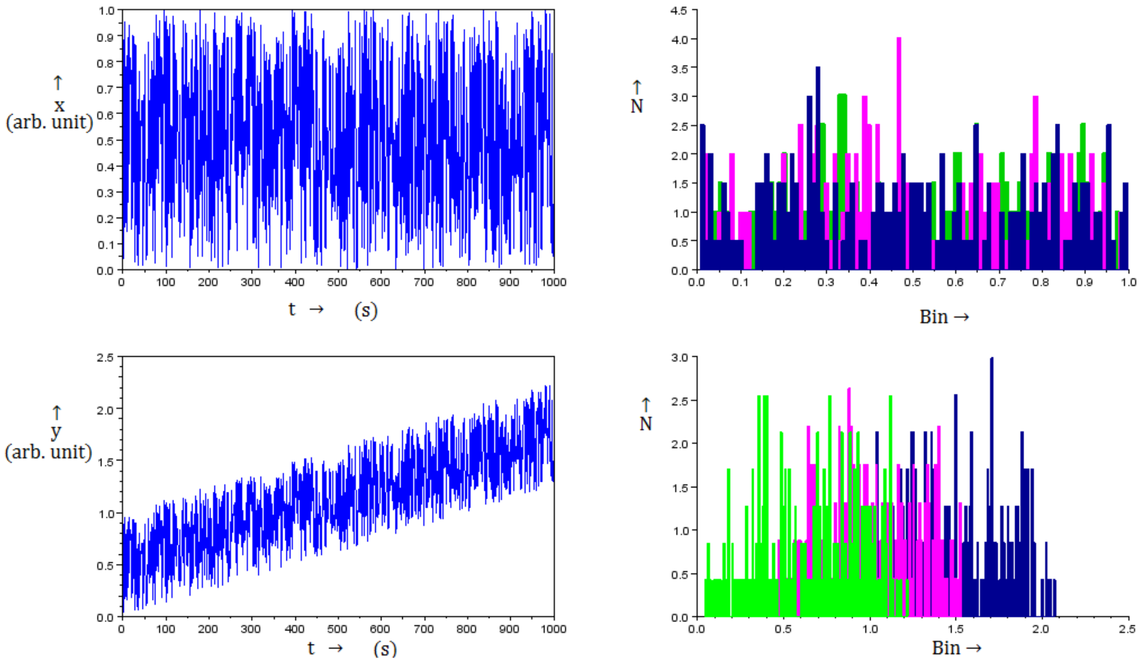


Figure 2.3: Stationary vs. Non-stationary signal.

Frame statistic for time domain data gives useful visual information about stationarity. Parameters such as mean or root mean square (RMS) can be used for such frame statistics. RMS value for a sample data can be calculated as;

$$X_{rms} = \sqrt{\frac{1}{N}\sum_{n=1}^{N}|x_n|^2} \tag{6}$$

The running RMS value is calculated over a defined value of window length, say W, such that;

$$X_{rms,W} = \sqrt{\frac{1}{N}\sum_{n=1+W}^{N+W}|x_n|^2} \tag{7}$$

where $W = 0,1,2,3,.........\infty$ for a continuously recorded data.

Figure 2.5 shows running rms value for two different signals.

In *frequency domain*, spectral analysis by using Fourier transform gives details about the frequency content of the signal. Figure 2.6 shows the FFT plot for signals with different fluctuation level.

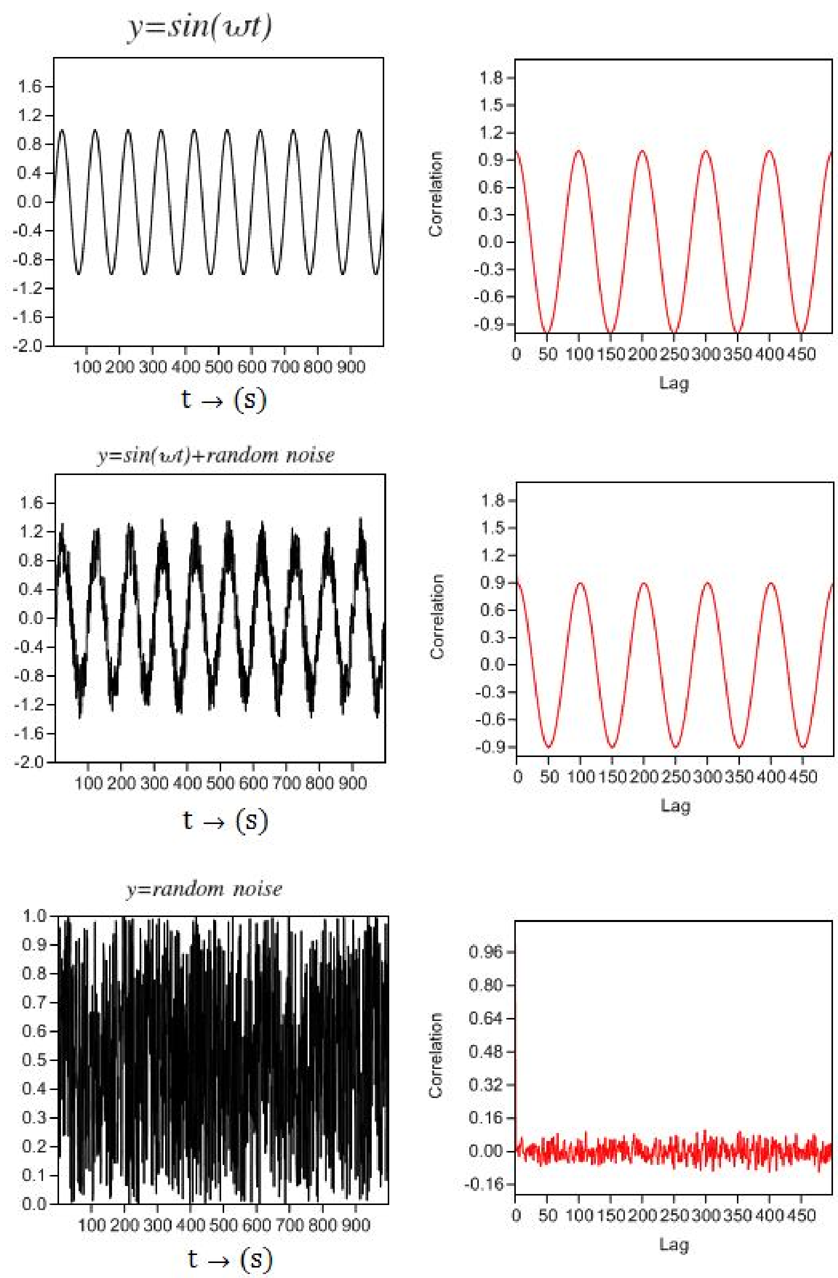


Figure 2.4: Autocorrelation plots.

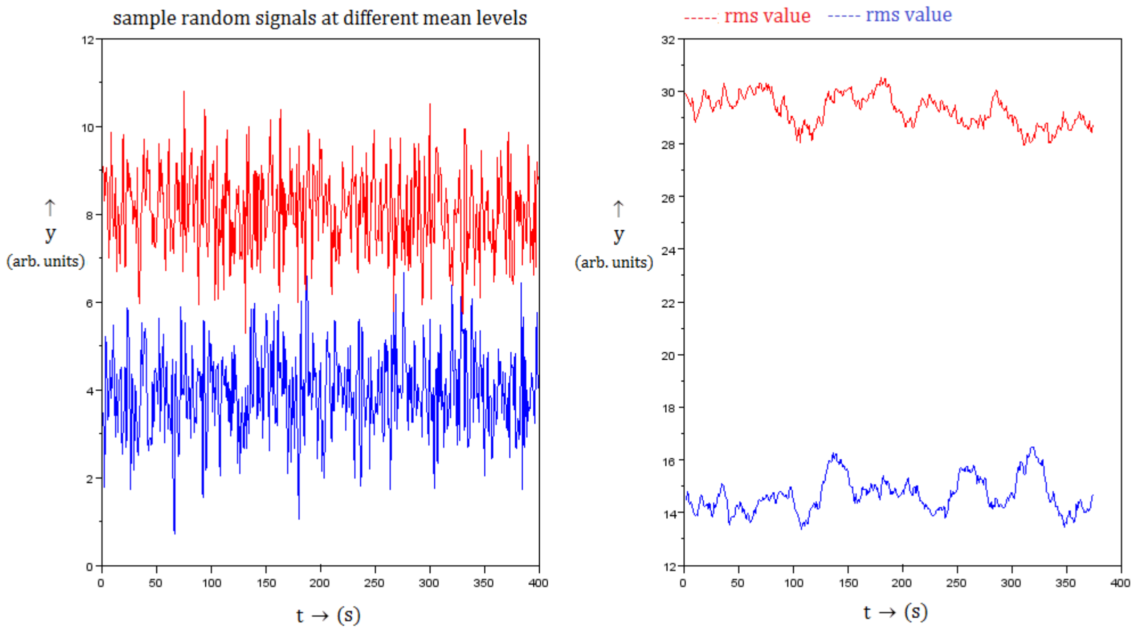


Figure 2.5: RMS plots.

The sample signals shown in figure 2.5 can be generated with the help of *grand* command in SCILAB with following syntax.

*grand(1,400,'nor',8,2)* and *grand(1,400,'nor',4,2)*

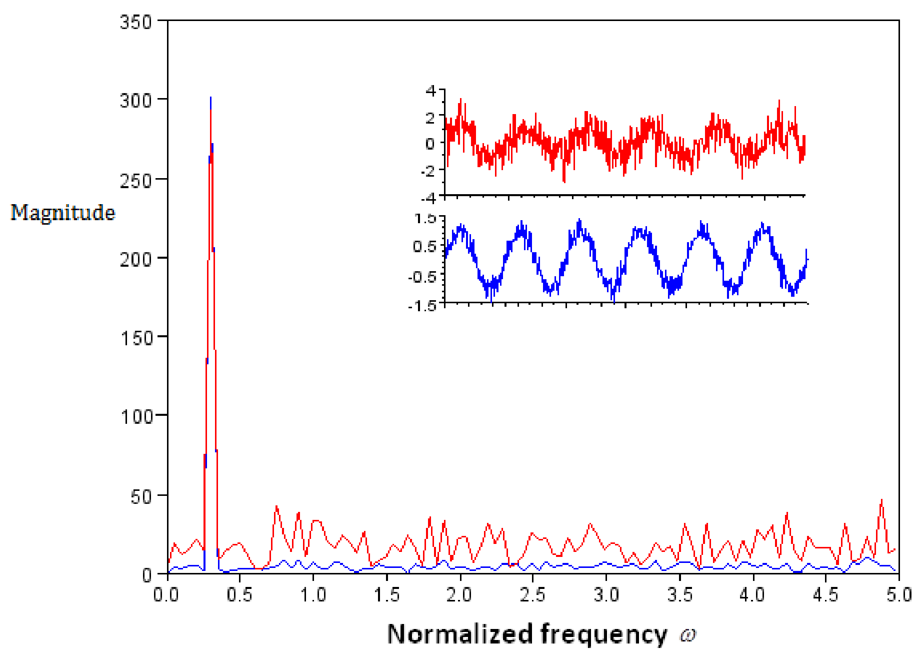


Figure 2.6: FFT plot.

*Time frequency analysis* is used to study a signal in both time and frequency domains simultaneously, by the use of time-frequency representations. The choice of representation depends on nature of the signal. The time frequency representations include Wigner-Ville distribution, time varying Power Spectral Density. (PSD), windowed Fourier transforms viz. (Short Time Fourier Transform (STFT), spectrogram, Gabor transform), altered function of time, instantaneous power spectrum, and energy density [36].

Each technique has its unique applicability which is discussed below.

- Wigner-Ville distribution - The WVD of a signal $s(t)$ is given by

$$W_z(t, f) = \underset{\tau \to f}{F}\{z(t+\tau/2)z^*(t-\tau/2)\} \tag{8}$$

where $z(t)$ is the analytic associate of signal s(t). One of the advantages of WVD is its high resolution and it gives good result when the signals under examination consist of a small number of higher harmonics.

- Time-varying PSDs - Time varying PSDs make use of the Wiener-Khintchine theorem, which relates PSD to autocorrelation function.

$$S_z(t, f) = \underset{\tau \to f}{F}\{R_z(t,\tau)\} \tag{9}$$

where $R_z(t,\tau)$ is the autocorrelation of $z(t)$. $S(t, f)$ is also known as Wigner-Ville Spectrum.

- Windowed Fourier Transform - STFT distribution is given as

$$F_s^{\omega}(t, f) = \underset{\tau \to f}{F}\{s(\tau)\omega(\tau - t)\} \tag{10}$$

where $s(\tau)$ and $\omega(\tau)$ are signal and window resp.

Spectrogram is the squared magnitude of STFT.

$$S_s^{\omega}(t, f) = \left|F_s^{\omega}(t, f)\right|^2 \tag{11}$$

Gabor transform is given as

$$c_{n,k} = \underset{k \to \Delta f}{F}\{s(\tau)\omega(\tau - n\Delta t)\} \tag{12}$$

where $c_{n,k}$ are the complex coefficients assigned to each logon, $(n,k)$ being time and frequency indices, respectively.

- Other transforms such as Continuous Wavelet Transform (CWT), scalogram etc. provide time-scale description equivalent to STFT, but uses different functional basis [36],[37].

$$\psi_{a,b}(t) = \frac{1}{\sqrt{|a|}}\psi\left(\frac{t-b}{a}\right) \qquad a, b \in \Re \, , a \neq 0 \tag{13}$$

where $\psi$ is the mother wavelet, $a$ and $b$ are scaling and time shift of the wavelet with respect to signal.

Scalogram is the magnitude squared version of CWT. Wavelets such as Haar, Morlet, Daubechies, Mexican hat, Symlet etc. are used for such purpose, amongst which Morlet wavelet is widely used as it is well localized in time and frequency domain. Morlet wavelet is obtained by modulation of a Gaussian, and given as

$$h(t) = (\pi t_o^2)^{-1/4} \exp\left\{-\frac{1}{2}\left(\frac{t}{t_o}\right)^2 + i2\pi\upsilon_o t\right\} \tag{14}$$

Figure 2.7 illustrates the performance of spectrogram and Wigner-Ville distribution in time-frequency/scale domain obtained using time frequency toolbox of SCILAB [38].

For the analysis of random signals, the scalogram and STFT give better time and frequency resolution as compared to other techniques. One such plot is shown in fig. 2.8, where it is observed that temporal resolution is better for scalogram, whereas STFT offers a better frequency resolution.

## 2.3 Visual Recurrence Analysis: Recurrence Plots

Recurrence plots were first proposed by Eckmann et al. [39] for nonlinear data analysis. These plots indicate the recurrence of a system state in phase space. A recurrence plot is mathematically expressed as

$$R_{i,j} = \Theta(\varepsilon_i - \|x_i - x_j\|),\; x_i \in \Re^m,\; i, j = 1....N \tag{15}$$

where, $N$ is the number of considered states $x_i$, $\varepsilon_i$ is threshold distance, $\|\ \|$ is 2-norm operator and $\Theta$ is Heaviside function [40].

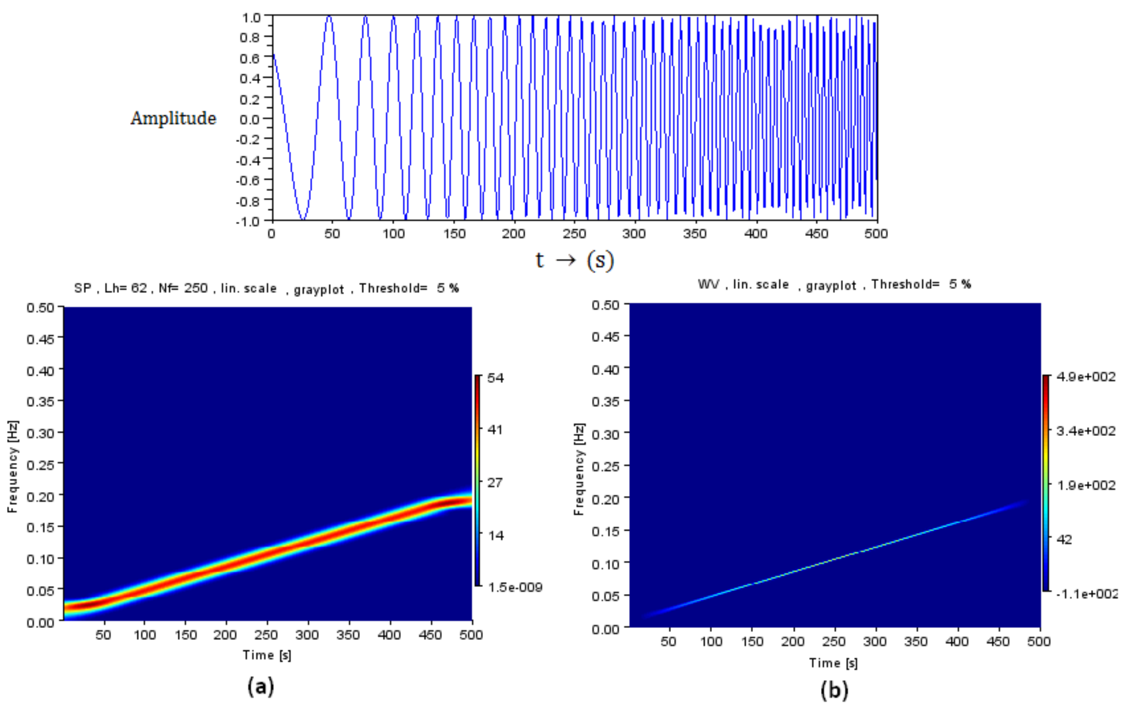


Figure 2.7: Time-frequency plot: frequency modulated signal.

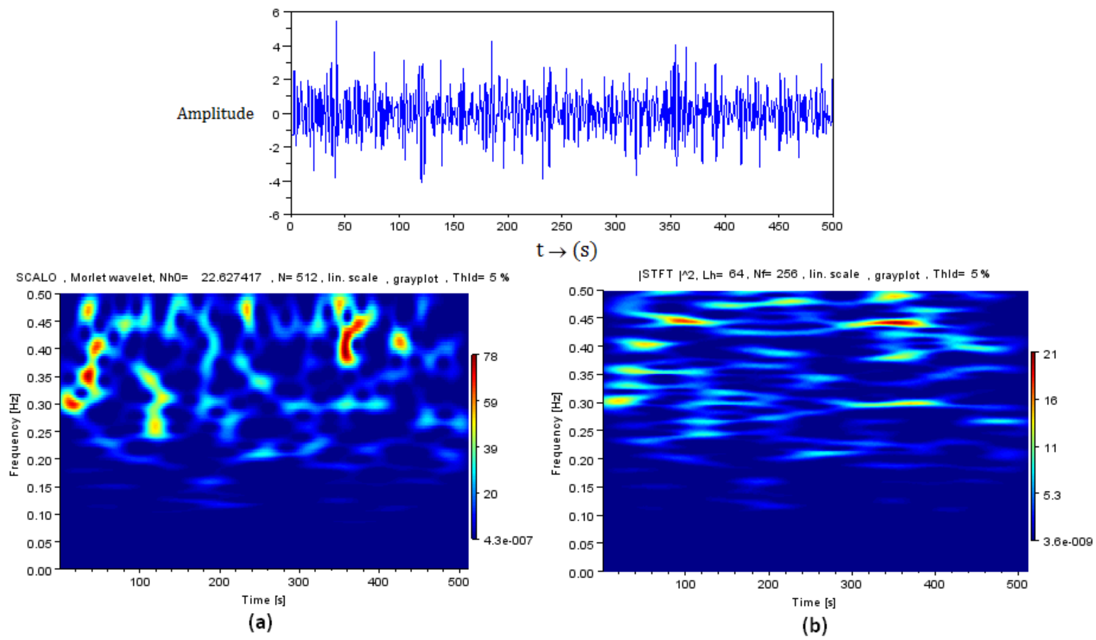


Figure 2.8: Time-frequency plot: random signal.

The visual details of RP give information about the evolution of system states. RPs contains small scale (texture) and large scale (typology) structures which are specific to different properties [41]. The typology consists of features such as homogeneous, periodic, drift and disrupted, whereas texture consists of single dots, diagonal, vertical and horizontal lines. Several work [42], [43], [44] based on this technique have been reported to derive system parameters. RP for two different time series is shown in figure 2.9, which are for sine and noise mixed sine wave.

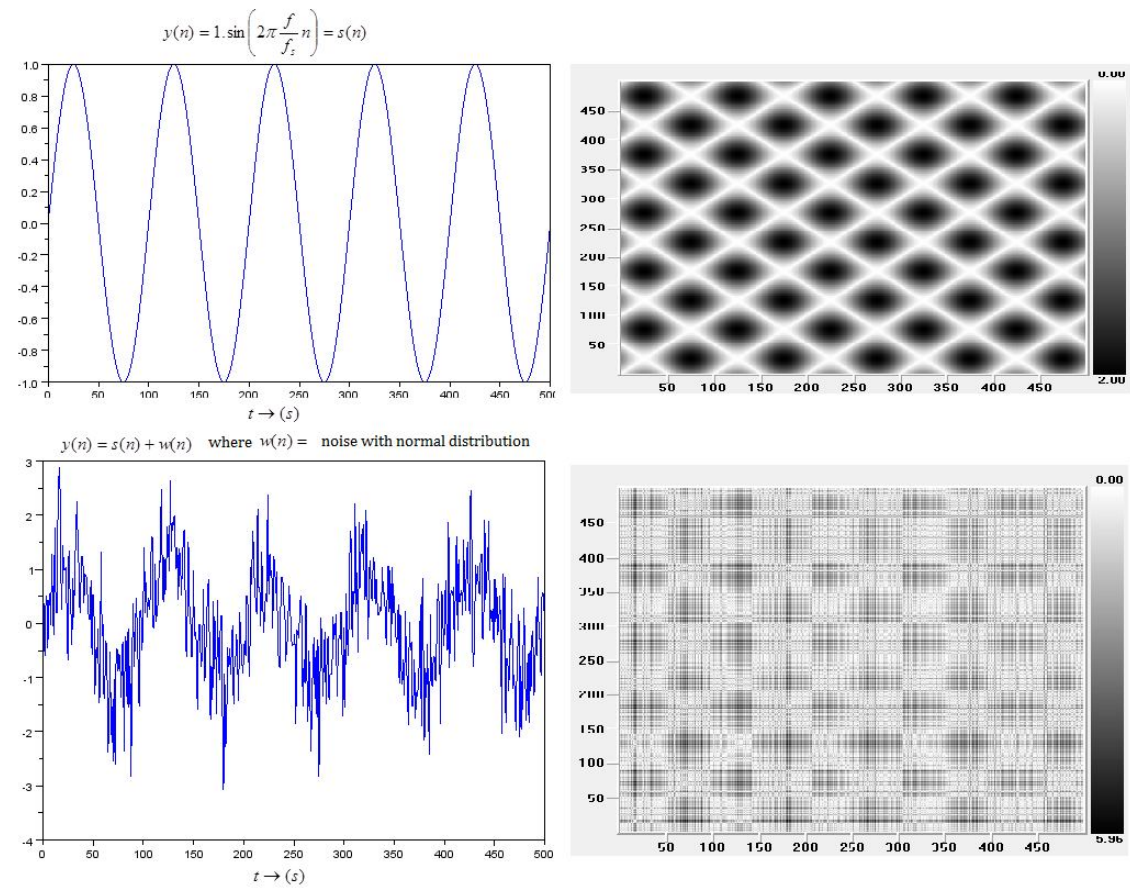


Figure 2.9: Recurrence plots.

As compared to the first plot, second plot reveals hidden patterns, even in the presence of noise. As shown in figure 2.9, the horizontal and vertical lines signify periodicity and homogeneity signifies stationarity of the signal.

## 2.4 Approximate Entropy as a Complexity Measure

Approximate entropy (ApEn) is a statistical parameter used to quantify the unpredictability of fluctuations in a time series. It was developed by Steve Pincus by using exact regularity statistic *Kolmogorov-Sinai entropy* [45]. ApEn reflects the likelihood of non repetitive occurrence of similar observations. Hence, a time series with smaller ApEn is highly predictable than a time series with higher ApEn statistics. ApEn is calculated as,

$$ApEn = (\Phi^m(r) - (\Phi^{m+1}(r)) \quad (16)$$

where $\Phi^m(r) = \dfrac{\sum_{i=1}^{N-m+1} \log\left[C_i^m(r)\right]}{N-m+1}$ and

$N$ = length of time series

$C_i^m$ is calculated as follows:

(1) First, $m$ and $r$ are defined ($m$=2, $r$=3). The value of $r$ can be changed without affecting the result.

(2) Then, the original time series $x = [x(1) \;\; x(2) \;\; x(3) \; .... \; x(N-m+1)]$ is divided into vectors of length $m$, such that

$$y(1) = [x(1) \;\; x(2)]$$

$$y(2) = [x(2) \;\; x(3)]$$

..

..

$$y(N-m+1) = [x(N-1) \;\; x(N)]$$

(3) $C_i^m$ is the no. of $y(j)$ divided by $(N-m+1)$ such that

$$d_{y(i),y(j)} \leq r \quad (17)$$

(4) The same process is repeated for $m$ replaced by $(m+1)$

It would be better to understand ApEn with the help of an example here. Let us assume two time series as shown in figure 10, which are required to be analyzed for regularity.

$$x = [22 \;\; 23 \;\; 23 \;\; 28 \;\; 20 \; 25 \;\; 22 \;\; 23 \;\; 22 \;\; 27], \; m = 2, r = 3$$
$$z = [22 \;\; 26 \;\; 22 \;\; 26 \;\; 22 \; 26 \;\; 22 \;\; 26 \; 22 \; 26], \; m = 2, r = 3$$

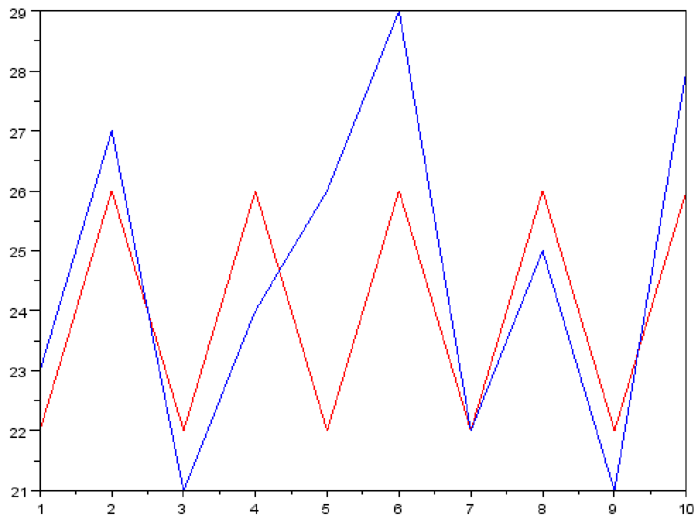


Figure 2.10: Example time-series.

Then,

$$y(1) = [22 \;\; 23]$$
$$y(2) = [23 \;\; 23]$$
$$y(3) = [23 \;\; 28]$$
$$y(4) = [28 \;\; 20]$$
$$y(5) = [20 \;\; 25]$$
$$y(6) = [25 \;\; 22]$$
$$y(7) = [22 \;\; 23]$$
$$y(8) = [23 \;\; 22]$$
$$y(9) = [22 \;\; 27]$$

$d[y(1), y(1)] = \max(abs([0 \;\; 0])) = 0$, which is $< r$

Similarly,

$$d[y(1), y(2)] = \max(abs([-1 \;\; 0])) = 1 \;< r$$
$$d[y(1), y(3)] = \max(abs([-1 \;\; -5])) = 5 \;> r$$
$$d[y(1), y(4)] = \max(abs([-6 \;\; 3])) = 6 \;> r$$
$$d[y(1), y(5)] = \max(abs([2 \;\; -2])) = 2 \;< r$$
$$d[y(1), y(6)] = \max(abs([-3 \;\; 1])) = 3 \;= r$$
$$d[y(1), y(7)] = \max(abs([0 \;\; 0])) = 0 \;< r$$
$$d[y(1), y(8)] = \max(abs([-1 \;\; 1])) = 1 \;< r$$
$$d[y(1), y(9)] = \max(abs([0 \;\; -4])) = 4 \;> r$$

$$\therefore \; C_1^2(3) = 6/(N-m+1) = 6/9$$

Similarly, $C_2^2(3) = 6/9$

$$C_3^2(3) = 3/9$$

$$C_4^2(3) = 2/9$$
$$C_5^2(3) = 7/9$$
$$C_6^2(3) = 6/9$$
$$C_7^2(3) = 6/9$$
$$C_8^2(3) = 6/9$$
$$C_9^2(3) = 3/9$$

$$\therefore \ \Phi^m(r) = \frac{\sum_{i=1}^{N-m+1} \log\left[C_i^m(r)\right]}{N-m+1} = -0.9139952$$
$$\Phi^{m+1}(r) = -1.5400377$$

Hence, $ApEn = -0.9139952 - (-1.5400377)$
$= 0.6260425$

In the same manner, the $ApEn$ value for $z$ comes out to be 0.1239686, which confirms the better regularity and predictability of $z$ than $x$.

## 2.5 Statistical Tests : KPSS, RAT and Runs test

Statistical tests are considered very important part of time series analysis. Various tests for randomness and stationarity check are discussed below.

*KPSS (Kwiatkowski–Phillips–Schmidt–Shin) Test:*

Though the stationarity test as proposed by Kwiatkowski et al. [46] was related to econometrics, its testing capabilities in signal processing were also recognized and utilized in [47], [48], and [49]. The null hypothesis $H_o$ in KPSS test is that the time series is stationary around a deterministic trend. $H_o$ is rejected if the KPSS test statistic is greater than the $100 \cdot (1-\alpha)\%$ quantile from the appropriate distribution. (for eg. Normal distribution). A stationary time series is represented as Integrated of zeroth order $I(0)$. If $H_o$ is rejected for a time series, and if it becomes stationary after performing $k^{th}$ order differencing; then the time series is represented as $I(k)$. Hence, KPSS test proves to be of immense utility in determining the mathematical transformations to be applied on original time series in part.

There are various software tools available for performing KPSS test, such as Gretl, R, Matlab, Scilab etc. Gretl is open source software and provides various options for performing a KPSS test. The KPSS critical values (quantiles) are listed in Table 2.1.

TABLE 2.1
Critical values for KPSS test

| | 10% | 5% | 1% |
|---|---|---|---|
| Critical values: | 0.347 | 0.461 | 0.743 |

*Reverse Arrangement test (RAT):*

While the earlier discussed method (KPSS) make assumptions about the distribution of the data, RAT is one of the non-parametric test procedures, where no assumption is required to be made about the distribution of the data. The test statistic [50] is calculated as follows.

- Let $x_i = x_1, x_2 \cdots\cdots x_N$ be the time series. Then, for $i = 1, 2 \cdots\cdots (N-1)$ and $j = i, i+1, \cdots\cdots N$

$$d_{ij} = \begin{cases} 1, x_i > x_j \\ 0, otherwise \end{cases} \tag{18}$$

- $$A = \sum_{i=1}^{N-1} \sum_{j=i+1}^{N} d_{ij} \tag{19}$$

$H_o$ in RAT is that the data is from a random source. $H_o$ is rejected if the calculated z-score is > 1.96. The z-score is calculated as follows.

$$z = \frac{A - \mu_A}{\sigma_A}$$

where $A$ is the no. of reverse arrangements, and

$\mu_A = \frac{N(N-1)}{4}$, $\sigma_A^2 = \sqrt{\frac{2N^3 + 3N^2 - 5N}{72}}$, $N$ is the length of time series

*Runs test:*

The runs test [51] is used to decide if a data set is from a random process. $H_o$ in runs test is that the data has been produced in a random manner. For 5 % significance level, a test statistic $|z| > 1.96$ indicates non-randomness. $z$ score is calculated as follows.

- The test data is divided into several groups (runs) whenever there is a transition above/below a certain fixed value. This fixed value can be rms, mean etc.
- Each group is consecutively designated as $n_1$ and $n_2$.
- Then, $z$ score is calculated as

$$z = \frac{r - \bar{r}}{\sigma_r} \tag{20}$$

where $r =$ is the total no. of runs

$\bar{r} =$ Expected no. of runs $= \frac{2n_1n_2}{n_1 + n_2} + 1$, and

$$\sigma_r^2 = \frac{2n_1n_2(2n_1n_2 - n_1 - n_2)}{(n_1 + n_2)^2(n_1 + n_2 - 1)} \tag{21}$$

## 2.6 Selection of Fast Breeder Test Reactor (FBTR) Data

To perform the above discussed tests, a large size and wide range of data is required. Hence, reactor core temperature data was collected for various power levels during *stable* as well as *transient* (shut-down and start-up) reactor operations. The data includes central subassembly outlet temperature, reactor outlet temperature, primary sodium flow and neutronic signals. K-type, Cr-Al (Chromel-Alumel) thermocouples without thermowell, directly in contact with sodium is used for measuring central subassembly outlet temperature for this purpose. This results in a faster response of thermocouple. As shown in figure 2.11, the thermocouple output is taken to a reference insulated junction box. The reference junction box temperature is measured with the help of an RTD (Resistance Temperature Detector). The output signals in mV (millivolts) are then fed to isolation amplifiers, where they are amplified and standardized to 0-10 V d.c. These standardized signals are then fed to Analog Input Card (AIC) of embedded computer system, where they are continuously monitored for various safety actions. The calibrated temperature data along with various other reactor parameters are logged to computer memory as *.CSV* (Comma Separated Value) file. These files consist of temperature time-series and can be taken at different times of reactor operation. Each time series is 2400 samples long, with each sample spaced 0.1 second apart. The reactor power ranges from few MWTh (thermal) to 18 MWTh.

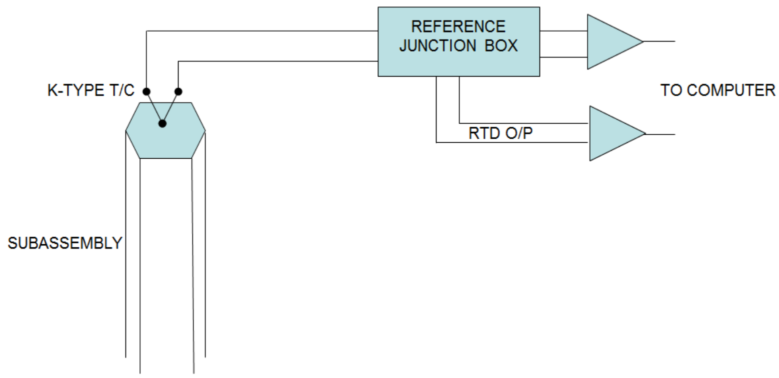


Figure 2.11: Data Acquisition setup.

The proposed analysis method involves utilization of CSA (Central Sub-Assembly) temperature time-series for various tests and analysis discussed so far; hence to give a meaningful insight of the signal processing architecture needed for the purpose of estimating power from temperature fluctuation data.

## 2.7 Conclusion

A process for data driven model based design approach was outlined for proposed temperature fluctuation analysis. A single domain or type of analysis would be insufficient in judging the characteristics of the data. Hence analysis in time, frequency and mutually correlated domain was introduced. The tests associated with extraction of main features of data i.e., determinism/stochasticity and stationarity/non-stationarity were discussed for their possible use in FBTR data time series analysis. It is found that performing such analysis would give sufficient information to build a mathematical model for signal processing of the dynamic temperature fluctuations.

# 3

# CORE TEMPERATURE ANALYSIS OF FAST BREEDER TEST REACTOR

This chapter discusses the various test results for core temperature of fast reactor. Central Subassembly (CSA) outlet temperature profile is used for the analysis. CSA exhibits highest temperature in the core. Though, the concept of flow zoning [52] is utilized for coolant flow in core to give a uniform temperature profile, there exist a minimum degree of fluctuation at each reactor power level [8]. Hence, a proper analysis is required in order to establish a correlation between thermal power and temperature fluctuations.

## 3.1 FBTR Data

The data in the form of a time series consists of various reactor parameters. These parameters are listed in Table 3.1.

TABLE 3.1: Signal Nomenclature for time-series

| Signal Name | Description |
|---|---|
| FML020A, FML030A, FME020B | Linear and log power safety channel |
| NNA000, NNA100, NNA101, NNA200, NNA201 | Sodium level in reactor, pump, IHX |
| PAR332 | Argon gas pressure |
| TNA000Z | Central subassembly temperature |

Figure 3.1 shows core structure of FBTR. The central subassembly (CSA) data in the time-series consists of 2400 samples spaced 0.1 s apart. This data is taken for a large power range i.e., from 1 MWTh to 18 MWTh, at reactor startup and shutdown, as well as few power levels at stable power. Figure 3.2 shows the CSA temperature profile at different power levels. Figure 3.3 shows temperature profile for stable power levels.

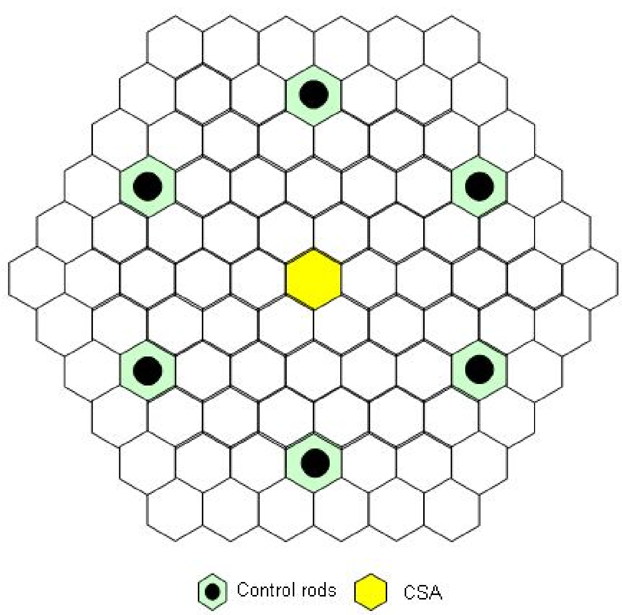


Figure 3.1: FBTR Core structure.

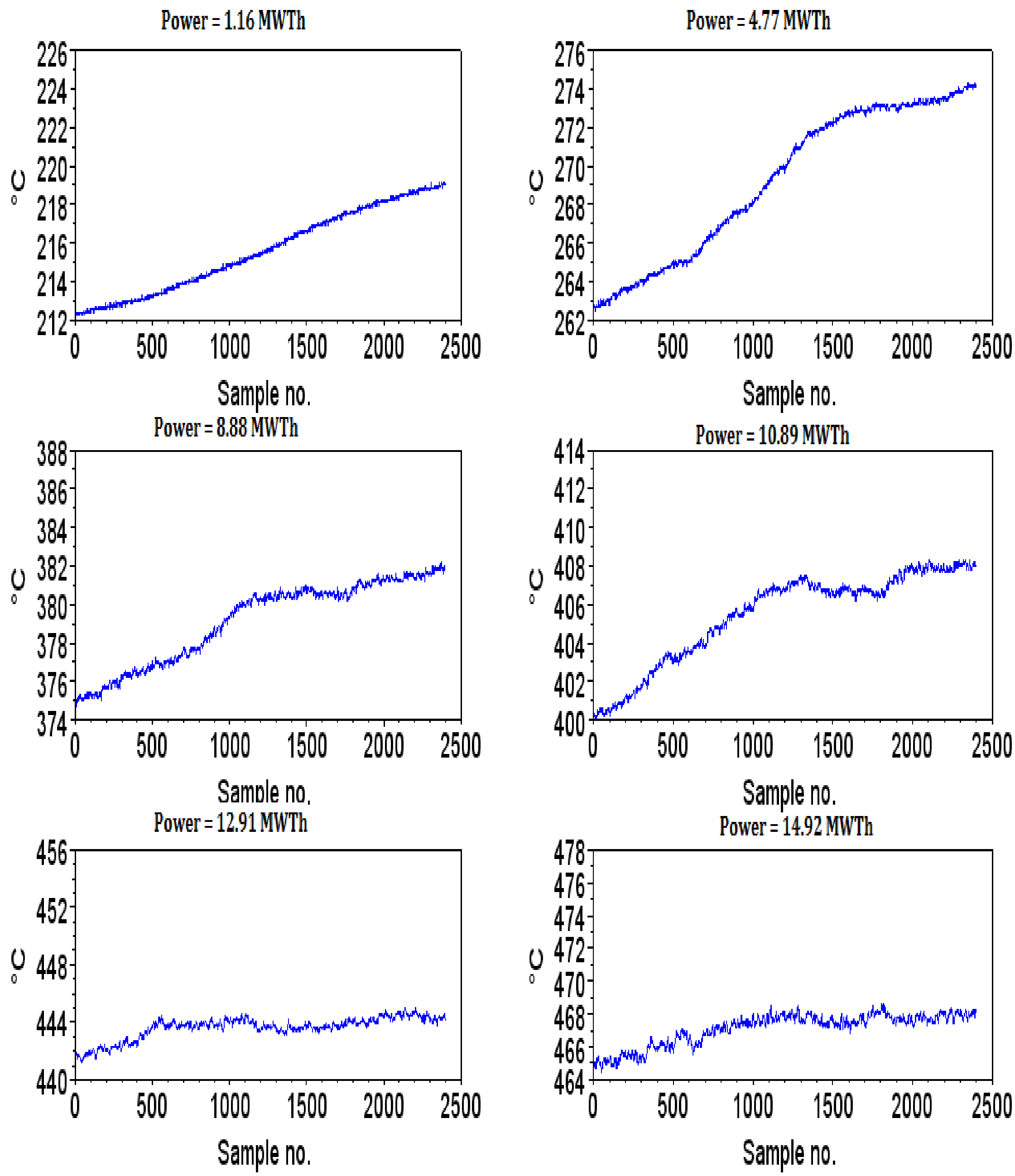


Figure 3.2: Temperature profile: reactor power increase.

A visual inspection of these profiles suggests that the degree of fluctuation increases with an increase in mean temperature value. This can be verified by taking note of maximum deviation from mean level at a particular reactor power. For e.g.; at 409.4 $^{o}$C and 512.3 $^{o}$C, the maximum deviation are 0.29 and 0.43 respectively. Further analysis would give valuable information about key building blocks of signal processing architecture required for fluctuation processing.

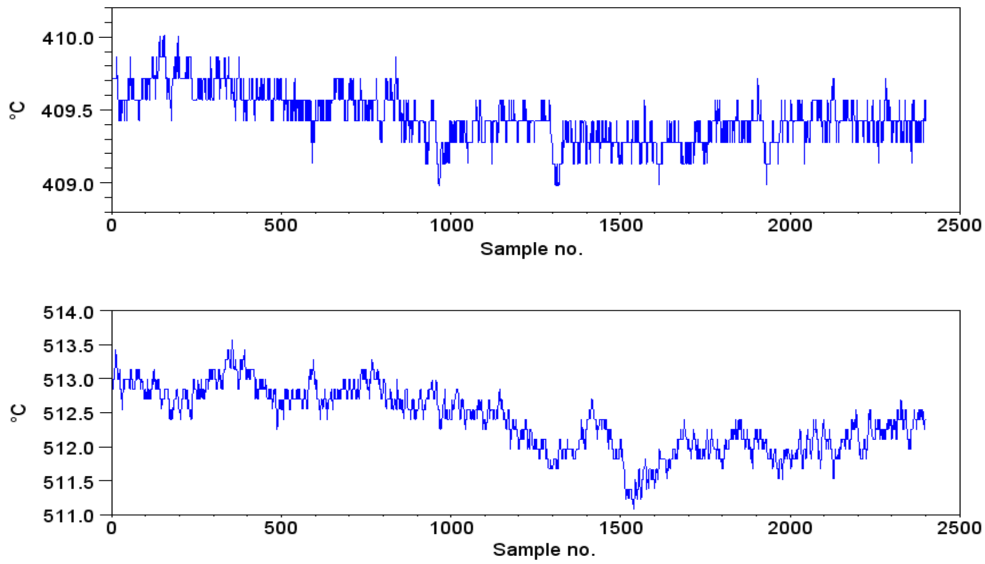


Figure 3.3: Temperature profile: Stable power.

## 3.2 Domain based Analysis

*Time-domain:* Autocorrelation plot of temperature profiles at various power levels gives information about similarity between time series and its time-shifted version. This gives clue about the inclusion of mathematical operation needed in the architecture.

Figure 3.4 shows the autocorrelation (ACF) plot of CSA temperature for different power levels obtained during raising of reactor power. The ACF plot for two different and stable power levels is shown in figure 3.5.

It is important to observe ACF plot for stable power, since the same plots for raising reactor power operation would convey less information about the nature of fluctuations. As can be seen in the above figures, the autocorrelation slowly decreases and doesn't crosses zero immediately. Also, the autocorrelation value at zero lag (mean square value) shows irregular behavior of fluctuations at different power levels.

The parametric signal source modeling for an AR(1) process can written as [53];

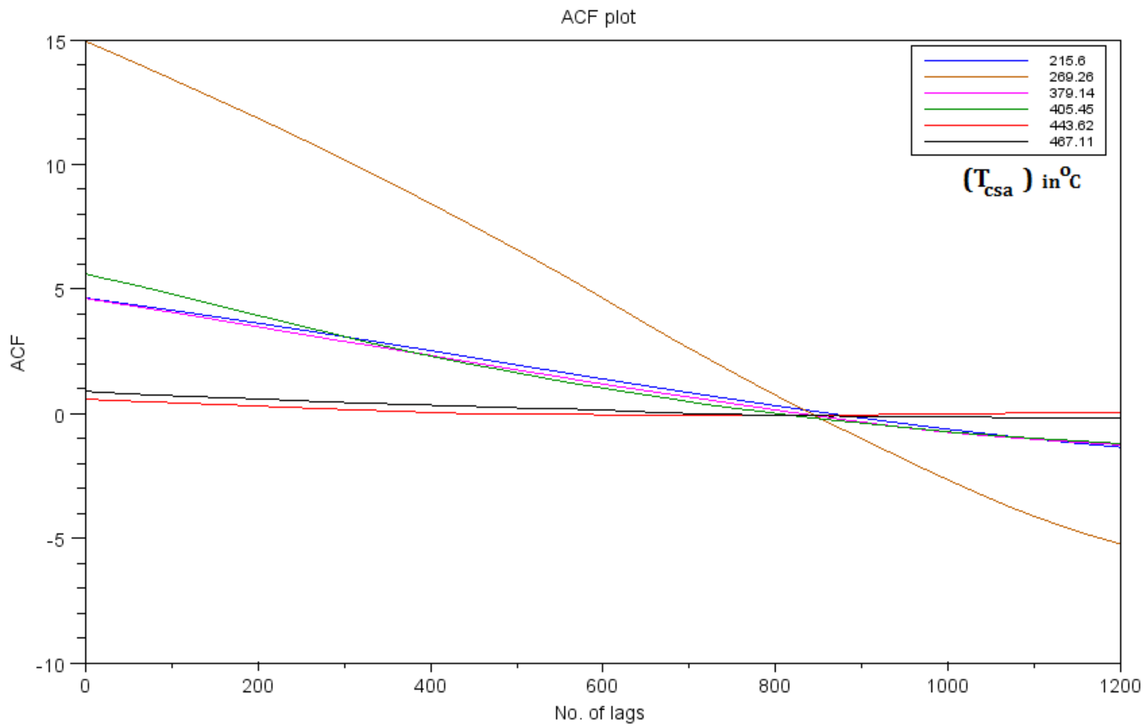


Figure 3.4: ACF plots - transient power level.

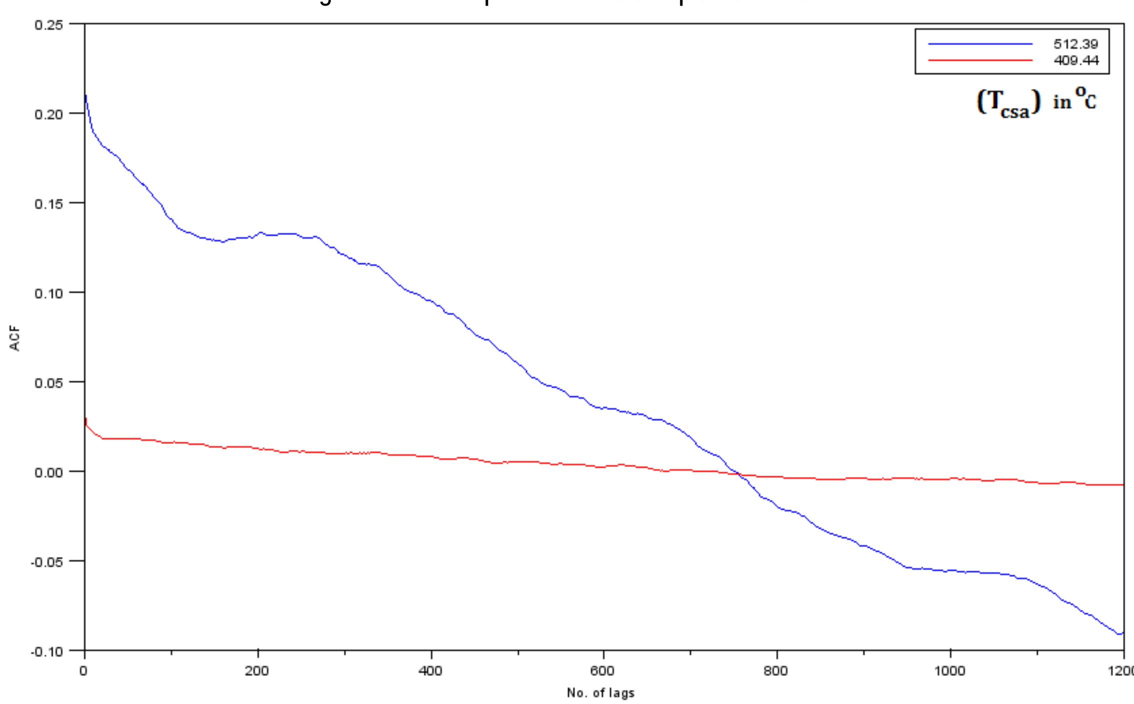


Figure 3.5: ACF plots – Stable power levels.

$$\tilde{x}(n) = x(n) - x(n-1), \text{where } x(n) \text{ is in } ^{o}\text{C}.$$

Another approach to obtain the fluctuation signal can be given as;

$$\tilde{x}(n) = x(n) - \bar{x}(n), \text{where } \bar{x}(n) \text{ is the mean level in } ^{o}\text{C}.$$

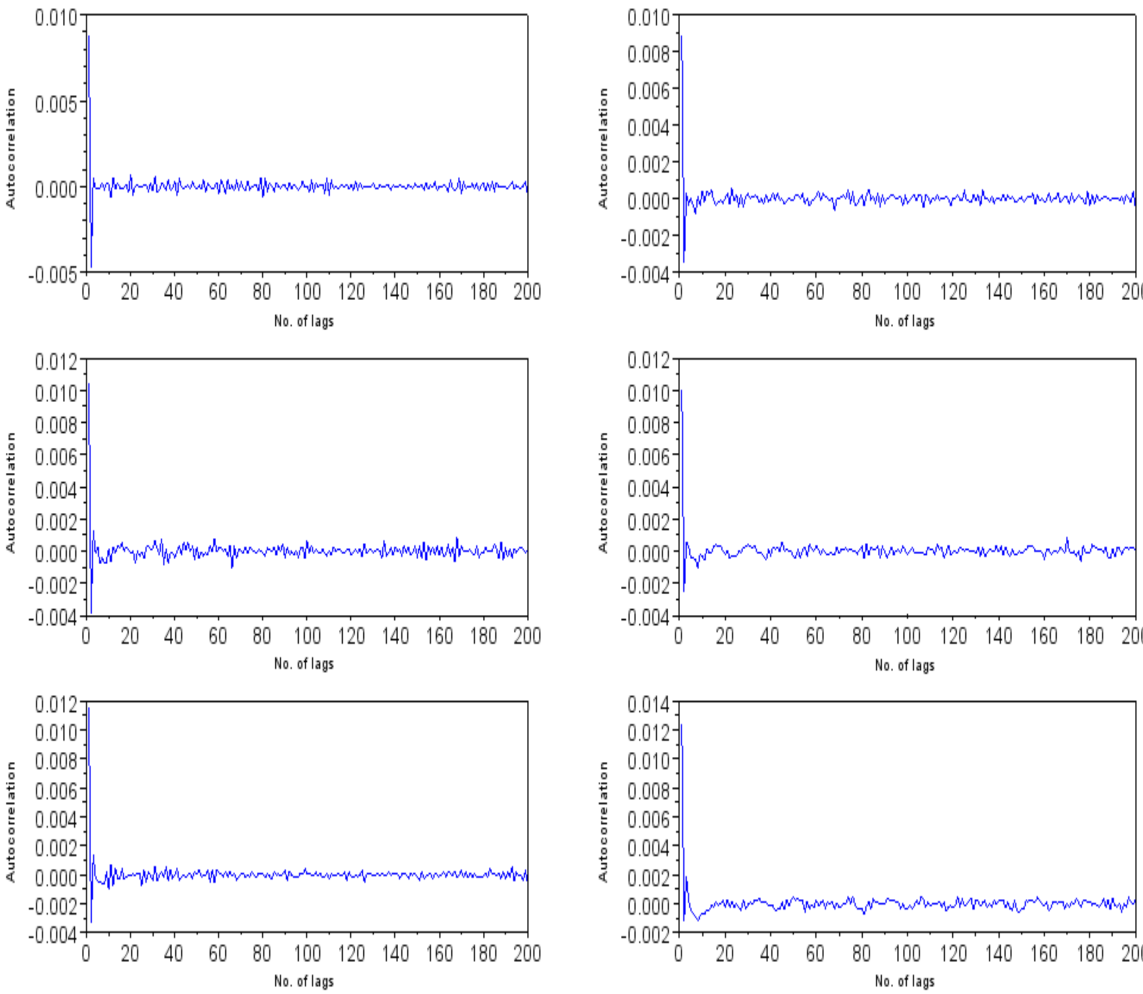


Figure 3.6: ACF plots – Differenced data.

With a view from making computationally easier operation, the first approach as mentioned above has been utilized here. The ACF plot for fluctuation signal (for reactor power-up operation) obtained by first order differencing at various temperature levels are shown in shown in figure 3.6 and 3.7.

The plots crosses the horizontal axis immediately and hence confirms the presence of AR(1) component in the signal, and has to be included in the model.

Histogram plots for time series at different mean CSA temperatures, and for its differenced version are shown in figure 3.8 and 3.9 respectively.

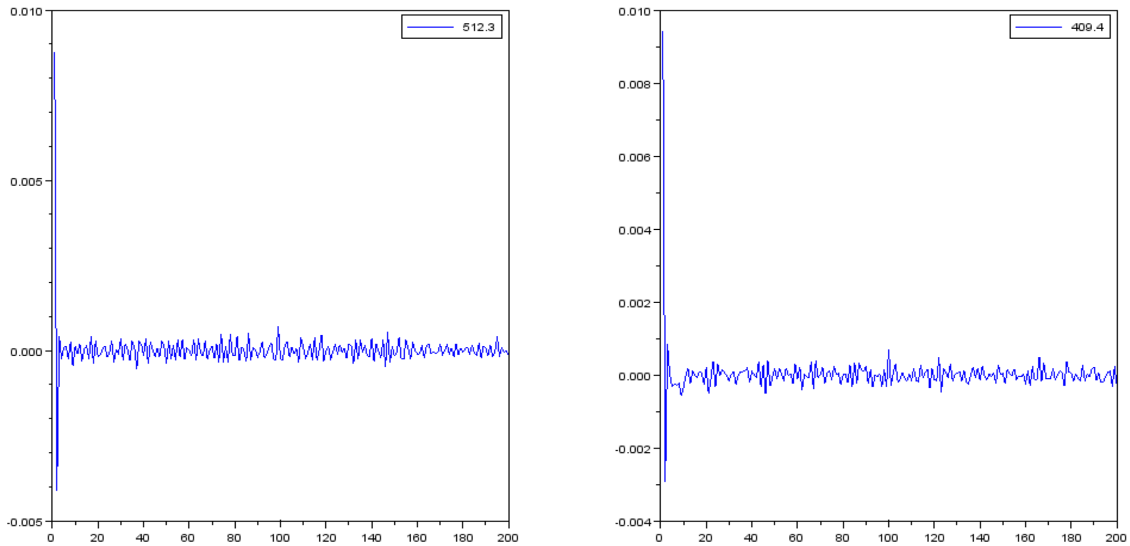


Figure 3.7: ACF plots – Differenced data (stable power).

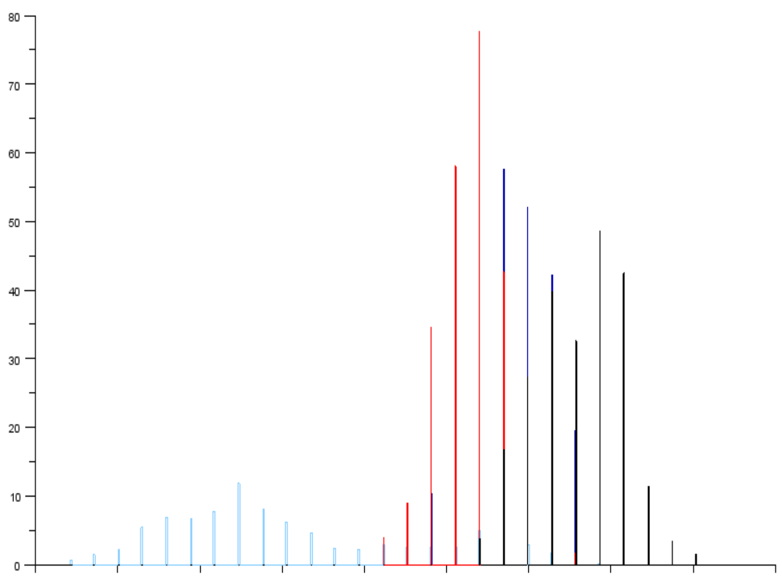


Figure 3.8: Histogram plot –at various mean $T_{CSA}$

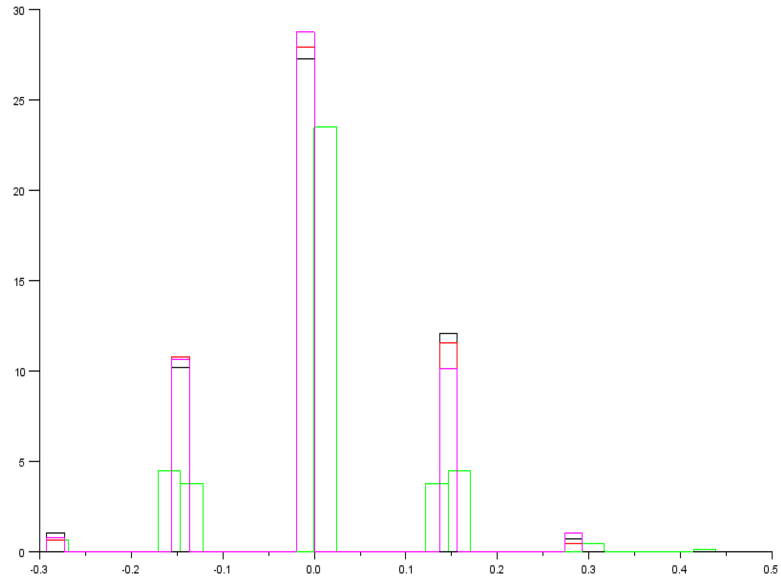


Figure 3.9: Histogram plot – for differenced time series at various mean $T_{CSA}$

It can be observed from above histogram plots that temperature values at different power levels (and hence at different $T_{CSA}$) gets distributed uniformly and hence becomes stationary after performing first order differencing.

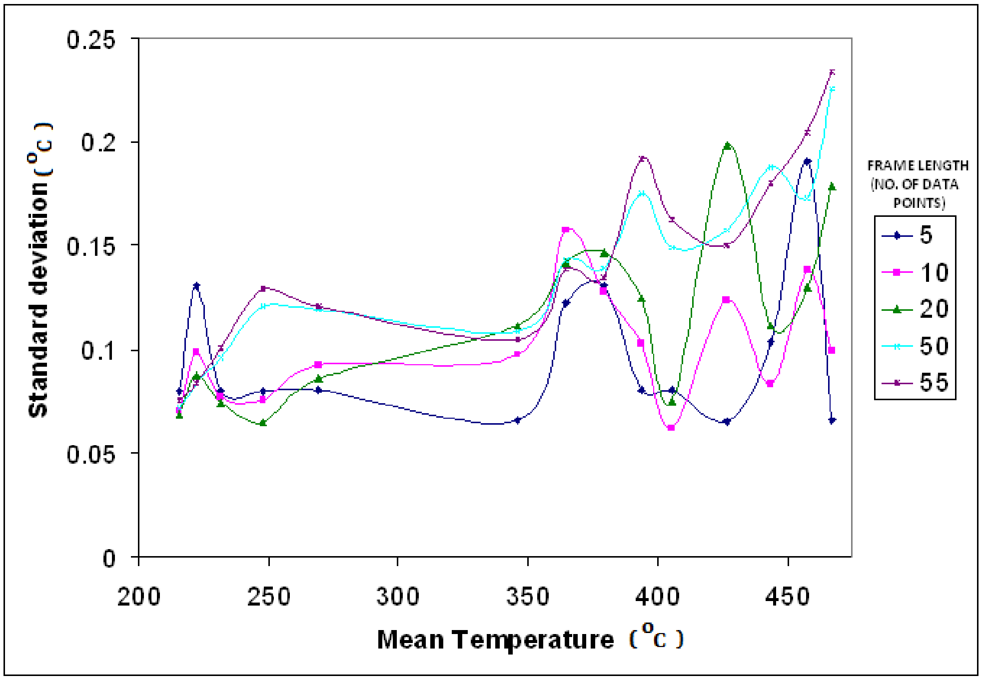


Figure 3.10: Frame statistics (std. deviation) for different temperature data.

Frame statistics of data at different temperatures and for various window lengths is shown in figure 3.10. For e.g., standard deviation for each set of 5 data points at different temperature levels is calculated. It is clear that the signal in its raw state may not be suitable for deriving the desired parameter.

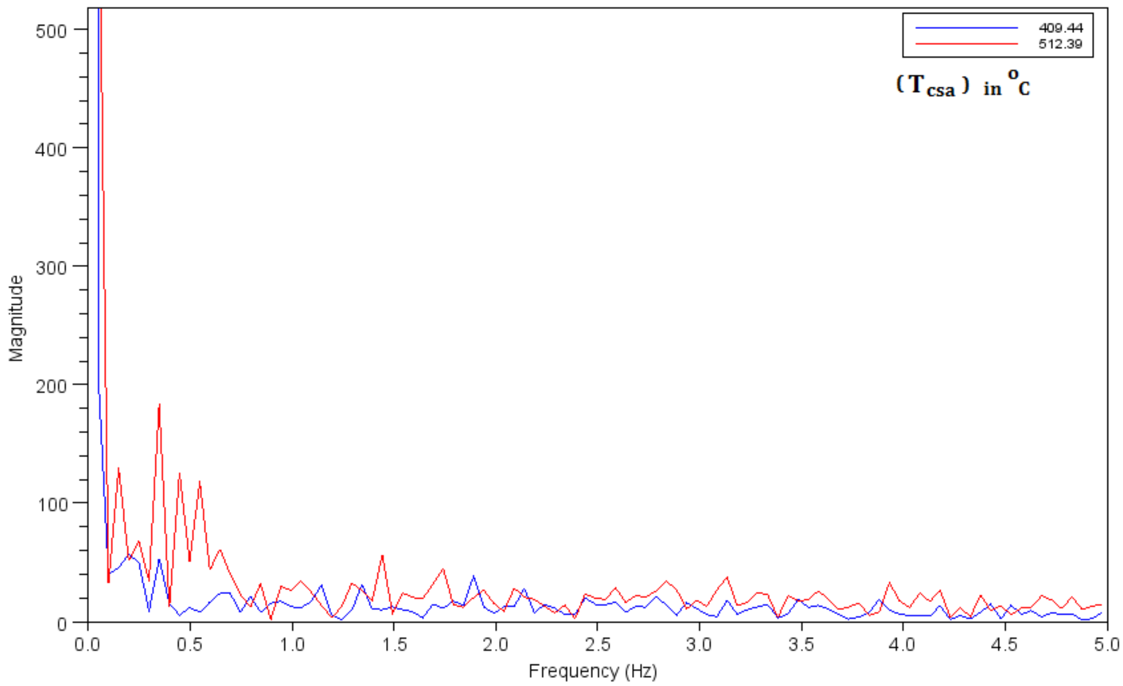


Figure 3.11: Fourier analysis.

Figure 3.11 shows the FFT (Fast Fourier Transform) plot for two different power levels. It is clear from the plot that there is an increase in fluctuation levels at comparatively higher temperatures. However, the fluctuations obtained even after differencing are non-linearly localized in time. To analyze its behavior in localized time and frequency domains, time-frequency plots at various power levels are shown in figure 3.12, 3.13 and 3.14.

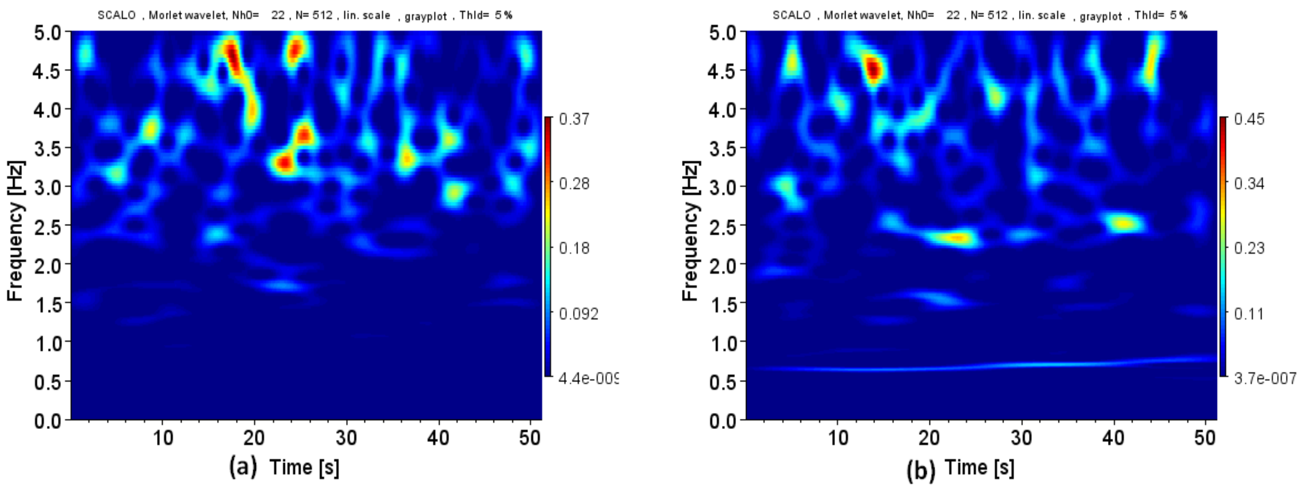


Figure 3.12: Time-frequency plot analysis (a) 215.6°C (b) 269.2 °C.

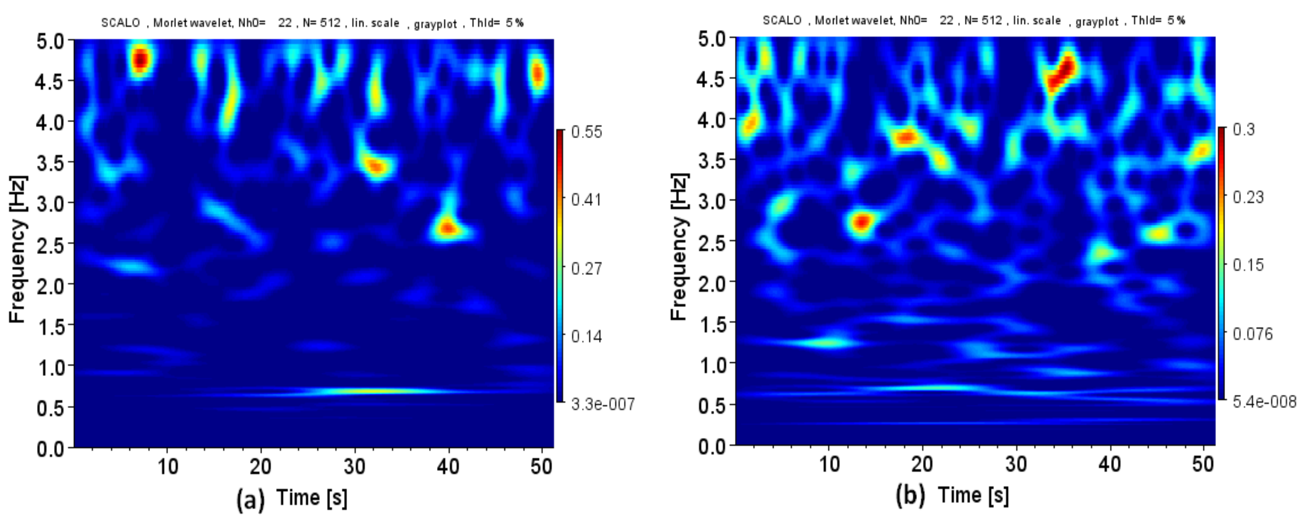


Figure 3.13: Time-frequency plot (a) 379.1°C (b) 405.4°C .

It is observed from the above plots that no. of fluctuations as well as their magnitude increases with temperature. However, it is also observed that the magnitude increase may deviate slightly at certain temperatures. This can be contributed to magnitude distribution amongst the no. of fluctuations [56].

Hence, for certain temperatures; even if the magnitude of fluctuations doesn't increases, the reduction is well reflected by increase in no. of fluctuations occurring. For eg., as shown in figure 3.13, the magnitude reduction is accompanied by increased occurrence of fluctuations.

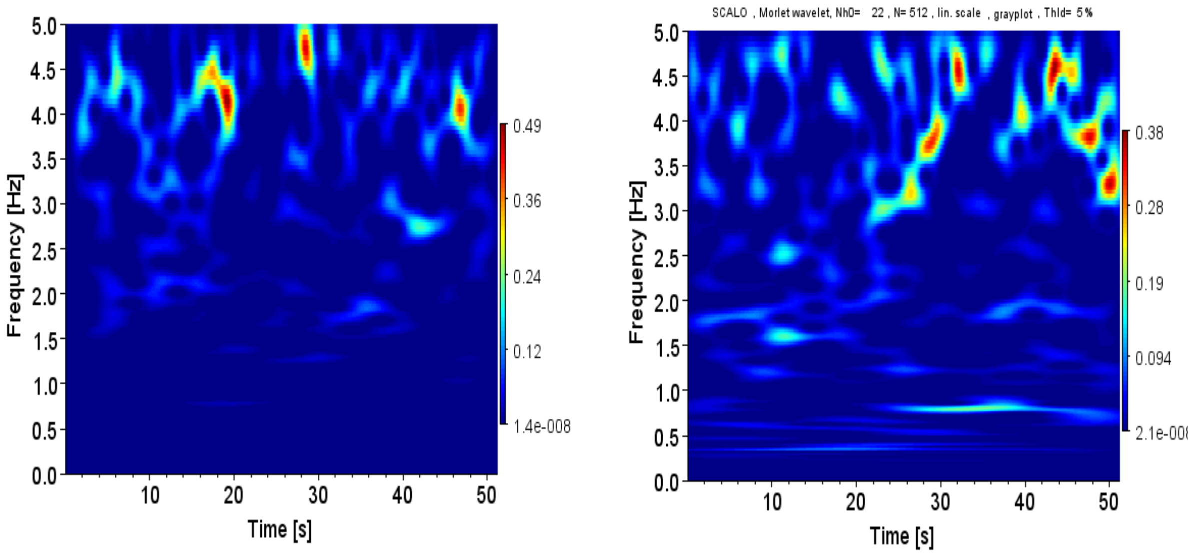


Figure 3.14: Time-frequency plot (a) 409.4°C (b) 512.3°C .

A detailed analysis explaining the observed CSA temperature fluctuation behavior with respect to thermal power has been discussed in section 3.6.

## 3.3 Recurrence plot analysis

Figure 3.15 shows the recurrence plots for differenced temperature data at various power levels. Small scale (texture) and large scale (typology) structures as visible in the figure explain the system evolution with increasing temperature. It confirms the presence of laminar states at discrete power levels, since the system state changes slowly with time. Also, the RP looks homogeneous which agrees with stationarity principle [57].

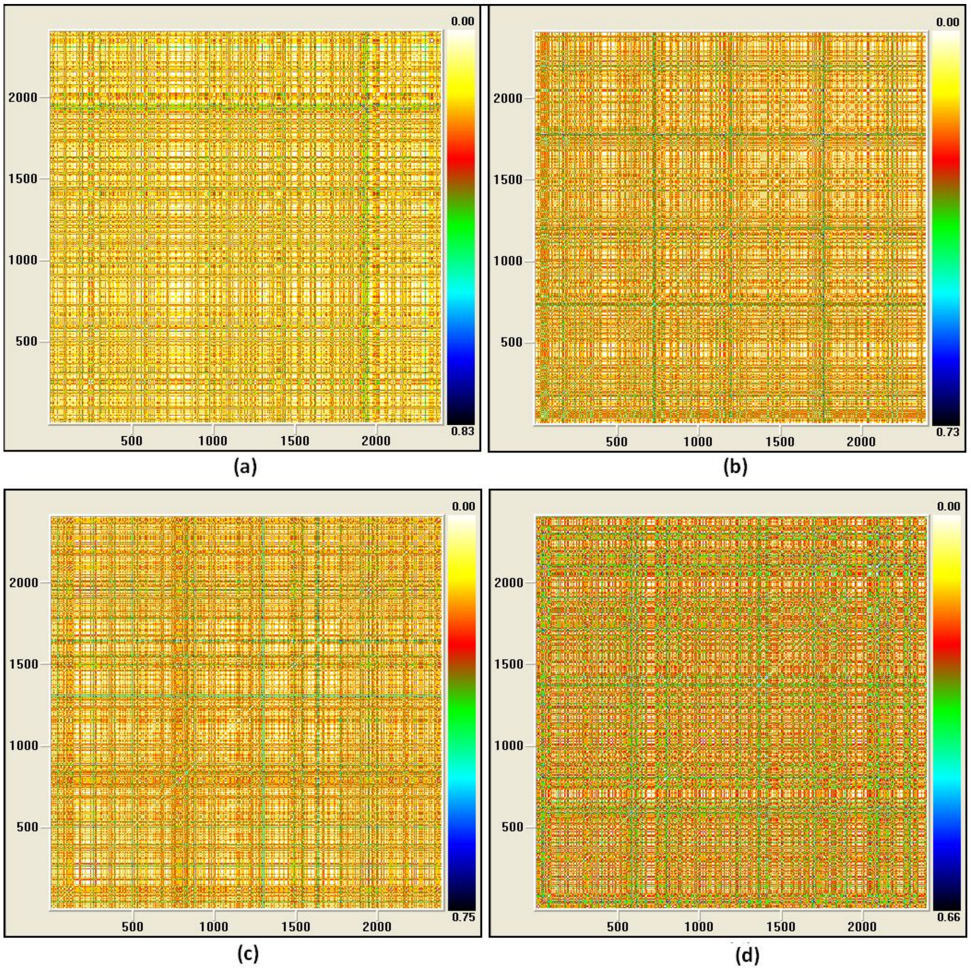


Figure 3.15: VRA (a) 215.6$^o$C (b) 269.2$^o$C (c) 379.1$^o$C (d) 405.4$^o$C.

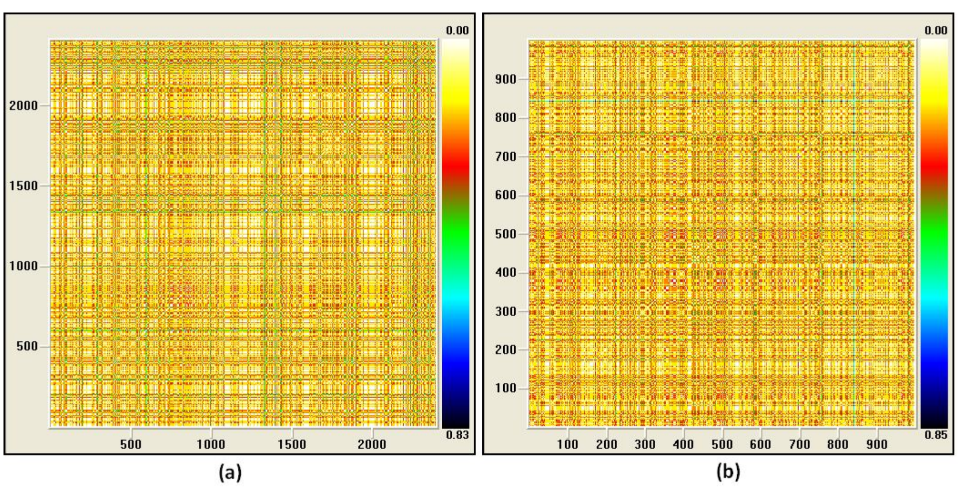


Figure 3.16: VRA (a) 409.4 $^o$C (b) 512.3$^o$C .

## 3.4 Approximate Entropy analysis

A time series with smaller ApEn is highly predictable than a time series with higher ApEn [58]. ApEn is a parameter used to quantify regularity in data and doesn't need prior knowledge of the system generating it. The ApEn statistics obtained for temperature data with pattern length (m) of 3, and similarity criterion (r) being multiple of variance of time series is shown in figure 3.17, which confirms the presence of statistical pattern in it. The ApEn value as compared to that for a pure random series is very less, thereby making it comparatively more predictable. Similar results in other studies in different domains have been found in [59], [60].

The ApEn statistics for the present study has motivated for further analysis of core temperature. The temperature fluctuations are not merely random observations and supports the idea of information extraction from the temperature fluctuations in reactor core.

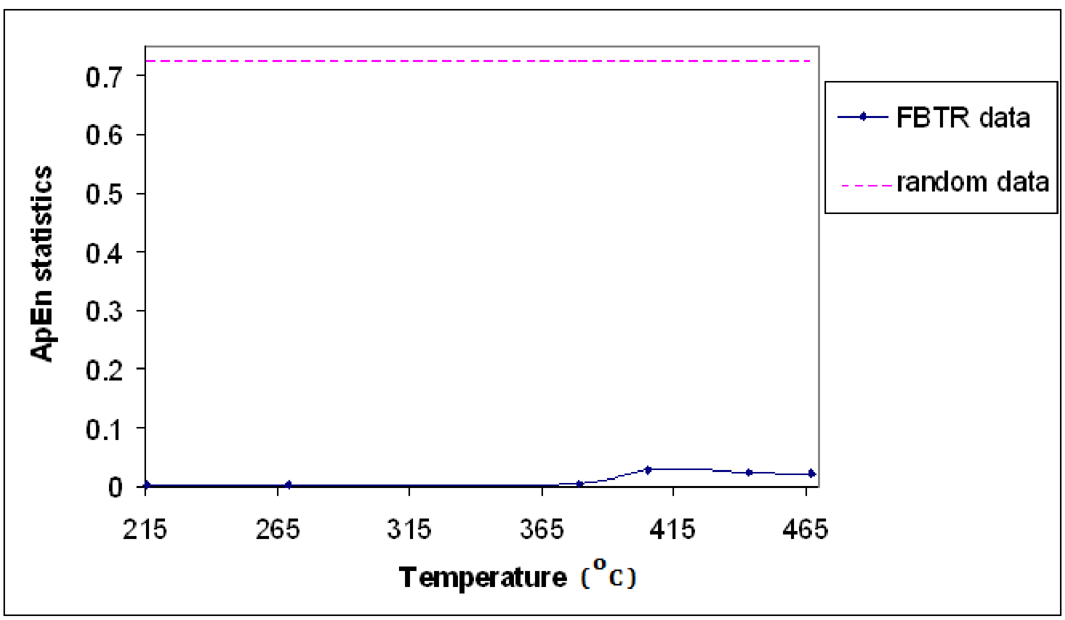


Figure 3.17: ApEn test statistic.

## 3.5 Statistical Test analysis

KPSS Test: The test result for temperature data at various power levels are shown in figure 3.18 and 3.19.

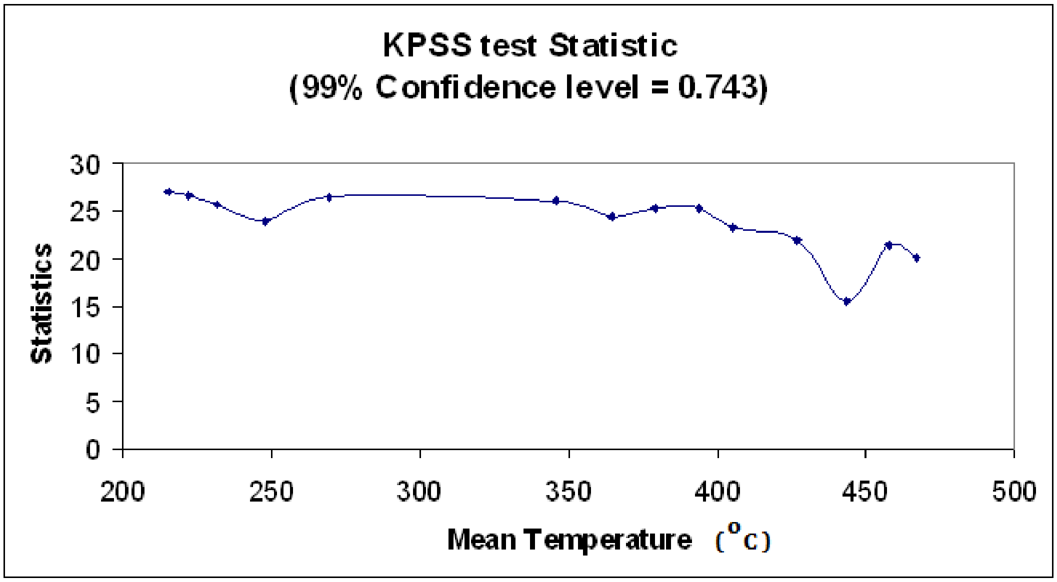


Figure 3.18: KPSS test statistic for raw data.

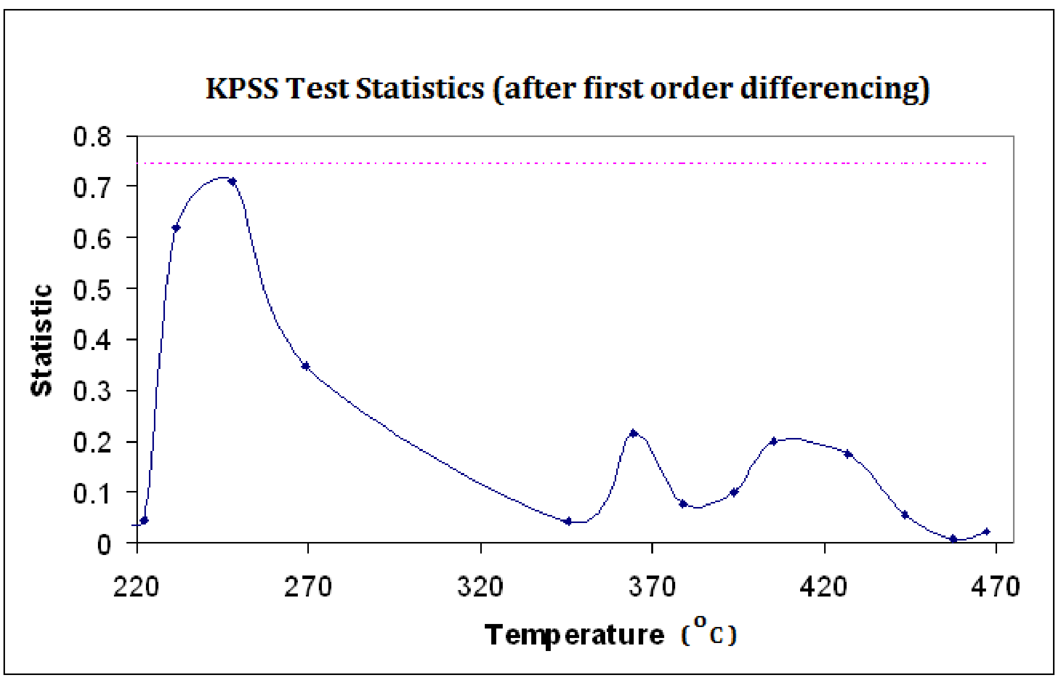


Figure 3.19: KPSS test statistic for 1st order diff. data.

KPSS test statistics in figure 3.18 shows that the data is non-stationary for all power levels. Since the aim is to correlate temperature fluctuations with reactor power, the mean

level value is removed by performing first order differencing, which in turn complies with stationarity . A KPSS test run for 1-D data is shown in figure 3.19. This data passes the $H_o$ (as explained in section 2.5), and hence becomes stationary. Similarly, the test statistics for stable power levels of 11 and 18 MWTh are [12.99, 17.88] (raw data) and [0.013, 0.019] (1st order differenced data) respectively.

Reverse Arrangement test (RAT): Figure 3.20 shows the test statistic behavior for temperature data. It is clear from the figure that data is not from a random process. However, the test result doesn't correctly differentiate between differenced and un-differenced signal time series, and thus necessitates the use of alternative test.

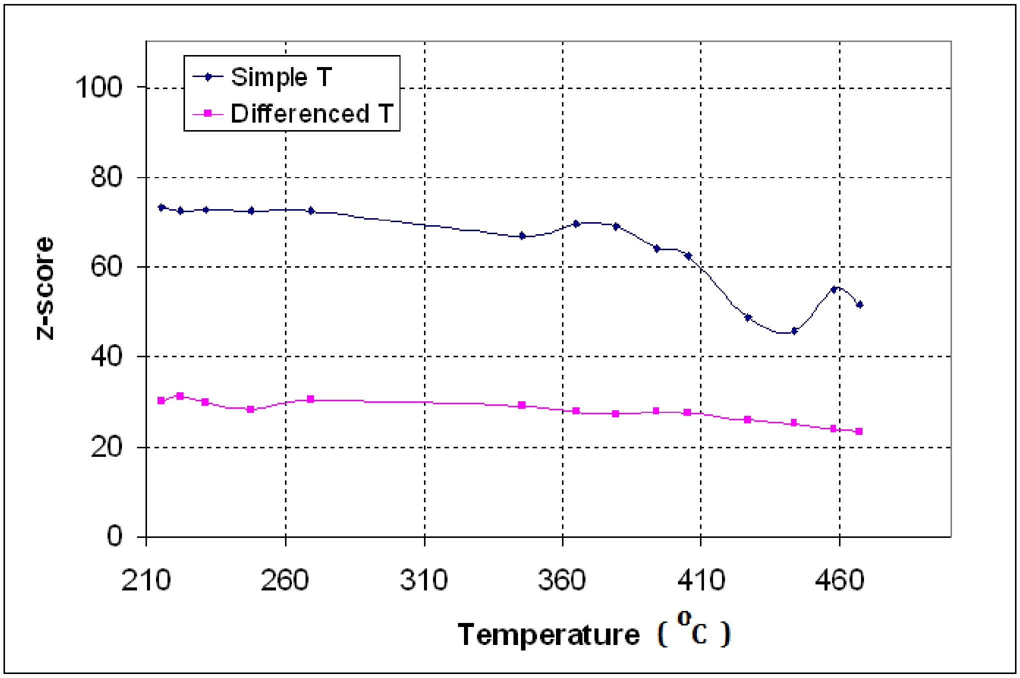


Figure 3.20: Reverse arrangement test statistic.

Runs test: As shown in figure 3.21, it is observed that the $H_o$ (data is from a random source) passes only after a certain value of mean temperature. However the p-value, which represents the evidence against $H_o$, also increases several folds. Hence temperature fluctuations tend to become more random with increase in power, but still following a unique statistical pattern [6], i.e. fluctuation behavior is related to the thermal power in reactor core.

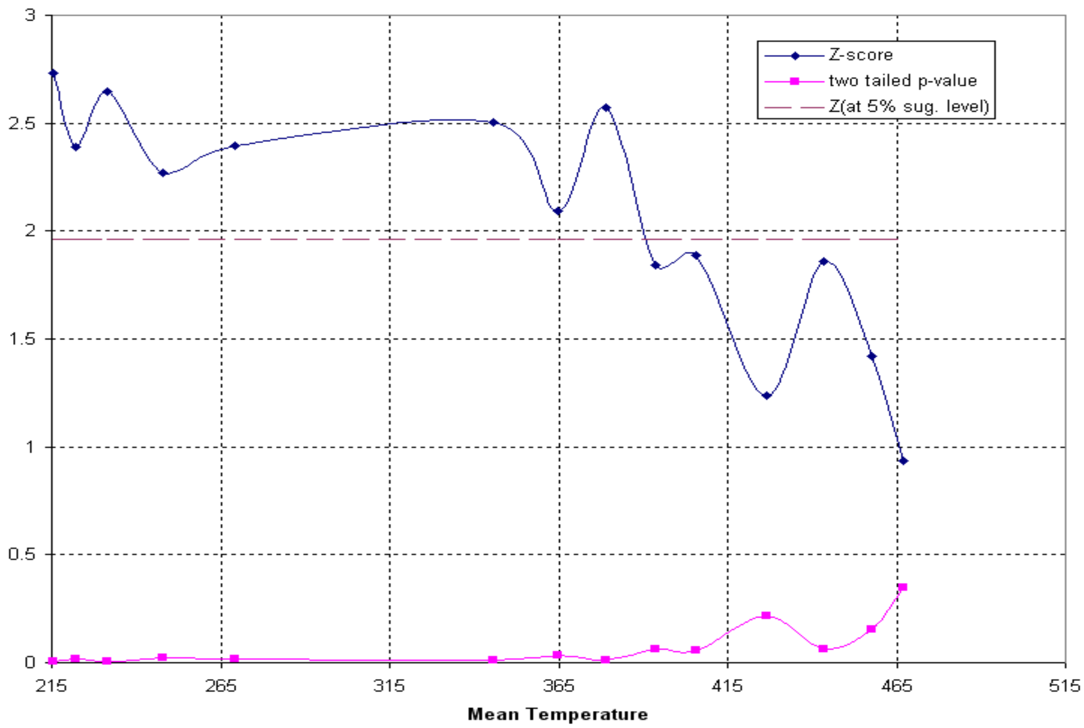


Figure 3.21: Runs test statistic for 1st order diff. data.

The statistical test results are summarized in Table 3.2. With appropriate data transformation, it is possible to extract useful information from the fluctuation data.

TABLE 3.2: Statistical test results.

| Test | Test statistic | | | Critical value (z) | Conclusion |
|---|---|---|---|---|---|
| | Increasing | Stable | | | |
| | | 11 MWt | 18MWt | | |
| KPSS | 0.007 to 0.71 | 0.0138 | 0.014 | 0.743 | $H_o$ accepted : Hence, Data becomes stationary after 1-D |
| RAT | 23.26 to 31.04 | 31.29 | 27.8 | 1.96 | $H_o$ rejected: Hence, Data is not from a random source |
| Runs* | 0.9 to 2.75 | 2.6488 | 2.17139 | 1.96 | $H_o$ rejected: Hence, Data is not from a random source |

* $H_o$ passes after a particular mean temperature level, but corresponding p-value also increases, suggesting against the passing of $H_o$

## 3.6 Discussion

Initial multi domain analysis helps in building the base for desired model. The necessary blocks to be included such as differencing, absolute/rms are the conclusive outcomes of domain analysis. Also, a comparative analysis of the properties of such blocks highlights the necessary complexity required for processing. For e.g., a larger window length beyond a level for rms or moving average may not further improve statistics [61]. The tests suggest that the data becomes stationary after processing. The random looking like signal in fact contains a lot of information about internal thermodynamics [62]. The temperature fluctuation behavior inherits a good correlation with thermal power. The model once developed has to be validated with reactor data. The use of various statistical tests also proved to be very helpful in understanding the fluctuation behavior.

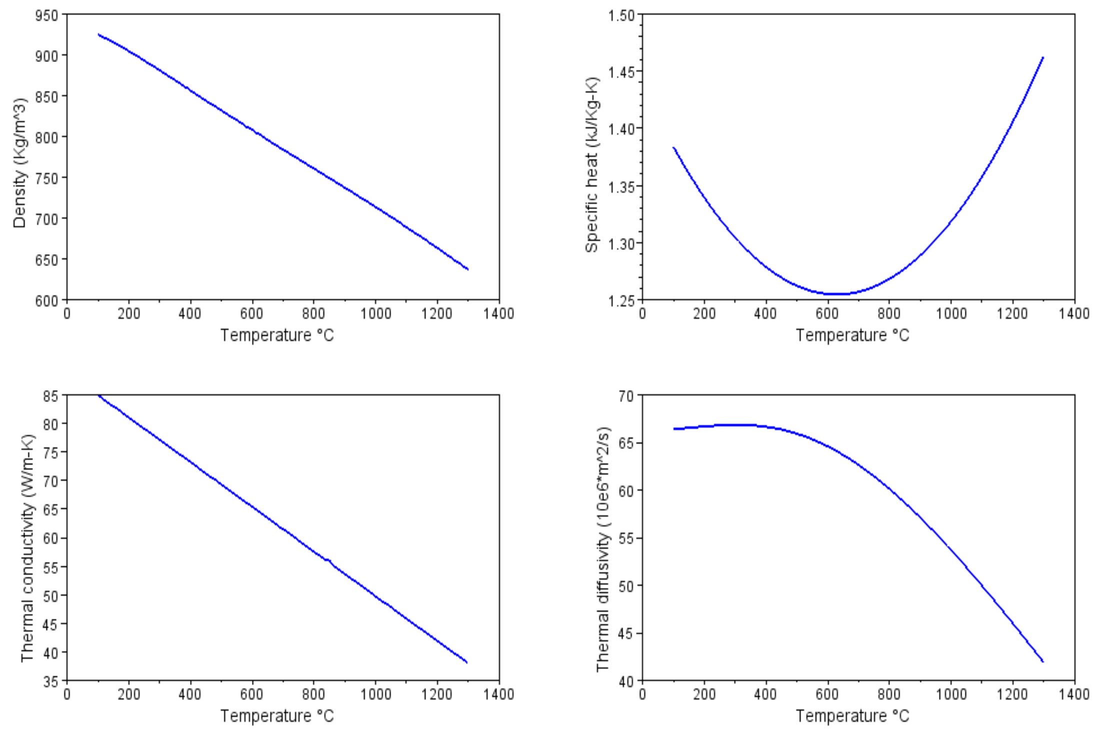


Figure 3.22: Thermophysical properties of sodium with Temperature.

*Effect of thermophysical properties of sodium:*

Figure 3.22 shows variations in various thermophysical properties of sodium (coolant) with temperature [63]. Heat transfer correlations in liquid metal fast breeder reactors are based on Peclet number ($P_e$), given as [2],

$$P_e = Pr * Re$$

where Pr and Re being Prandtl and Reynolds no. respectively. The coolant flow through subassemblies is turbulent forced convection type due to high value of Reynolds no. for liquid sodium [64]. The value of Pr is very small (P r<0.01). The $P_e$ value is high and more than 100 for LMFBRs [65]. At low $P_e$, molecular diffusion (conduction) is the prominent heat transfer mechanism whereas at higher $P_e$, mechanical mixing (convection) dominates [66]. Nusselt's no. which defines the overall heat transfer characteristics, is given as,

$$Nu = a + b(P_e)^c$$

where a is the contribution due to conduction and the remaining portion is due to forced convection. Presence of a is due to high thermal conductivity of sodium [67]. As shown in figure 3.22, value of thermal conductivity (k) decreases with increasing temperature. Hence, the heat transfer contribution due to conduction further decreases. Figure 3.23 shows that Pr value, which is already low for liquid sodium, further decreases with temperature. There is a relative 70% decrease in Pr value from 0.0075 (200$^o$C) to 0.0044 (470$^o$C). This results into slight enlargement of thermal boundary layer (figure 3.24).

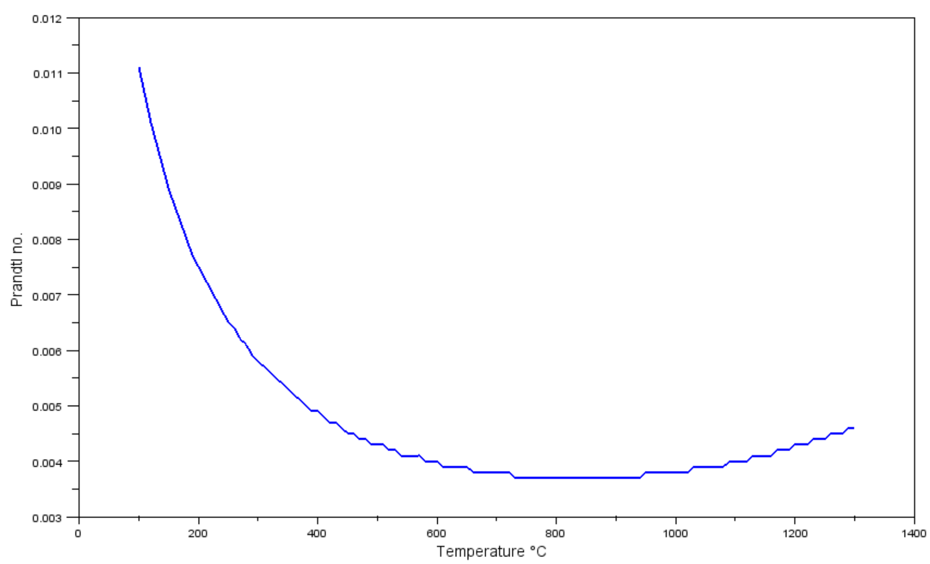


Figure 3.23: Pr vs. Temperature.

The same correlation can be understood by the relationship between $P_e$ and thermal diffusivity (α) as [68],

$$P_e = UD/\alpha$$

where U is the velocity, and D is the characteristic dimension. From figure 3.22, it can be observed that α remains fairly constant in the range 200-470°C (0.73% decrease).

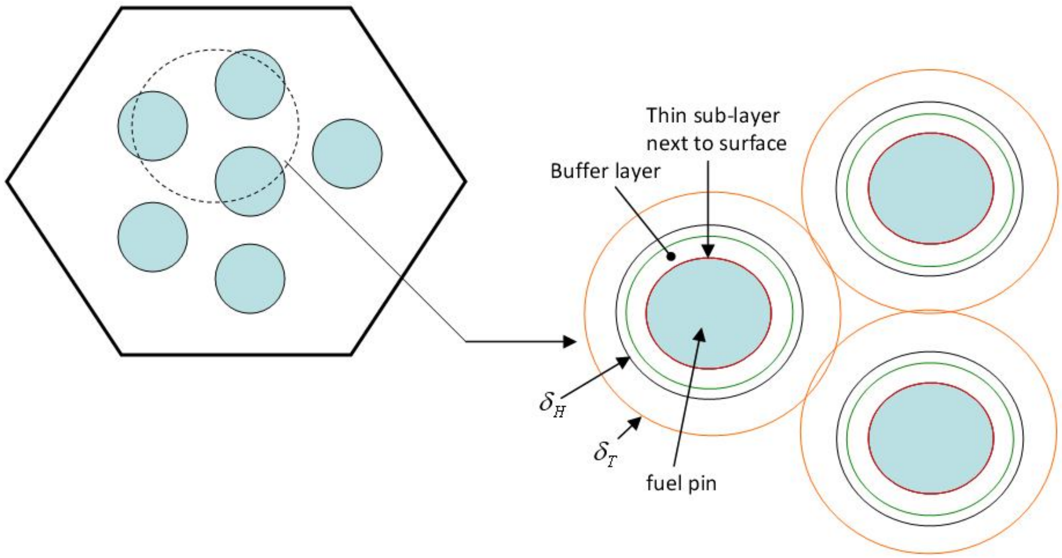


Figure 3.24: Thermal boundary layer ($\delta_T$) vs. Temperature.

However, as temperature further increases, value of α falls by 5% (480-700°C). The net effect is a relative increment towards $P_e$ value after a certain temperature. Hence with increasing temperatures, more convective heat transfer takes place. It is concluded from the above discussion that the convective heat transfer dominates the one due to conduction, and this domination increases with increase in temperature.

The radial core temperature distribution depends on neutron flux profile in core, flow through each subassembly etc [69]. Measures are adopted to maintain a flat radial temperature distribution in the core. Since for the present study, CSA temperature profile is utilized; the fluctuations so observed are mainly due to the coupled effect of turbulent flow and slight temperature differences amongst the fuel pins. The thermal power is directly proportional to the temperature difference and coolant flow rate.

Since the flow rate is almost maintained constant (figure 3.25), the increase in thermal power is attributed to increase in core temperature.

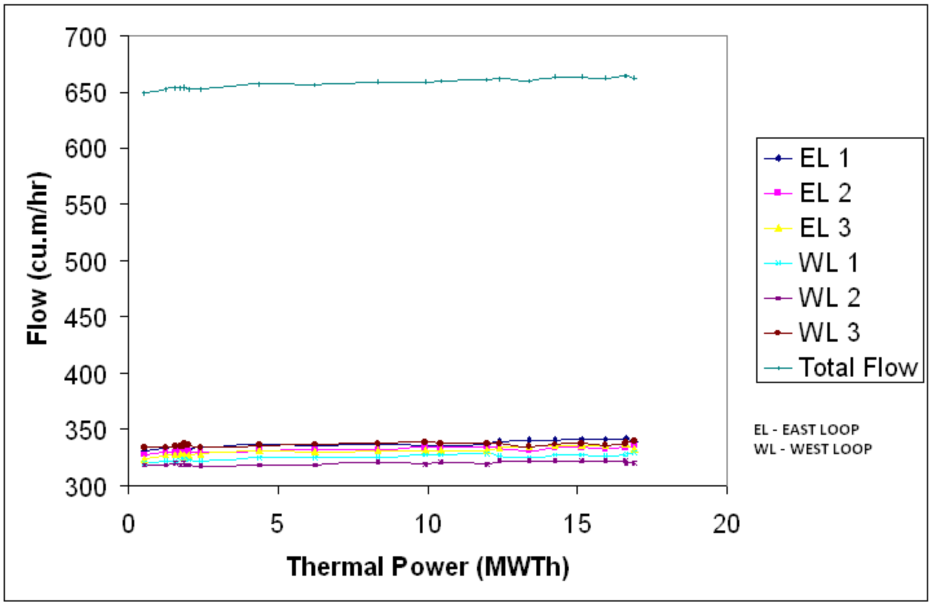


Figure 3.25: Primary coolant flow.

Any increment in CSA temperature means a slight increase in temperature difference amongst individual fuel pins within the CSA [70]. This gives rise to increase in magnitude and frequency of temperature fluctuations at the outlet of subassembly, and gets reflected in the signal as sensed by thermocouple.

## 3.7 Conclusion

Analysis of CSA outlet temperature data suggests the presence of a strong correlation between temperature fluctuation and thermal power in a fuel subassembly. It is possible to derive a proportional parameter with the help of mathematical transformation of raw temperature data. The usability of various tests in time series analysis is also highlighted for complex fluctuation signal analysis. The mathematical operations include first order difference, absolute/rms and moving average.

# 4

# MODELLING & SIMULATION FOR SIGNAL PROCESSING ARCHITECTURE

This chapter discusses the model development and simulation procedure for an appropriate signal processing scheme. The model is validated for reactor data. A comparison is presented here to differentiate between blockage induced fluctuations with that of fluctuations generated under normal operation. The effect of variations in thermocouple time-constant on the sensing of temperature fluctuations is also studied.

## 4.1 Temperature fluctuation correlation with thermal power

Fluctuations in coolant temperature occur due to many reasons for all possible reactor operations. For e.g., in case of a blockage, temperature fluctuations are generated due to formation of vortex [7]. Under normal operating condition, fluctuations are sensed due to variations in thermophysical properties of sodium with temperature and turbulent mixing. But in both the cases, increase in fluctuations resembles increase in thermal power. Hence, the modelling of temperature fluctuations is divided into two parts; one considering a blockage scenario and the second for normal operations. In first case, it is assumed that the overall fluctuation level increases after a blockage happens, since the temperature around blockage spot keep on increasing in the absence of sufficient heat removal. However in second case, the generation of fluctuations is dominated by statistical parameters associated with thermophysical quantities, and is relatively complex to model. Both models are data-driven.

## 4.2 Model design

### 4.2.1 Model under blockage condition

This analysis requires the knowledge of mean temperature value at a particular power level. Roychowdhry et.al. [71] reported a considerable increase of 36.85$^{o}$C of temperature across a 30% blockage. With increase in temperature being a function of blockage size, the temperature fluctuation generation can be modeled at different blockage size. Figure 4.1 shows the central subassembly outlet temperature at different power levels.

With the initiation of flow blockage, the fuel pin temperature begins to increase and give rise to temperature fluctuations in coolant passing by, due to difference in relative temperature. The mean over which these fluctuations lie, also increases with time. The continued presence of such blockage may shoot the temperature to a dangerous level, sacrificing the safety of reactor core.

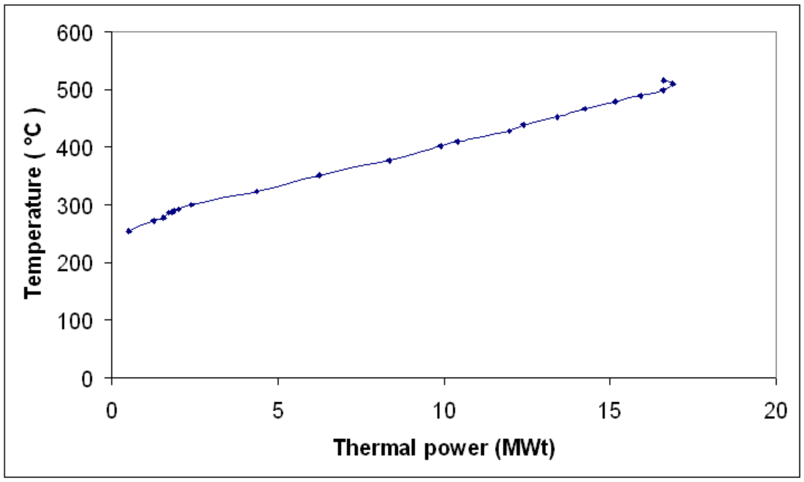


Figure 4.1: $T_{CSA}$ vs. $P_{th}$.

The temperature readings for central subassembly (CSA) are used for model design and determine model parameters as shown in figure 4.2. While maximum and minimum temperature values are used here to generate fluctuations, the standard deviation around a particular mean temperature value at discrete thermal power values was used for the validation of the code. The statistical analysis of the readings suggested a proper design and use of bandpass filter using mathematical details. Table 4.1 gives the bandpass filter specifications.

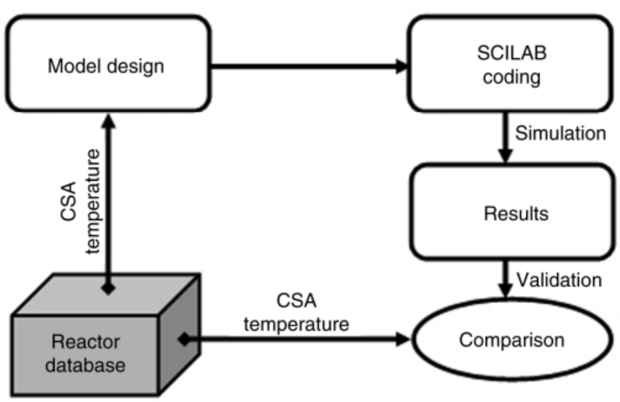


Figure 4.2: Model development methodology.

Table 4.1: Bandpass Filter Specification

| | | |
|---|---|---|
| 1 | $f_{c1}$ (lower cut-off frequency) | 0.1 Hz |
| 2 | $f_{c2}$ (upper cut-off frequency) | 50 Hz |
| 3 | $f_s$ (Sampling frequency) | 100 Hz |
| 4 | $A_s$ Stopband attenuation | 31 dB |
| 5 | $A_p$ Passband gain | 0.34 dB |
| 6 | $R_p$ Passband ripple | 1.39 |

The lower, upper and sampling frequencies, respectively chosen are 0.1, 50 and 100Hz. Hence, the normalized frequencies are

$$f_{n1} = f_{c1} / f_s = 0.001 \text{ and}$$

$$f_{n2} = f_{c2} / f_s = 0.5$$

The magnitude squared response of an elliptic filter is given as,

$$\left|H(\omega)\right|^2 = \frac{1}{1+\varepsilon^2 R_n^2(\omega)} \tag{22}$$

where $\varepsilon$ is the pass band ripple factor and $R_n(\omega)$ is the Jacobian elliptic function. A bilinear transformation method is used here for designing the bandpass filter. For that, a low pass filter is designed and then transformed to a bandpass filter. The SCILAB commands associated with such designs are,

$$[\mathrm{hz}] = \mathrm{iir}(\mathrm{n}, \mathrm{ftype}, \mathrm{fdesign}, \mathrm{frq}, \mathrm{delta});\ \mathrm{hzt} = \mathrm{trans}(\mathrm{hz}, \mathrm{tr\_type}, \mathrm{frq});$$

where n, ftype, fdesign, frq, delta are filter order, filter type, cutoff frequencies and error values, respectively. The stopband attenuation (As) and passband ripple (Rp) are predefined with 31dB and 1.39, respectively for further calculations. Then, the error values are calculated as follows:

$$d1 = \frac{k-1}{k+1}, \text{ and } d2 = (1+d1)\times 10^{-A_s/20} \quad (23)$$

$$\text{where } k = 10^{R_p/20}$$

delta = [d1 d2]

The passband gain (PBG) of the filter is given as:

$$PBG = \frac{1}{\sqrt{1+(1.39)^2}} = 0.3402dB \quad (24)$$

Using the predefined values, values of 0.08 and 0.03 are obtained for d1 and d2 respectively.

A model representing the temperature fluctuation generation due to blockage is shown in figure 4.3. The model works on the basis of defined maximum and minimum value of temperature. The temperature values so obtained are sensed and correspondingly shaped by thermocouple transfer function. Most of these fluctuations lie in extreme low frequency range. Hence, a band pass filter is incorporated into the model. As a pure indicator of fluctuation level, rms (root mean square) is calculated.

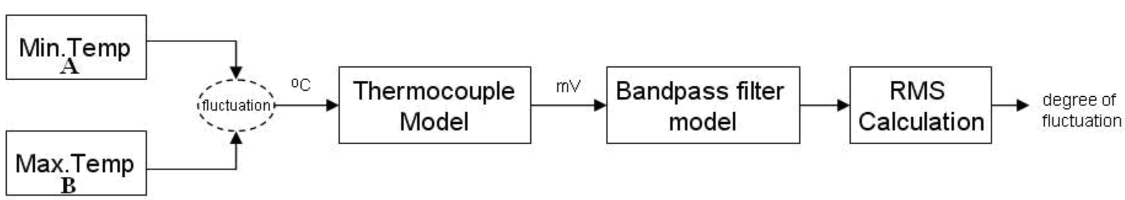


Figure 4.3: Simulation model.

The fluctuations are generated assuming a uniform distribution $u(x, y)$ at particular power levels. The degree of temperature variation is decided by setting x and y values, where x and y denotes the minimum and maximum temperature for a particular test. The lower value is set according to practical data obtained from various sources for a fixed power level. The upper limit is adjusted during simulation in correspondence to the desired fluctuation level. The variation value is incremented in various ways. First, a temperature fluctuation variation is achieved in steps of 10$^o$C, 20$^o$C, 30$^o$C, 40$^o$C and 50$^o$C over time, for slower increase. Then the temperature variation is achieved in steps of 50$^o$C and 100$^o$C. The standard deviation $\sigma$ in both the cases is quite different. Hence, if a phenomenal sudden increase in $\sigma$ is to that of abnormal occurrence is observed in coolant flow, blockage can be predicted.

For determination of a maximum safe limit for the degree of fluctuations, a worst case scenario can also be considered, in which the temperature starts fluctuating over 120-130$^o$C in few seconds. In the analysis of neutron flux noise, it was found that the noise in frequencies lower than $1.5 \times 10^{-2}$ Hz are mainly due to the inlet temperature noises, which should be eliminated. Hence, a proper bandpass filter is required. For a k-type thermocouple, whose response time is 300ms, it is fairly good enough to consider a sampling rate of 100 samples per second. Any two successive temperature fluctuation values are 0.01s apart. It is to be noted as shown in Fig. 4.3, the modeled units prior to thermocouple is actually the analog component of signal detection scheme. The remaining signal processing can be performed digitally either in a real time computer or FPGA [72] board. Hence, this procedure gives the possibility of program development of FPGA with simulated fluctuations in temperature.

*Results*: Figure 4.4 shows the case in which there is a slow increase in fluctuation (10$^o$C, 20$^o$C, 30$^o$C, 40$^o$C and 50$^o$C). The sample number on x-axis denotes the data element index of the signal matrix.

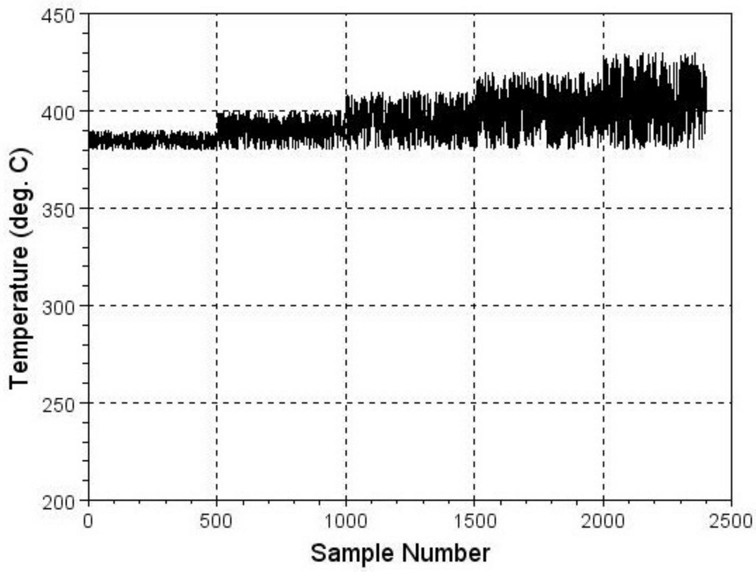


Figure 4.4: Gen. Temperature profile: A=380$^{o}$C, variation=10$^{o}$C, 20$^{o}$C, 30$^{o}$C, 40$^{o}$C, 50$^{o}$C.

The minimum temperature A is kept at 380$^{o}$C. Hence, value of B attains 390$^{o}$C, 400$^{o}$C, 410$^{o}$C, 420$^{o}$C, 430$^{o}$C and 440$^{o}$C in 2400 iterations. The thermocouple response time is taken as 300ms and the sampling rate is 10 samples per second. Hence for 2400 samples, equivalent time taken is 4 mins. Figure 4.5 shows the thermocouple response for temperature range up to 700$^{o}$C.

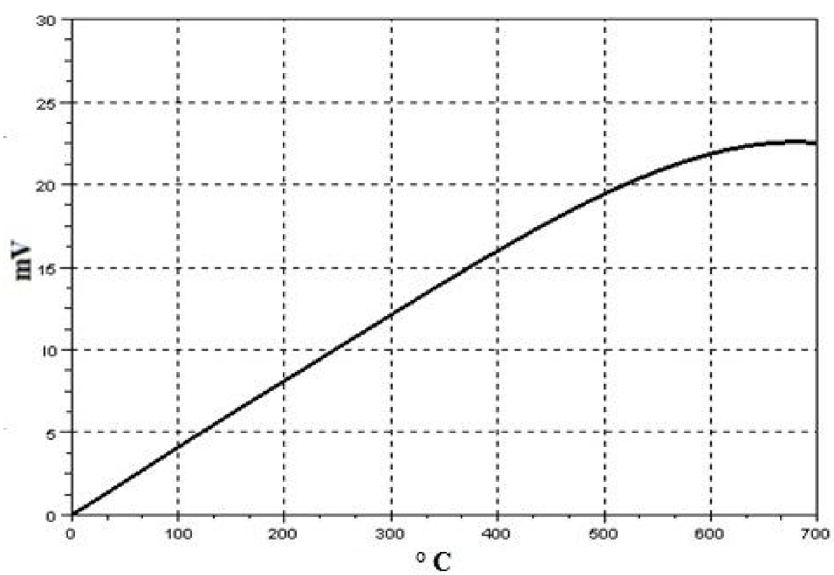


Figure 4.5: Simulated thermocouple response.

As explained earlier, analysis of neutron flux noise [73] reveals that inlet temperature noises fall in the region lower than $1.5 \times 10^{-2}$ Hz, which are not suitable for the purpose of blockage detection or which might otherwise affect relevant signal considerably. Hence, it is necessary to filter the signal in a narrow specific frequency range. The generated signal is passed through a bandpass filter with specifications given in Table 4.1. RMS value is then calculated for the generated data, and the data profile so obtained is shown in Fig. 4.6 for thermocouple response time $(\tau)$ of 0.3s. In running RMS calculations, two successive data elements say $x_1$ and $x_2$ are taken and a coefficient is calculated as;

$$\sqrt{\frac{1}{2}\left(x_1^2 + x_2^2\right)}$$

For calculation of next rms value, $x_1$ takes the previous value of $x_2$ and $x_2$ gets a new value. Figure 4.7 shows the running RMS values for the case in which the temperature fluctuations rapidly shoots up to a higher limit in 50$^{o}$C and 100$^{o}$C.

It can be observed from Figs. 4.6 and 4.7 that the RMS value increases from 0.16$^{o}$C to 0.5$^{o}$C due to sudden increase in fluctuations.

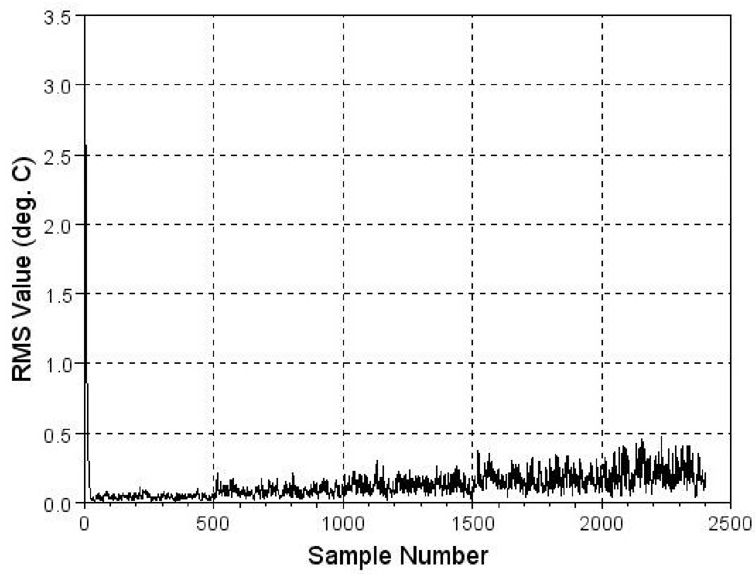


Figure 4.6: Running RMS, variation = 10°C, 20°C, 30°C, 40°C and 50°C, $\tau$ =300ms.

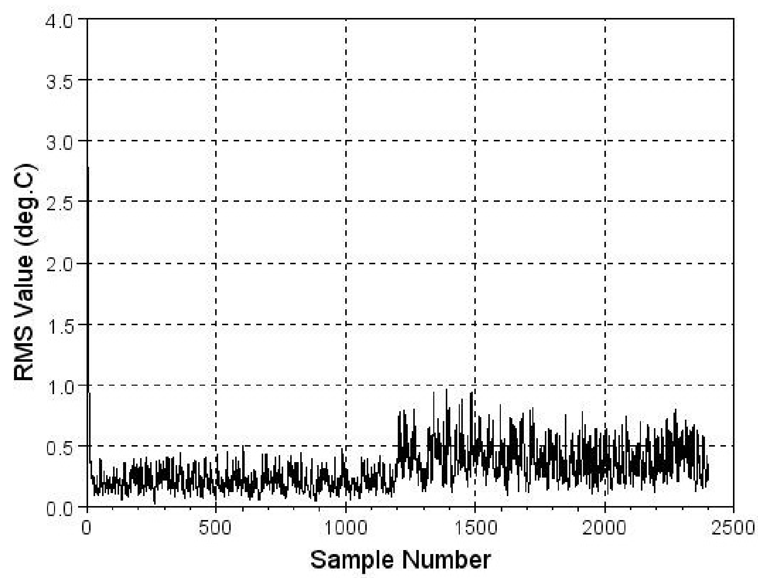


Figure 4.7: Running RMS, variation = 50°C, and 100°C, $\tau$ =300ms.

If simulation is performed for a sequence of 110°C, 115°C and 120°C, its RMS values reflects a shift in mean level as shown in Fig. 4.8. It would also be useful to see the effect of small fluctuations which arise due to turbulent mixing of fluid (2°C, 3°C and 4°C).

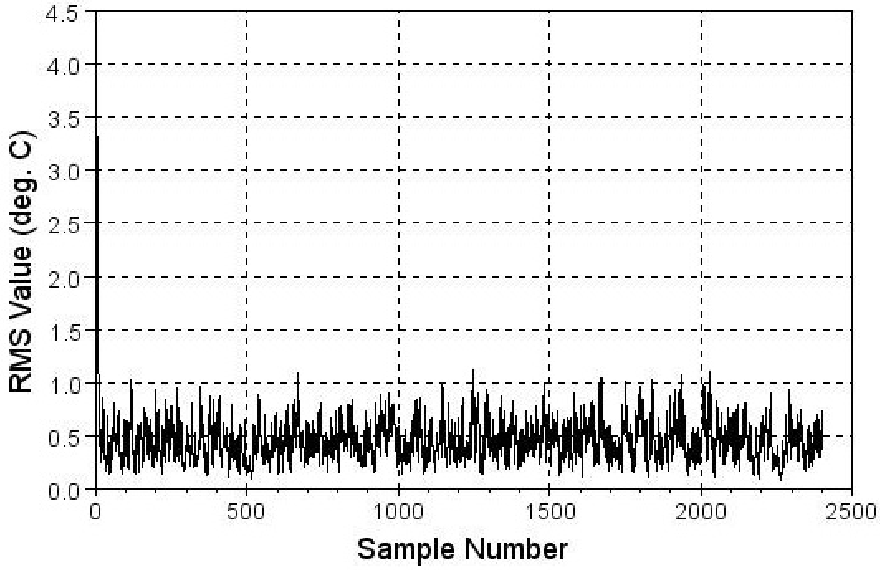


Figure 4.8: Running RMS, variation = 110$^o$C, 115$^o$C and 120$^o$C, $\tau$ =300ms.

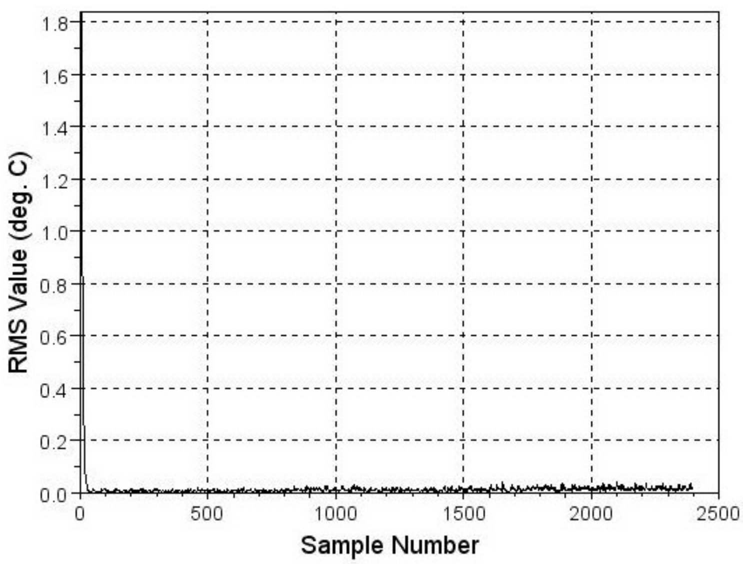


Figure 4.9: RMS for very less fluctuations: A=380$^o$C, variation=2$^o$C, 3$^o$C and 4$^o$C, $\tau$ =300ms.

It is clear from figure 4.9 that RMS value or a function of RMS value itself could be useful for the purpose of detecting malfunctions.

One more advantage of such an analysis could be the fact that these fluctuations not only represent the effect of rising temperature due to improper cooling in case of a blockage, but also can be used to point out the size of blockage. As the size of blockage increases, the chances of mixing or fading up of the fluctuations throughout downstream of subassembly decreases [74], thereby generating greater fluctuations at the outlet. Although in such cases, the location of blockage plays a significant role. Also, the flow rate of coolant would have a direct impact on fluctuations. The higher the flow rate, lesser is the fluctuation value due to better turbulent mixing. However, it would be possible to detect malfunction for a steady power operation for which the values of flow, heat flux are constant throughout the operation.

It would be useful to understand the impact of using a thermocouple which is placed inside a thermowell in order to have a longer sensor life time. This results in a longer response time (5-6s). Under such condition, the RMS values for two cases viz. 10°C, 20°C, 30°C, 40°C, 50°C and 50°C, 100°C are shown in Figs. 4.10 and 4.11.

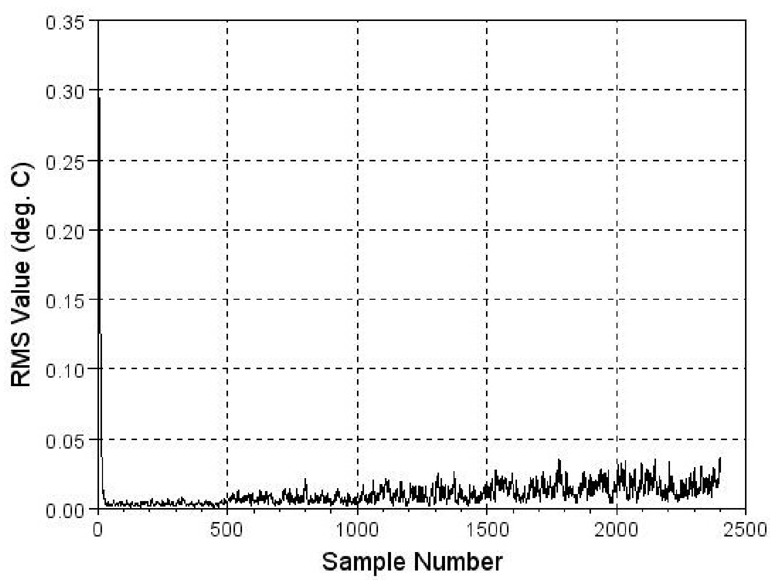


Figure 4.10: Running RMS, variation = 10°C, 20°C, 30°C, 40°C and 50°C, $\tau$ =6s.

It is clear that the mean RMS level drops to a very low value and also increases the time required to digitally calculate RMS values for the same period. Hence, it is always better to use a faster thermocouple for the intended purpose. For getting an insight into the spectral content of such fluctuations, Fourier analysis is performed for the thermocouple output as shown in Fig.4.12. It is clear that presence of fluctuations appears in the frequency range of few Hz, which suggests the possible use of extremely low frequency (ELF) bandpass filter.

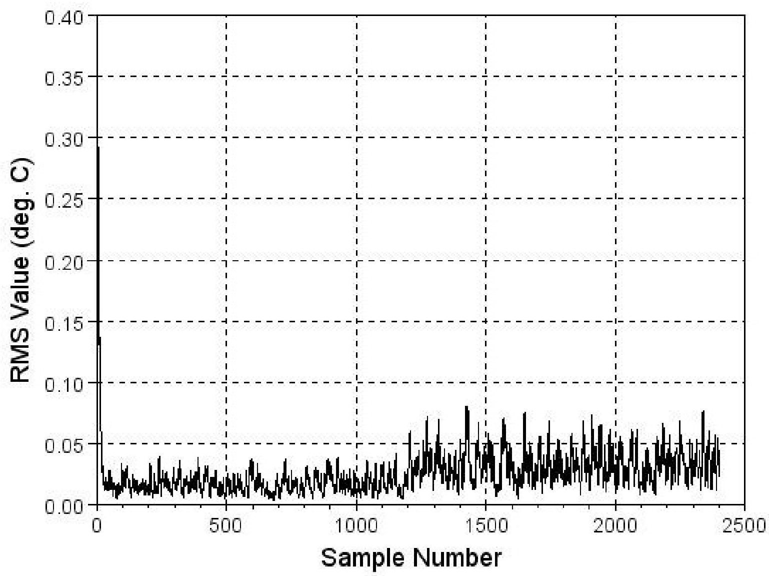


Figure 4.11: Running RMS, variation = 50°C and 100°C, $\tau$ = 6s.

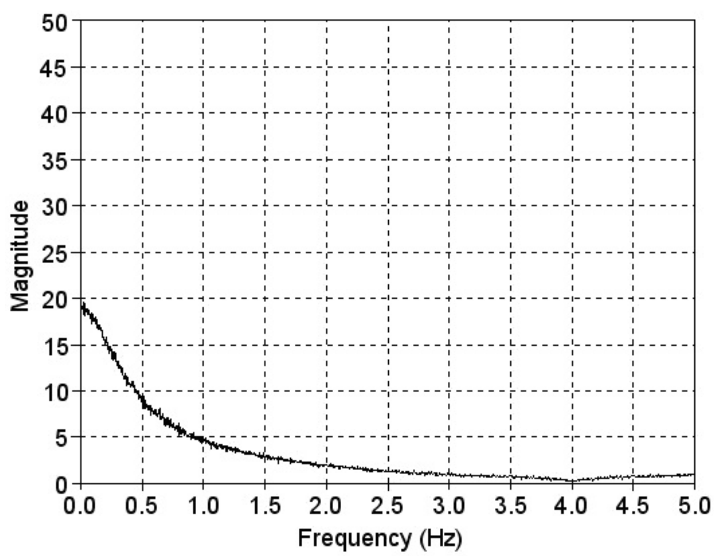


Figure 4.12: Fourier analysis with variation of 2°C, 3°C and 4°C.

Figure 4.13a:Phase response with variation of 2°C, 3°C and 4°C.

*Fluctuation due to fluid mixing*: A subassembly is surrounded by many other similar subassemblies through which coolant flows as depicted in Fig. 4.13. Let us consider a condition where partial blockage occurs in one such subassembly, along with normal coolant flow in other neighboring subassemblies. Then the subassembly outlet where the sensors are located, witnesses the mixing of fluid from two channels. With a liberal approach to analyze the effect of mixing on fluctuation properties, a Fourier analysis of running RMS values obtained from mixed fluid temperature signal is performed, as shown in Fig. 4.14.

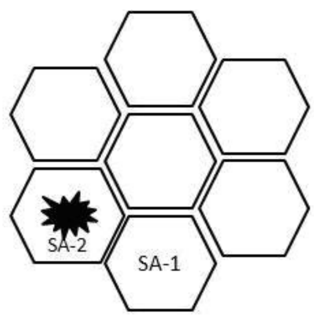


Figure 4.13: A section of subassembly arrangement.

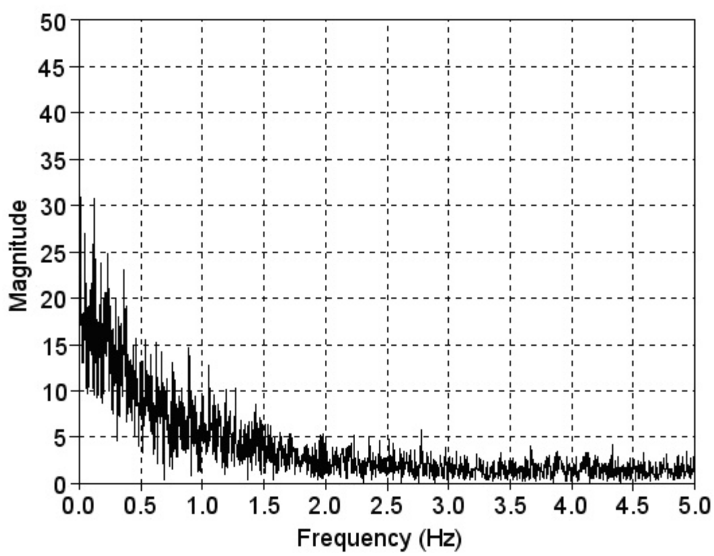


Figure 4.14: Fourier analysis in case of fluid mixing: $\tau$ =300ms, SA1 - variation 2 ◦C, 3◦C, and 4◦C, SA2 - variation 50–100◦C

*Model Validation*: For validation of the model, reactor data in the form of CSA temperature was collected during FBTR power range from 1 to 15MWt. CSA location has highest temperature due to highest flux levels in that region. However, standard deviation tends to fluctuate; a best possible set of standard deviation of temperature values for each discrete power level of the reactor is considered. This data is used to simulate the fluctuations in SCILAB model. Figure 4.15 shows the comparison of standard deviation of the experimental data and synthetic data at each power level.

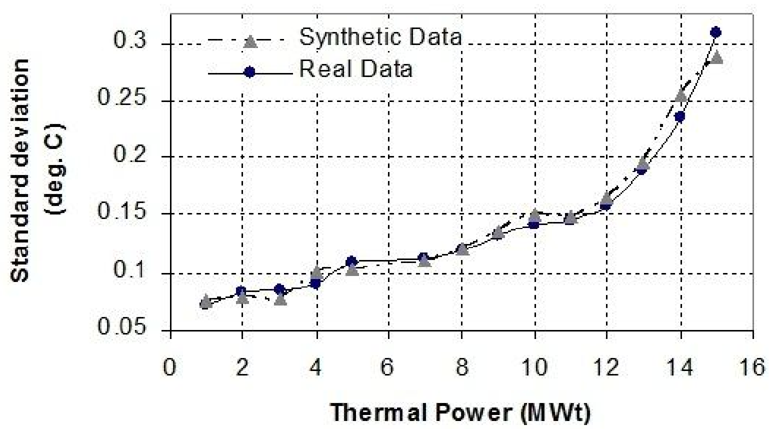

Figure 4.15: Simulated vs real time data.

### 4.2.2 Model under normal reactor operation

With the help of results obtained in chapter 3, a mathematical model (figure 4.16) is formulated which expresses the correlation between thermal power and temperature fluctuations.

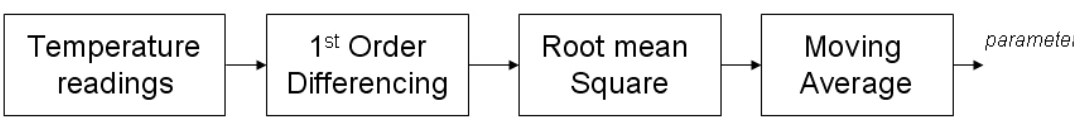

Figure 4.16: Proposed Model.

The parameter (CP) calculated on the basis of such correlation is found to be proportional to the reactor thermal power ($P_{th}$).

$$CP = f(P_{th}) \tag{26}$$

Let the time-series under analysis be X, such that

$$X = x_1,\ x_2,\ x_3,\ x_4 \,\ldots\ldots\ldots\, x_N \tag{27}$$

The AR(1) term is equivalent to the first order difference of the time series,

$$D = x_n - x_{n-1}\text{; where } n \to (2 \text{ to } N)$$

Pure fluctuation levels can be extracted as, A = |D| (absolute of difference) or rms(D)

The MA($w$) (moving average)term is calculated as,

$$MA(k,w) = \frac{1}{w}\sum_{i=k}^{k+w-1} A(i)\text{, where } k \to \left(1 \text{ to } (N-1)/w\right) \tag{28}$$

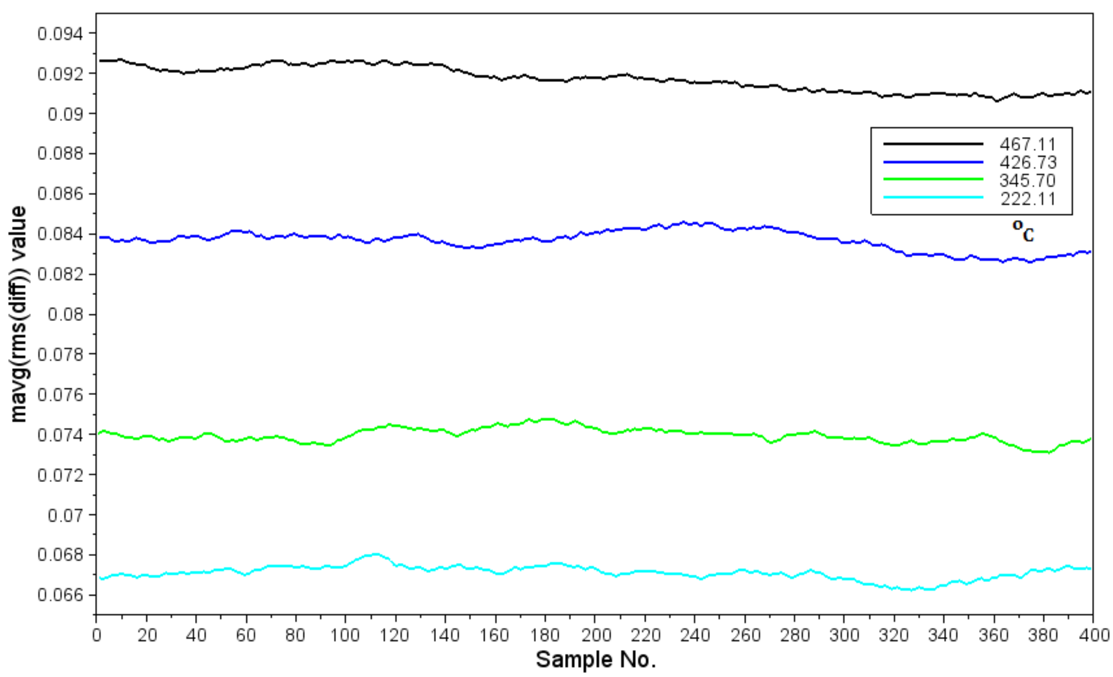


Figure 4.17: Calculated parameter at different power levels.

The window length $w$ is large owing to the response time of thermocouple. But with appropriate digital signal processing, this effect can be minimized. For eg., if a window length of 1000 samples is required, then initially all the data elements (1000) in the memory can be initialized with the first sampled signal. Subsequently, parameter calculation can be achieved by giving a left shift to the data set and adding the newly sampled data to the set.

The results for temperature data at different power level are shown in figure 4.17 and 4.18. The reasons for presence of increased fluctuations at higher power levels have been discussed in detail in section 3.6.

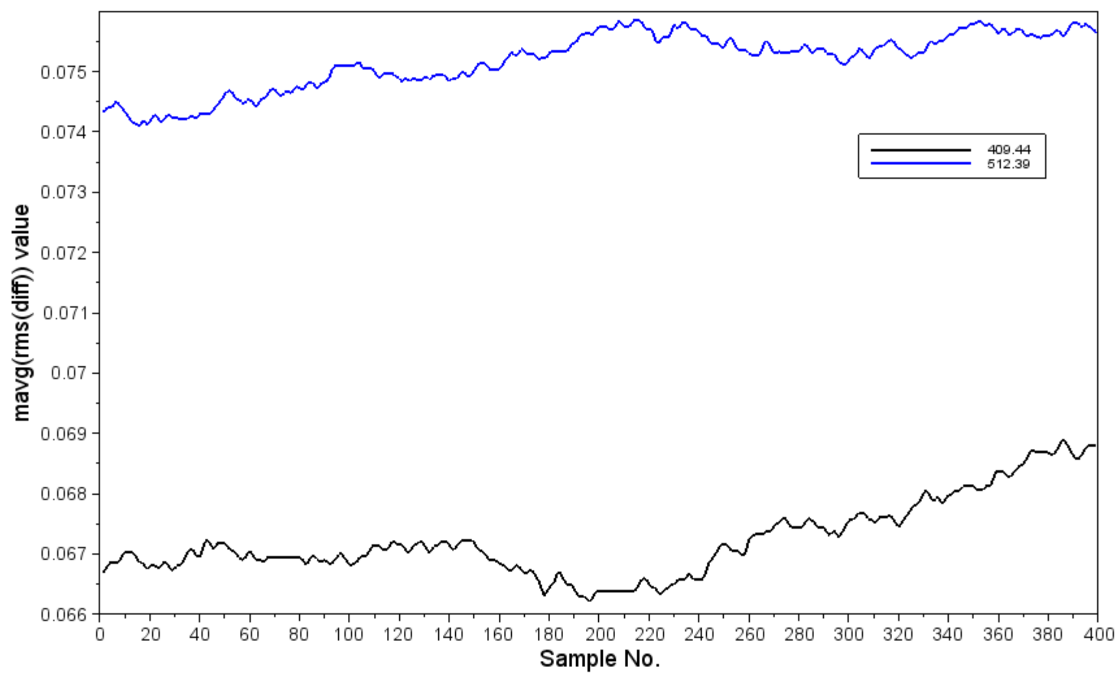


Figure 4.18: Calculated parameter at different power levels.

It is clear from these figures that the parameter calculated on the basis of coolant temperature fluctuation reflects a strong correlation with thermal power in the reactor.

## 4.3 Effect of variations in thermocouple time-constant

Time-constant of thermocouples which are used for measuring coolant temperature in fast reactor, varies owing to various factors. Hence, it becomes necessary to investigate the effect of change in time-constant on sensed fluctuations. A SCILAB model consisting of source temperature profile, second order thermocouple and histogram calculation is designed here. Simulation is performed for various levels of fluctuations, fix and variable thermocouple time-constants. Kurtosis for each condition is calculated with the help of histogram. Thermocouple time-constant value plays an important role in detecting these fluctuations, as smaller time-constants are more efficient in recording them [75]. In order to study the factors affecting the fluctuations, an analysis is attempted while considering thermocouple parameters, source temperature and fluctuating time-constants. The details about sensor and its typical arrangement in a fast reactor subassembly are discussed here.

*Thermocouple*

Thermocouple is widely used in numerous industrial applications including nuclear reactors due to there range, ruggedness and accuracy. A first order model is generally used to describe thermocouple. However, thermocouple time constant is considered multiordered [76].

A second order model of thermocouple can be given as

$$H(s) = \frac{1}{\tau s^2 + s + 1} \tag{29}$$

where τ is the thermocouple time-constant (time taken to reach 63.2% of the final value). Thermocouple response time vary with various configurations such as directly exposed (few ms), grounded sheathed (100 ms), ungrounded sheathed (few 100 ms), inside thermowell (5-7 seconds). Time-constant depends on the mass of thermocouple (m), specific heat of thermocouple wire material (c), convective heat transfer coefficient (h) of local medium and the surface area (A) [77] and given as

$$\tau = \frac{mc}{hA} \tag{30}$$

The bandwidth of a thermocouple is [78] given as

$$\omega_B = kd^{m-2}v^m \tag{31}$$

where K is some invariant constant, m is constant (0.3⩽m⩽0.7), d is wire diameter and v is coolant velocity. In terms of wire diameter, τ is represented as [79]

$$\tau = \frac{\rho cd}{4h} = \frac{\rho cd^2}{4N_u\lambda_g} \tag{32}$$

where ρ is wire material density, $N_u$ is Nusselts number, $\lambda_g$ is thermal conductivity of fluid around thermocouple. $N_u$ is a function of Reynolds number, Grashoff number and Prandtl number.

$$N_u = f(\mathrm{Re}, Gr, \mathrm{Pr})$$

It is clear from these equations that τ is dependent on many parameters involving the construction and geometry of the sensor as well as the operating conditions. The effective bandwidth offered by a thermocouple depends on coolant flow, which in turn affects τ.

The parameters which are used for modelling and simulation are mean temperature value (μ) and corresponding standard deviation σ, where σ represents the degree of fluctuation. Hence a higher power level would have a high values of μ and σ. It is to be noted that though σ increases with power, it is non-linearly localized in time, since the source of such fluctuations is due to mixing of highly turbulent coolant streams passing through a subassembly. The value of (μ, σ) is (409.44, 0.17)$^{o}$C for 11 MWTh and (512.39, 0.45)°C for 18 MWTh. Table 4.2 represents unique (μ, σ) for increasing reactor power. The differenced series is added to the overall mean of actual series. If *a* is the original time series, *b* being the differenced series, stationary time series *c* is calculated as,

$$c = \mu + \sigma$$

Table 4.2

| | μ | Recalculated σ |
|---|---|---|
| 1 | 221.86 | 0.091 |
| 3 | 378.66 | 0.102 |
| 4 | 409.44 | 0.17 |
| 5 | 512.39 | 0.45 |

By using the collected reactor data, a simulation model is proposed as shown in fig. 4.19. K-type thermocouple is modeled for various values of τ ranging from 0.05 s to 0.5 s using polynomial coefficients from NIST database [80]. Based on the reactor data, source temperature profile with fixed mean and standard deviation is obtained using grand function of SCILAB [81]. Mean value is fixed at 300°C for closer approach towards analysis of the effect of variable fluctuations in source (coolant) (σ) itself. The following conditions were analyzed for fixed μ to observe their relative effect:

-Various constant values of σ and τ

-Various fluctuating levels of σ and τ

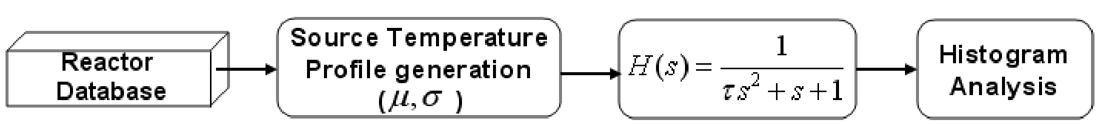


Figure 4.19: Simulation methodology.

Response to fluctuating (variable) values of $\tau$ is calculated by multiplexing even and odd terms of two different $\tau$ response values. Histogram plot gives frequency versus variable information of the data and is performed for the calculation of mean and standard deviation from the simulated sensor output. From these two parameters, kurtosis is calculated which gives an estimate of probability distribution (frequency distribution) of the data. So for all the test conditions, data profiles are simulated and kurtosis is calculated by using histogram. The mean ($\mu_h$), standard deviation ($\sigma_h$) and kurtosis ($\beta_2$) is calculated as follows.

$$\mu_h = \frac{1}{n}\sum_{i=1}^{n} f_i x_i \qquad (33)$$

$$\sigma_h = \sqrt{\frac{1}{n}\sum_{i=1}^{n} f_i (x_i - \mu)^2} \qquad (34)$$

$$\beta_2 = \frac{\sum_{i=1}^{N} (X_i - \mu)^4}{(N-1)\sigma^4} \qquad (35)$$

Maximum possible value of kurtosis is given as [82],

$$\beta_{2,\max} = \frac{(N-1)^3 - 1}{N(N-1)} \qquad (36)$$

Many works have been reported on the use of kurtosis in signal processing such as [83], [84]. The main characteristic of kurtosis is that it accurately depicts the peak and distribution of the data. Any change in the distribution of observation data would reflect in a different $\beta_2$ value. The idea is to observe the relative effect on $\beta_2$ for ±x% fluctuations in $\sigma$, keeping $\tau$ constant and vice versa, i.e.; to observe the effect on $\beta_2$ for ±x% fluctuations in $\tau$, keeping $\sigma$ constant.

Simulation results are obtained to study the effect of various combinations of parameters on the fluctuations. Table 4.3 indicates the variation of $\beta_2$ with $\sigma$, which shows a relative variation of 3.8 for $\beta_2$. Similarly, table 4.4 gives variation of $\beta_2$ with $\tau$. In this case, the relative variation is 0.043. It is clear that variations in source (coolant) temperature have higher impact on $\beta_2$.

Table 4.3: $\beta_2$ vs $\sigma$, $\mu = 300^{o}C$, $\tau = 0.1s$

| $\sigma$ | $\beta_2$ |
|---|---|
| 0.05 | 0.087 |
| 0.1 | 0.350 |
| 0.15 | 1.059 |
| 0.2 | 1.819 |
| 0.25 | 2.270 |
| 0.3 | 3.893 |

Table 4.4: $\beta_2$ vs $\tau$ , $\mu = 300^{o}C$, $\sigma = 0.1^{o}C$

| $\tau$ | $\beta_2$ |
|---|---|
| 0.05 | 0.416 |
| 0.1 | 0.425 |
| 0.15 | 0.434 |
| 0.2 | 0.443 |
| 0.25 | 0.451 |
| 0.3 | 0.459 |

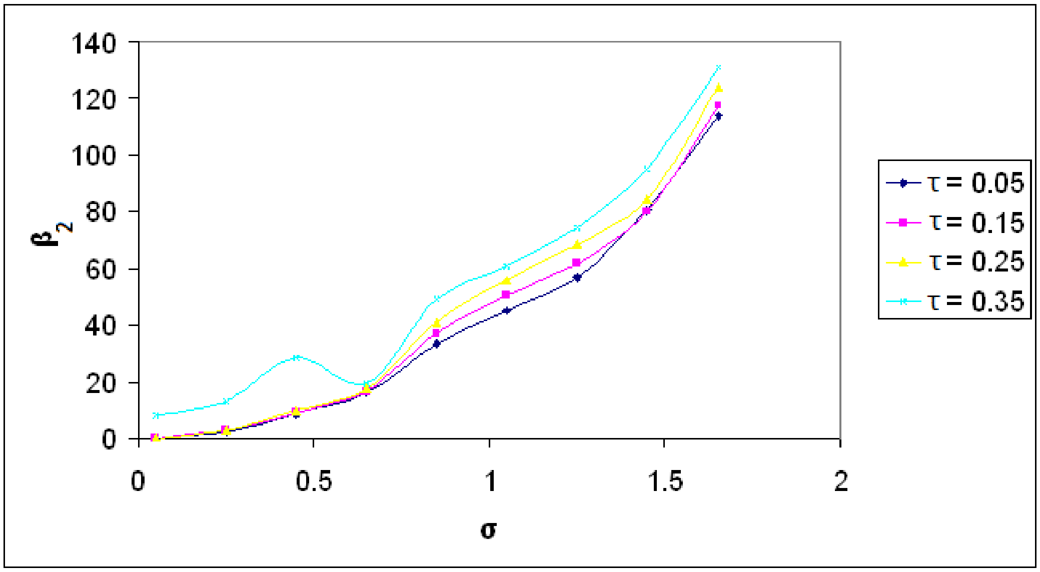


Figure 4.20: $\beta_2$ vs $\sigma$ .

Fig. 4.20 shows the kurtosis variation for different values for τ and σ. For analyzing variable σ and τ (i.e. both source profile as well as thermocouple time constant tend to fluctuate due to reactor thermodynamic conditions), various levels of source and time-constant fluctuations are generated by specifying the minimum and maximum threshold values. Results for various combinations of source and time-constant behavior are shown in fig. 4.21 and 4.22.

The mean value of σ and τ are fixed at $0.1^{o}$C and 0.1 s respectively. Fluctuation levels of 5-35% around these mean values were simulated in different cases.

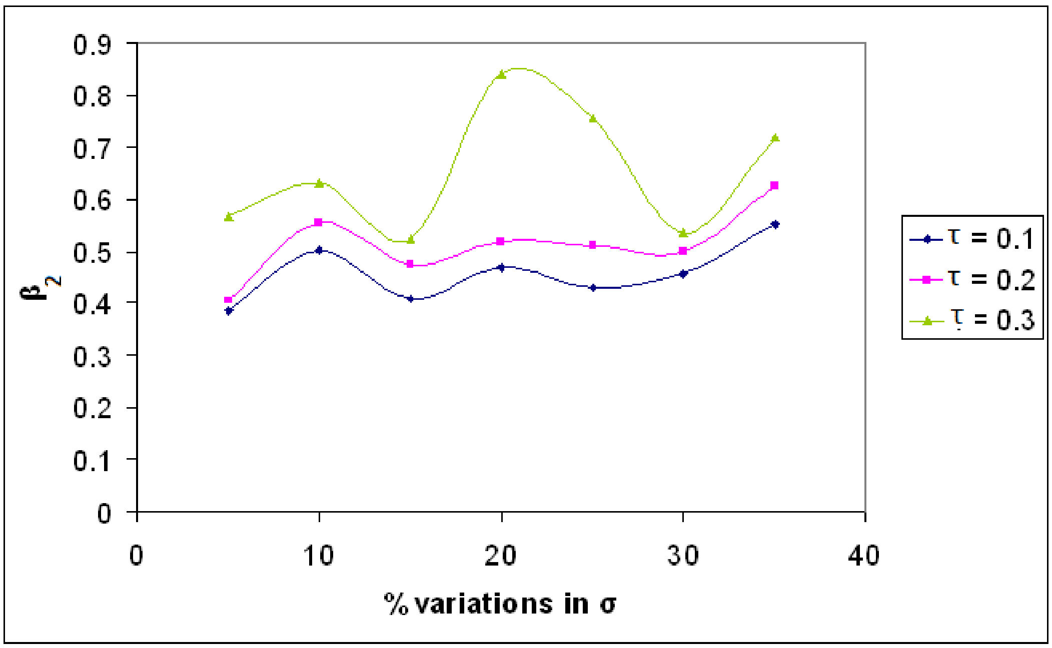


Figure 4.21: $\beta_2$ vs variations in σ .

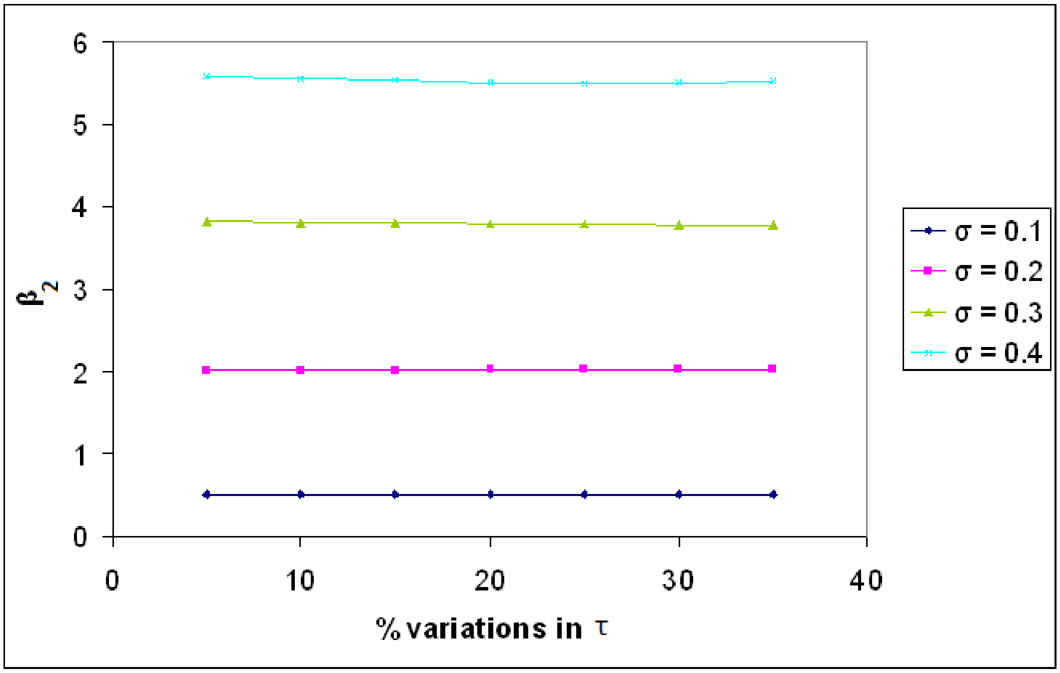


Figure 4.22: $\beta_2$ vs variations in $\tau$.

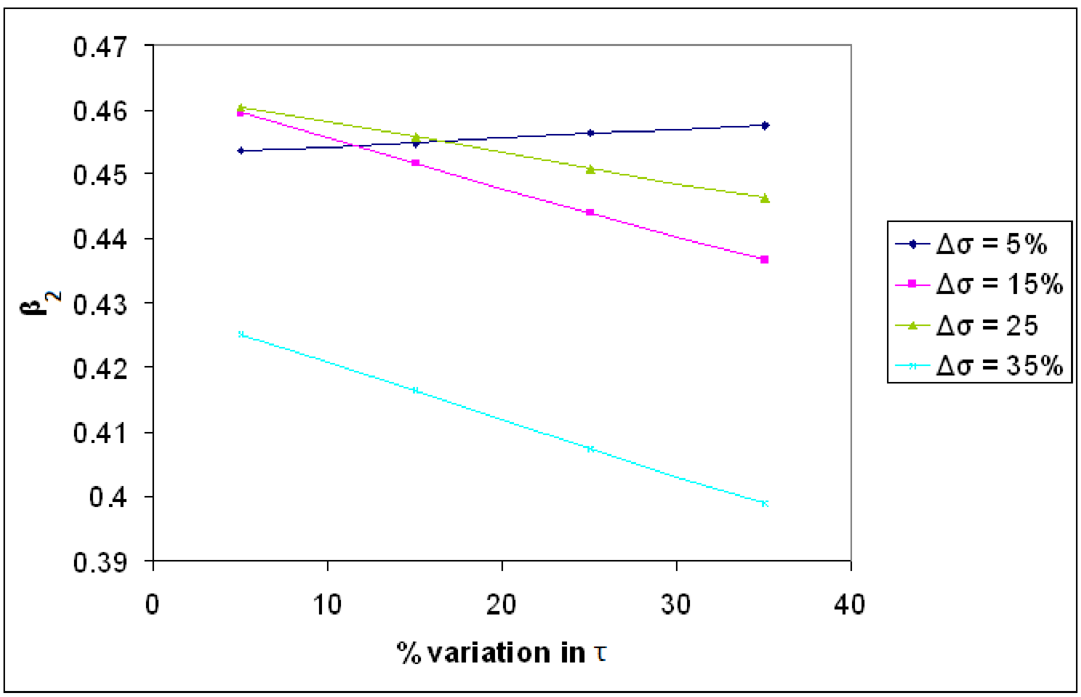


Figure 4.23: $\beta_2$ vs variations in $\tau$.

To simulate a more realistic condition, where both source and time-constant tend to vary, both $\sigma$ and $\tau$ are allowed to swing between fixed levels in many possible combinations. For eg., 5% fluctuation in $\sigma$ with ±(5,15,25,35)% fluctuations in $\tau$ and vice versa. The result is shown in fig.

4.23. The cases so far considered comprises of values which vary around mean values of $\sigma = 0.1^{o}C$ and $\tau = 0.1$ s. Result for the values of σ, τ constant and analyzed with respect to fluctuating levels mutually are shown in fig.4.24. It is clear that the degree of change in kurtosis is far greater for fluctuating σ, than that of fluctuating τ i.e. fluctuations observed in thermocouple readings are largely due to the fluctuations in source (coolant) itself and hence a good indicator of coolant temperature with time.

Any change in kurtosis value denotes a shift in the signal properties by means of the frequency distribution. In a fast reactor, where the mean temperature level as well as the associated fluctuations increases with thermal power, kurtosis acts as an indicator of change in the frequency distribution of the signal. As it is observed that kurtosis increases with σ, it explains why the fluctuations at higher power level attain a sharper and narrow distribution.

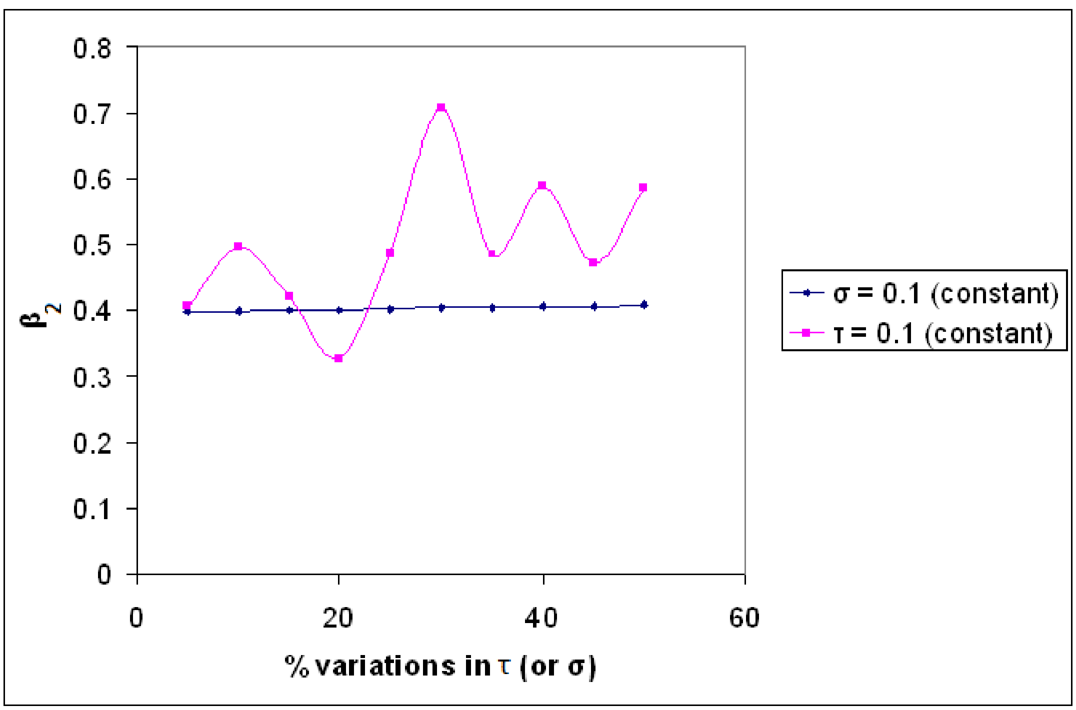


Figure 4.24: $\beta_2$ behavior.

It means that the core temperature signal is broadly distributed with lesser peakedness at low thermal power than at higher power. These results give sufficient confidence in estimating parameters based on temperature fluctuations. Also, it supports the idea of using fluctuations in spite of its non-stationarity. As already discussed, non-stationarity can be removed by performing first order differencing.

## 4.4 Discussion

The fundamental difference between fluctuation generation under two different conditions viz. blockage and normal operation can be understood by analyzing the related data. For analysis, maximum and minimum values of temperatures are set, and corresponding data is generated. For example, the profile for fluid temperature varying in the range of 380-390$^{o}$C is shown in figure 4.25.

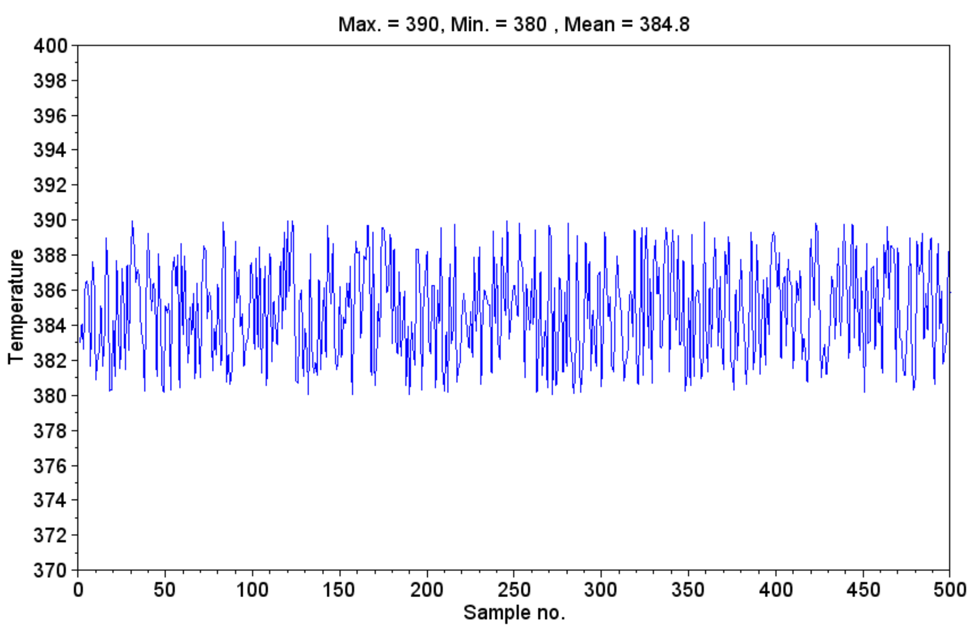


Figure 4.25: Temperature profile in case of blockage.

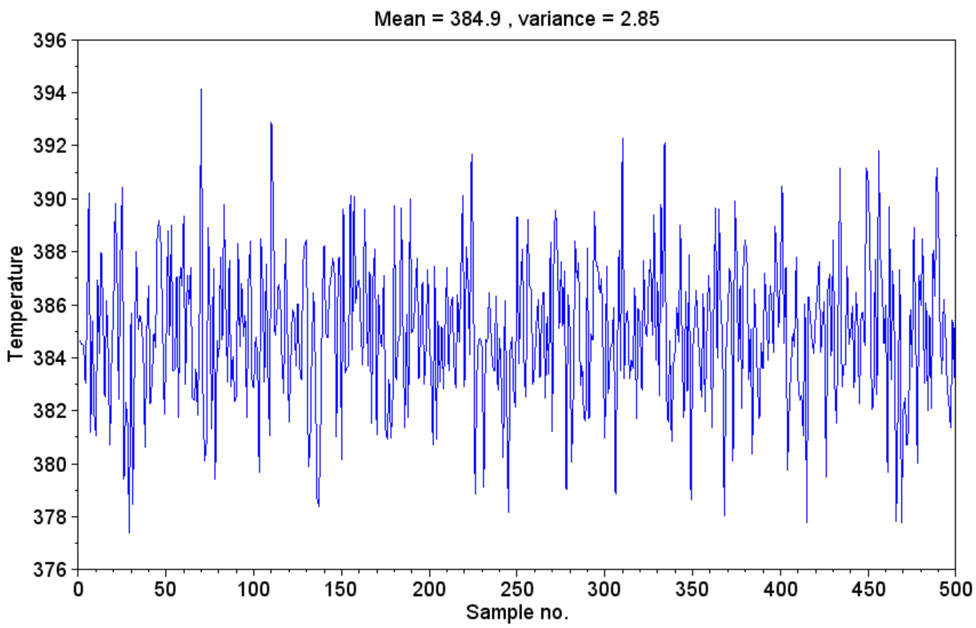


Figure 4.26: Temperature profile for normal condition.

Temperature profile with similar mean and variance is generated for normal operation and is shown in figure 4.26. Visual inspection suggests that peaks in case of normal operation can be assumed to be distributed non-linearly, whereas the fluctuations in case of blockage tend to become more stationary, making them easier to detect. However, mean temperature increases under continued presence of blockage. This in turn makes the fluctuations behave like as if there is an increase in thermal power. Hence, with the same algorithmic approach for estimating thermal power from fluctuations, presence of blockage can be detected if there is any unusual deviation in the calculated parameter.

Figure 4.27 shows the variation in calculated parameter with thermal power, which also validates the proposed model. The curve defined in the figure as “No weights” is obtained as;

$$CP = M_{avg}\{abs(diff_{1-order})\} \tag{37}$$

whereas the curve obtained as “with weights” is calculated by providing a fixed weightage to the CP for particular thermal power, given as;

$$CP = A_{P(MWTh)}[M_{avg}\{abs(diff_{1-order})\}] \tag{38}$$

where $A_{P(MWTh)}$ = weightage given to CP at particular thermal power.

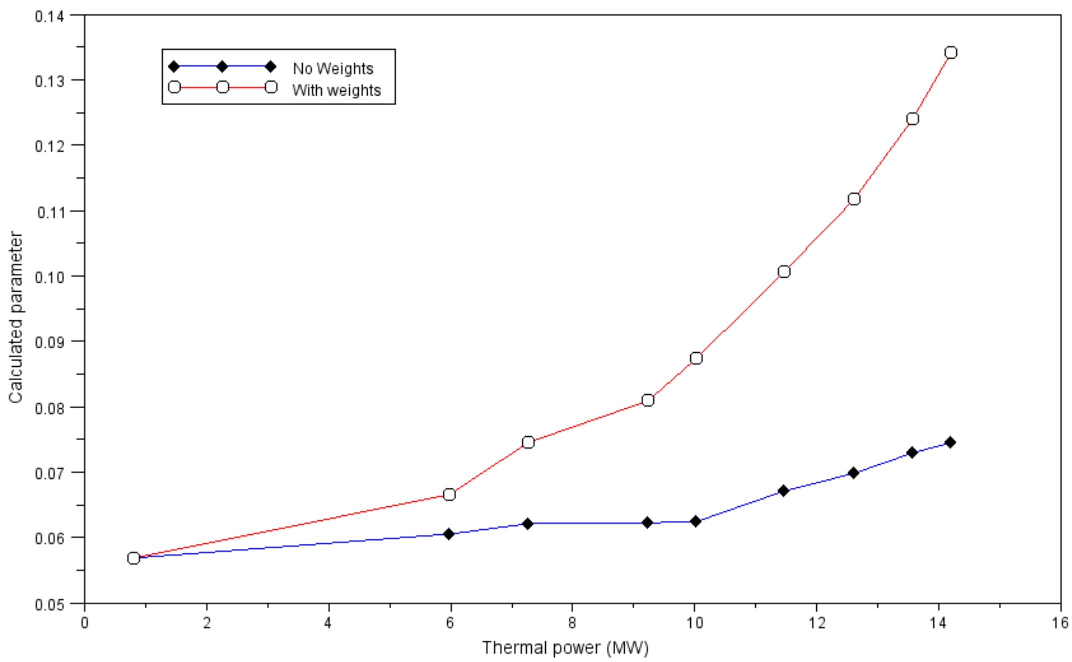


Figure 4.27: Calculated parameter vs thermal power.

## 4.5 Conclusion

A mathematical model was derived and simulated for various operational conditions. It was found that temperature fluctuation behavior is unique for variations in thermal power and that it initially differs from blockage induced fluctuations. Since the net effect of blockage is an overall increase in temperature, fluctuation behavior also changes. The fluctuation based calculated parameter shows strong relationship with thermal power. Hence, temperature fluctuations can be used for the purpose of estimating reactor power assuming a constant flow rate and use of thermocouple with small time-constant.

# 5

# RESOURCE UTILIZATION FOR PRACTICAL IMPLEMENTATION

This chapter discusses the technical aspects for practical implementation of the proposed mathematical approach on a FPGA based platform. Various tools for design, synthesis, simulation and testing of the proposed approach are explained.

## 5.1 Altera Quartus II & SOPC builder

Altera Quartus II® 12.0 web edition is free programmable logic device design software. User can analyze and synthesize HDL designs, perform compilation, timing analysis, examine RTL diagrams, simulate, and programme the target device. SOPC Builder is a part of Quartus II tool used for system development. FPGAs can implement logical functions with great flexibility. The FPGA design flow is shown in figure 5.1.

System design is the description of individual modules or whole system in hardware description languages such as VHDL, verilog, system C etc. [85]. The design entry can be block level also where logic gates are connected to implement the system. SOPC is also a means for system design.

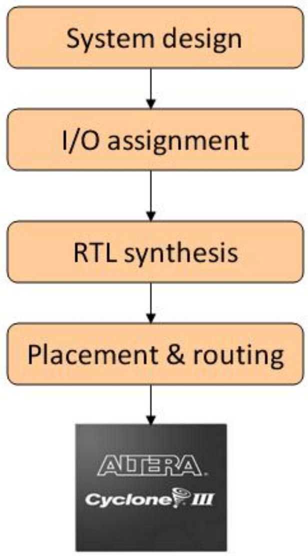


Figure 5.1: FPGA design flow.

System design and I/O assignment are accompanied by functional simulation, design rule check and RTL viewer. Power analysis, timing analysis, gate level simulation and signal integrity analysis are performed during placement and routing. TimeQuest timing analyzer and PowerPlay are available for such purpose as a part of Quartus II. The final generated bitmap file is ready to be loaded onto FPGA. The FPGA type has to be pre-defined in order to obtain a correct binary file. For the proposed signal processing approach as shown in figure 5.2, Cyclone III family FPGA development board DE0 is used, which is equipped with EP3C16F484C6 FPGA device comprising of 15,408 LEs(Logic Elements). The board provides 346 user I/O pins.

## 5.2 Implementation statistics

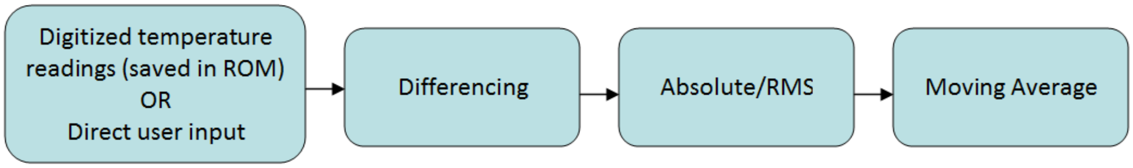


Figure 5.2: various math blocks.

As shown above, the input to system design has either temperature readings saved in a ROM or it can be direct user input for simulation purpose. The implementation cost for each module is as shown below.

*Differencing + Absolute:*

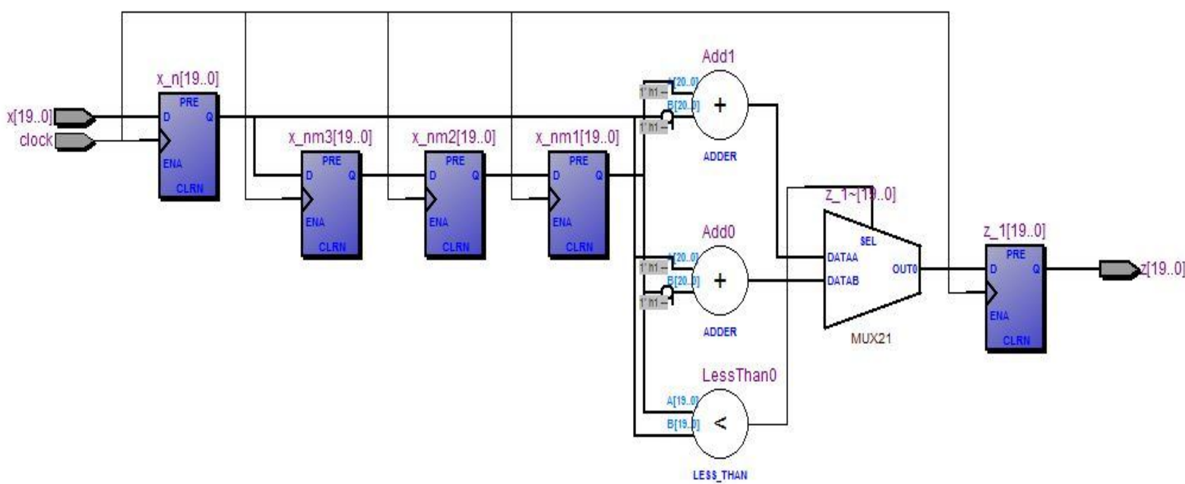


Figure 5.3: RTL diagram.

| Flow Summary | |
|---|---|
| Revision Name | abs_sub |
| Top-level Entity Name | abs_sub |
| Family | Cyclone III |
| Device | EP3C16F484C6 |
| Timing Models | Final |
| Total logic elements | 80 / 15,408 ( < 1 % ) |
| Total combinational functions | 67 / 15,408 ( < 1 % ) |
| Dedicated logic registers | 44 / 15,408 ( < 1 % ) |
| Total registers | 44 |
| Total pins | 41 / 347 ( 12 % ) |
| Total virtual pins | 0 |
| Total memory bits | 60 / 516,096 ( < 1 % ) |
| Embedded Multiplier 9-bit elements | 0 / 112 ( 0 % ) |
| Total PLLs | 0 / 4 ( 0 % ) |

Figure 5.4: Flow summary.

Figure 5.3 shows the generated RTL map of the mathematical operation. The usage summary is as shown in figure 5.4. For a 20 bit operation, the resource consumption is very less even for a mid range FPGA. The simulation results are obtained using Altera Quartus II for random user inputs, and are shown in figure 5.5 and 5.6 with the help of gtkwave software for vcd (value change dump) file format.

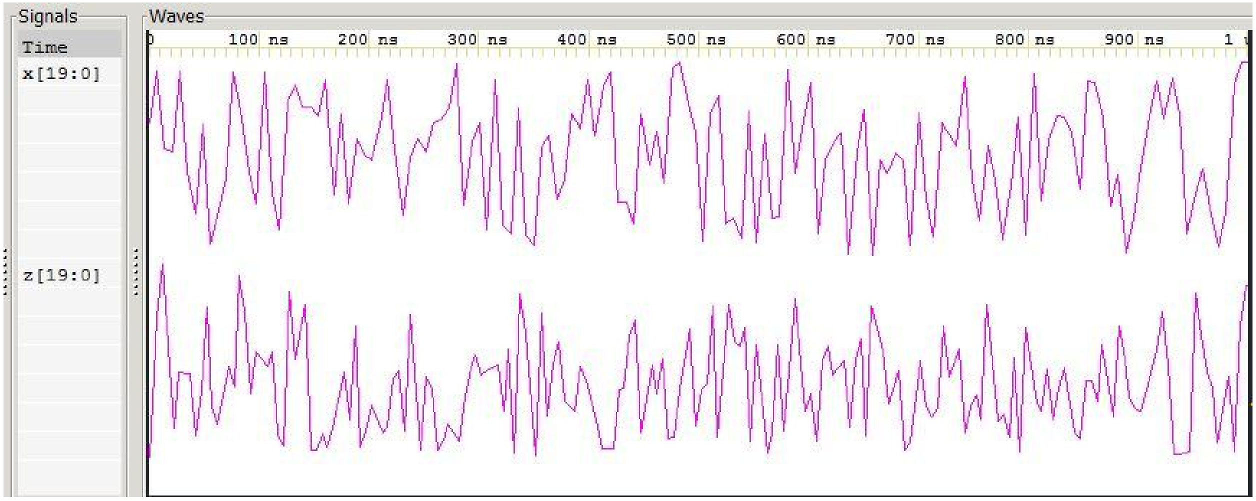


Figure 5.5: Input (upper) and Output (lower) for absolute and differencing operation.

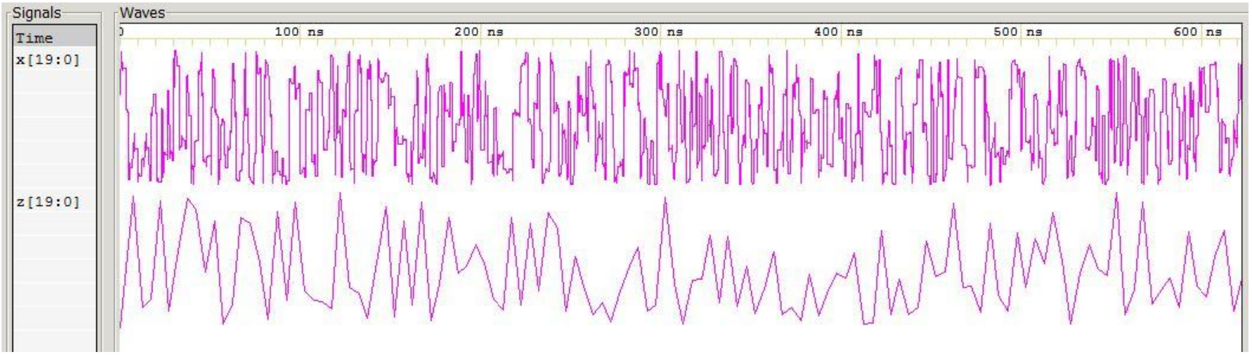


Figure 5.6: For another type of input: absolute and differencing operation.

It is interesting to note that increasing the no. of input bits (40 bit) leads to total logic elements requirement to increases from 80 to 167, which is still very less than actual available resources. Hence, future upgrades for system doesn't put any limits on the hardware.

Moving Average:

Figure 5.7 shows the RTL map of the moving average filter with a window length of four. The usage summary is shown in figure 5.8.

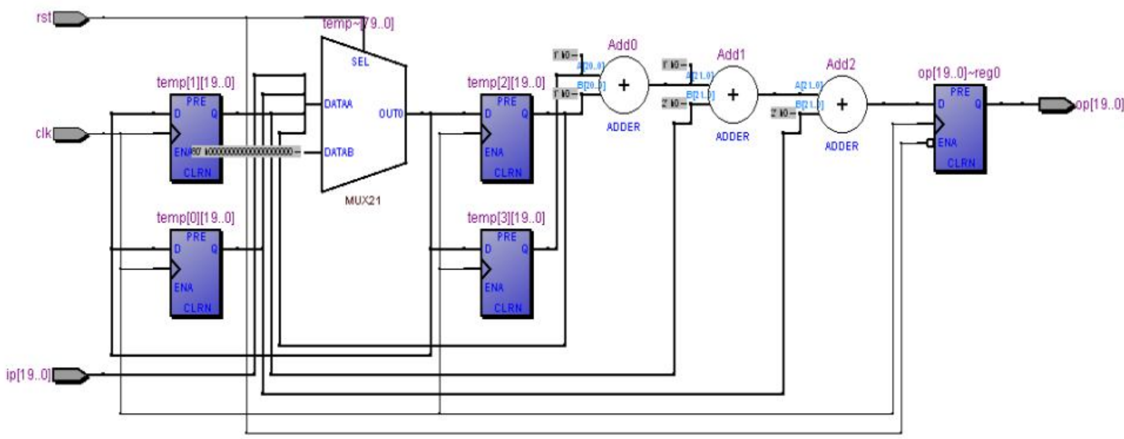


Figure 5.7: RTL diagram: moving average.

**Flow Summary**

| | |
|---|---|
| Revision Name | mavg2 |
| Top-level Entity Name | mavg2 |
| Family | Cyclone III |
| Device | EP3C16F484C6 |
| Timing Models | Final |
| Total logic elements | 144 / 15,408 ( < 1 % ) |
| Total combinational functions | 144 / 15,408 ( < 1 % ) |
| Dedicated logic registers | 100 / 15,408 ( < 1 % ) |
| Total registers | 100 |
| Total pins | 42 / 347 ( 12 % ) |
| Total virtual pins | 0 |
| Total memory bits | 0 / 516,096 ( 0 % ) |
| Embedded Multiplier 9-bit elements | 0 / 112 ( 0 % ) |
| Total PLLs | 0 / 4 ( 0 % ) |

Figure 5.8: Flow Summary: moving average.

The simulation result (using gtkwave viewer) for moving average block with a window length of four is shown in figure 5.9. The simulation result for window lengths of 25 and 50 are shown in figure 5.10.

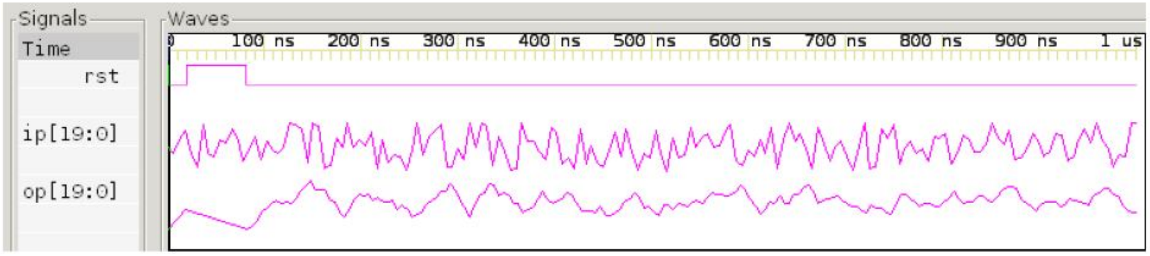


Figure 5.9: Simulation result – moving average of window length four.

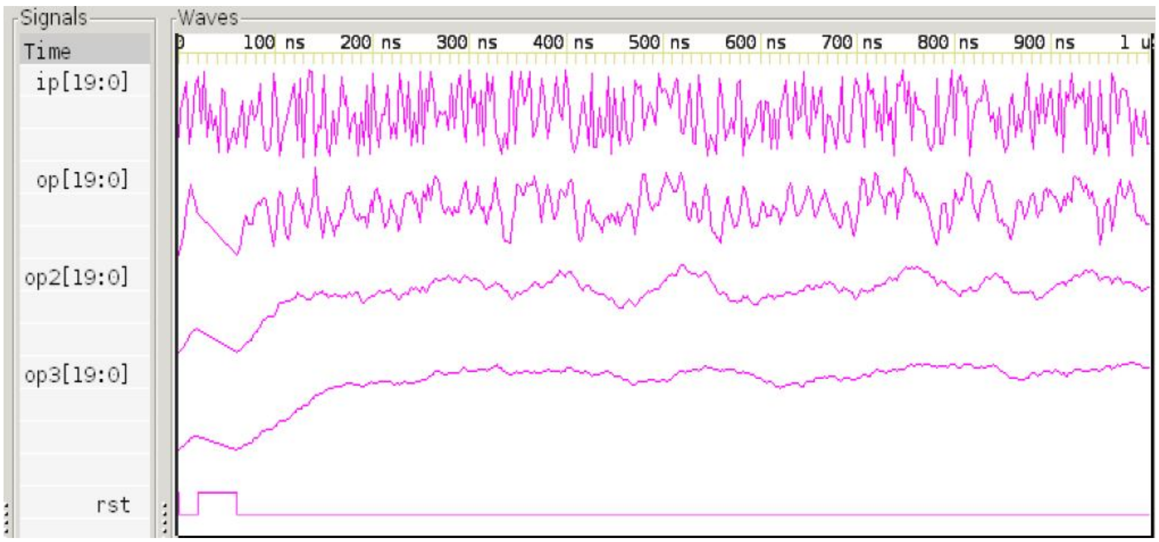


Figure 5.10: Simulation result- moving average of window length 4, 25 and 50 respectively.

| Flow Summary | |
|---|---|
| Revision Name | mavg |
| Top-level Entity Name | mavg |
| Family | Cyclone III |
| Device | EP3C16F484C6 |
| Timing Models | Final |
| Total logic elements | 3,376 / 15,408 ( 22 % ) |
| Total combinational functions | 3,372 / 15,408 ( 22 % ) |
| Dedicated logic registers | 1,060 / 15,408 ( 7 % ) |
| Total registers | 1060 |
| Total pins | 82 / 347 ( 24 % ) |
| Total virtual pins | 0 |
| Total memory bits | 0 / 516,096 ( 0 % ) |
| Embedded Multiplier 9-bit elements | 0 / 112 ( 0 % ) |
| Total PLLs | 0 / 4 ( 0 % ) |

Figure 5.11: Flow summary- moving average for simultaneous operation.

The resource usage status for simultaneous applications of moving average operation for all the thee window lengths viz 4, 25 and 50 is shown in figure 5.11, from which it is clear that even simultaneous operation is possible on the FPGA (EP3C16F484C6). Hence, a wide variety of processing algorithms can be used in parallel on the same platform without any compromise in functionality.

Though a minimal resource usage makes it possible to implement it on a microcontroller too, the choice for selecting FPGA as platform is very specific. It is possible to include the findings of other researches in the area of dynamic temperature analysis based on the current work. Hence, FPGA could accommodate the increased resource usage requirements which may otherwise arise. Figure 5.12 shows a simple C code to implement the proposed algorithm, which makes it platform independent. It may be noted that the input to the code are the values stored in local memory, which are temperature values.

```
#include<stdio.h>
#include<math.h>

#define N 13
#define M 10

#if N < M
#error N must be greater than M
#endif


int main()
{
    float x_n [N] ;
    float x2_n [N-1] ;
    float y[M] ;

    int i,j;

    for ( i = 0; i < N ; ++i)
    {
        scanf("%f",&x_n[i]);
    }

            ......cont.
```

```
    ......contd.
for ( i = 0; i < N-1 ; ++i)
{
    x2_n[i] = fabs(x_n[i] - x_n[i+1]) ;
}

for (i = 0 ; i < M ; ++i)
{
if ( N - i < M )
    y[i] = 0;
else
{
        float summation_of_y = 0 ;
        for ( j = 0 ; j < M; ++j )
        {
                summation_of_y += x2_n[i+j] ;
        }
        y[i] = summation_of_y / (M+1) ;
}
}

for (i = 0 ; i < M ; ++i )
{
    //printf("y(%d) = %f\n",i,y[i]);
    printf("%f\n",y[i]);
}
```

Figure 5.12: C-code for the proposed algorithm.

## 5.3 Conclusion

The details related to practical implementation of proposed algorithm was discussed. It was found that FPGAs are perfect for implementing complex mathematical operation as a part of signal processing architecture. Their use has grown enormous in present world applications. Also, the biggest advantage offered is in terms of re-configurability. The present study also highlights the usage of free software available for the analysis.

# 6

# SUMMARY AND FUTURE DIRECTIONS

## 6.1 Summary

This thesis has put forward the use of temperature fluctuation in fuel subassemblies to estimate reactor power. The overall research flow can be summarized as:

- The work presented in the thesis is novel in terms of system identification, model development and parameter estimation based on temperature fluctuations in CSA, with respect to reactor thermal power.
- A detailed and multi domain analysis approach of outlet temperature fluctuations for a fuel subassembly (CSA) in a fast reactor.
- Study on the correlation of temperature fluctuations with reactor thermal power.

- Use of data driven model based design in development of suitable signal processing methodology for fluctuation processing.
- Development of a simulation model to generate temperature profile of desired characteristics for fluctuation studies.
- Effect analysis of thermocouple time constant on the sensing of temperature fluctuations

## 6.2 Key findings of the work

- The technique presented in this work has helped to establish a proper correlation between the calculated parameter (moving average of absolute first order differenced data) to that of thermal power.
- Standard deviation ( $\sigma$ ) was observed to increase with thermal power. However, with non-linear localization in time, the trend being highly dependent on the sample window length.
- Temperature fluctuations have been found to be in the extreme low frequency range of 0.001 Hz to 5 Hz.
- Time-frequency analysis proved to be of immense use for understanding the temperature fluctuation behavior.
- The statistical test results have shown that it is possible to extract the information present in the fluctuations, and a proper mathematical formula was derived.
- Analysis regarding the implementation cost in terms of required logic element showed that a mid-level FPGA with few thousand of logic elements (LEs) would

be sufficient for the purpose.

## 6.3 Future directions

- Since only central subassembly features a fast response thermocouple, it would be helpful to study the temperature fluctuation behavior for other fuel subassemblies with a faster response thermocouple.
- It has been found that coolant flow rate has a direct impact on temperature fluctuations, with lesser fluctuation amplitude for high flow rates. Hence, it would be interesting to study effects of flow rate under various reactor power conditions.
- A similar approach of fluctuation analysis can be effectively used for other industrial dynamic system also, where a lot of system state information is present in the form of fluctuations.

## References


[1] Srinivasan, G., Suresh Kumar, K. V., Rajendran, B., & Ramalingam, P. V. (2006). The fast breeder test reactor—design and operating experiences.Nuclear Engineering and Design, 236(7), 796-811.

[2] Waltar, A. E., & Reynolds, A. B. (1981). Fast breeder reactors. Pergamon.489.

[3] Swaminathan, P. (2004). Computer based on-line monitoring system for Fast Breeder Test Reactor, India. In Technical Meeting on Increasing Instrument Calibration Interval through Online Calibration Technology (p. 3).

[4] DuBridge, R. A., Neissel, J. P., Boyd, L. R., Green, W. K., & Pielage, H. W. (1965). Reactor Control Systems Based on Counting and Campbelling Techniques. 6EAP-4900, July.

[5] Harrer, J. M., & Beckerley, J. G. (1973). Nuclear power reactor instrumentation systems handbook. Office of Information Services, US Atomic Energy Commission.

[6] Tsunoda, T. (1976). Application of temperature fluctuation to anomaly detection in fuel assemblies. Journal of Nuclear Science and Technology, 13(3), 103-110.

[7] Miyazaki, K., Kimura, J., Ogawa, M., & Okada, T. (1978). Temperature fluctuation of sodium in annular flow channel heated by single-pin with blockage. Journal of Nuclear Science and Technology, 15(1), 10-23.

[8] Greef, C. P. (1979). Temperature fluctuations: an assessment of their use in the detection of fast reactor coolant blockages. Nuclear Engineering and Design, 52(1), 35-55.

[9] Krebs, L., & Weinkötz, G. (1977). Detection of local boiling in an LMFBR subassembly by temperature fluctuations analysis at the outlet. Progress in Nuclear Energy, 1(2), 507-515.

[10] Inujima, H., Ogino, T., Haga, K., & Kikuchi, Y. (1982). Detection of local sodium boiling in a simulated LMFBR fuel subassembly. Progress in Nuclear Energy, 9, 107-121.

[11] B.O. Wey, G. Hughes, and R.S. Overton (1982). Prediction of temperature fluctuations at the outlet of a blocked subassembly. Proceedings of the LMFBR Safety Topical Meeting, European Nuclear Society 4, Lyon, France, 207–216, July 19–23.

[12] L. Krebs and G. Weinkotz (1984). Survey on the German research programme for blockage detection within LMFBR fuel elements by measurements and analysis of temperature fluctuations at the coolant outlet, Spec. Meeting on Methods and Tools to Detect Thermal Noise in Fast Reactors IAEA, Bologna, Italy.

[13] Ogino, T., Inujima, H., & Kazuo, H. A. G. A. (1984). Feasibility study of LMFBR local core anomaly detection by use of temperature and flow fluctuations. Journal of Nuclear Science and Technology, 21(3), 172-186.

[14] Nomoto, S., Yamamoto, H., Sekiguchi, Y., & Tamura, S. (1980). Measurement of subassembly outlet coolant temperature in the JOYO experimental fast reactor. Nuclear Engineering and Design, 62(1), 233-239.

[15] Takeda, T., Sonoda, Y., Aya, K., & Sekiya, T. (1982). Analysis of root-mean-square temperature noise in fast reactor fuel assembly with local blockage.Progress in Nuclear Energy, 9, 233-242.

[16] Takeda, T., Ohta, S., Yoshiyuki, T., & Sekiya, T. (1985). Analysis of root-mean-square temperature noise in FBR wire-spacered assembly with local blockage.Progress in Nuclear Energy, 15, 807-814.

[17] Yoshiyuki, T., Nakajima, A., Takeda, T., & Sekiya, T. (1986). Analysis of temperature noise propagation in a large fuel subassembly of FBR. Nuclear engineering and design, 91(3), 263-275.

[18] Lord, D. J., & Crowe, D. S. (1985). Reactivity noise on the United Kingdom prototype fast reactor. Progress in Nuclear Energy, 15, 473-481.

[19] Edelmann, M., Massier, H., Berlin, C., & Le Guillou, G. (1985). Intercomparison of noise analysis and perturbation techniques for measuring fast reactor fuel element performance characteristics. Progress in Nuclear Energy, 15, 43-53.

[20] Edelmann, M., Girard, J. P., & Massier, H. (1988). Experimental investigations of correlations between neutron power and fuel element outlet temperatures of SUPER PHENIX 1. Progress in Nuclear Energy, 21, 367-376.

[21] Seong, S., Jeong, H., Hur, S. E. O. P., & Kim, S. (2007). Establishment of a Neural Network Model for Detecting a Partial Flow Blockage in an Assembly of a Liquid Metal Reactor. NUCLEAR ENGINEERING AND TECHNOLOGY, 39(1), 43.

[22] Velusamy, K., Natesan, K., Selvaraj, P., Chellapandi, P., Chetal, S. C., Sundararajan, T., & Suyambazhahan, S. (2006, September). CFD studies in the prediction of thermal striping in an LMFBR. In CFD4NRS Conference, Garching, Munich, Germany.

[23] Velusamy, K., Chellapandi, P., Chetal, S. C., & Raj, B. (2010). Overview of pool hydraulic design of Indian prototype fast breeder reactor. Sadhana, 35(2), 97-128.

[24] Chapuliot, S., Gourdin, C., Payen, T., Magnaud, J. P., & Monavon, A. (2005). Hydro-thermal-mechanical analysis of thermal fatigue in a mixing tee. Nuclear engineering and design, 235(5), 575-596.

[25] Kasahara, N., Nakamura, K., Morishita, M., Shibamoto, H., & Inoue, K. (2008). Main R&D issues for fast reactor structural design standard. Nuclear Engineering and Design, 238(2), 287-298.

[26] Chandran, R. K., Banerjee, I., Padmakumar, G., & Reddy, K. S. (2011). Investigation of Thermal Striping in Prototype Fast Breeder Reactor Using Ten-Jet Water Model. Heat Transfer Engineering, 32(5), 369-383.

[27] Mesquita, A. Z., & Rezende, H. C. (2010). Thermal methods for on-line power monitoring of the IPR-R1 TRIGA Reactor. Progress in Nuclear Energy, 52(3), 268-272.

[28] Keesman, K. J. (2011). System Identification: An Introduction. Springer.

[29] Korovessi, E., & Linninger, A. A. (Eds.). (2005). Batch processes. CRC.

[30] Harris, B. (Ed.). (1967). Spectral analysis of time series. John Wiley & Sons.

[31] Friston, K. J., Jezzard, P., & Turner, R. (1994). Analysis of functional MRI time-series. Human Brain Mapping, 1(2), 153-171.

[32] Huang, N. E., Shen, Z., Long, S. R., Wu, M. C., Shih, H. H., Zheng, Q., ... & Liu, H. H. (1998). The empirical mode decomposition and the Hilbert spectrum for nonlinear and non-stationary time series analysis. Proceedings of the Royal Society of London. Series A: Mathematical, Physical and Engineering Sciences, 454(1971), 903-995.

[33] Jardine, A. K., Lin, D., & Banjevic, D. (2006). A review on machinery diagnostics and prognostics implementing condition-based maintenance. Mechanical systems and signal processing, 20(7), 1483-1510.

[34] Chatfield, C. (2003). The analysis of time series: an introduction (Vol. 59). Chapman & Hall/CRC.

[35] García Barrón, L., & Pita, M. F. (2004). Stochastic analysis of time series of temperatures in the south-west of the Iberian Peninsula. Atmósfera, 17(4), 225-244.

[36] Boashash, B. (2003). Time frequency signal analysis and processing: a comprehensive reference. Elsevier Science Limited.

[37] Cariolaro, G. (2011). Unified signal theory. Springer.

[38] Time Frequency Toolbox, Toolbox developed for the analysis of non-stationary signals using time-frequency distributions, SCILAB. http://atoms.scilab.org/toolboxes/stftb

[39] Ruelle, D., Eckmann, J. P., & Kamphorst, S. O. (1987). Recurrence plots of dynamical systems. Europhys. Lett, 4.

[40] Recurrence plots and cross recurrence plots. http://www.recurrence-plot.tk/

[41] Marwan, N., Carmen Romano, M., Thiel, M., & Kurths, J. (2007). Recurrence plots for the analysis of complex systems. Physics Reports, 438(5), 237-329.

[42] Thiel, M., Romano, M. C., Read, P. L., & Kurths, J. (2004). Estimation of dynamical invariants without embedding by recurrence plots. Chaos: An Interdisciplinary Journal of Nonlinear Science, 14(2), 234-243.

[43] Cazares-Ibáñez, E., Vázquez-Coutiño, G. A., & García-Ochoa, E. (2005). Application of recurrence plots as a new tool in the analysis of electrochemical oscillations of copper. Journal of Electroanalytical Chemistry, 583(1), 17-33.

[44] Rohde, G. K., Nichols, J. M., Dissinger, B. M., & Bucholtz, F. (2008). Stochastic analysis of recurrence plots with applications to the detection of deterministic signals. Physica D: Nonlinear Phenomena, 237(5), 619-629.

[45] Pincus, S. M. (1991). Approximate entropy as a measure of system complexity. Proceedings of the National Academy of Sciences, 88(6), 2297-2301.

[46] Kwiatkowski, D., Phillips, P. C., Schmidt, P., & Shin, Y. (1992). Testing the null hypothesis of stationarity against the alternative of a unit root: How sure are we that economic time series have a unit root?. Journal of econometrics, 54(1), 159-178.

[47] Casaseca-de-la-Higuera, P., & de-Luis-Garcıa, R. (2005). Weaning from mechanical ventilation: Feature extraction from a statistical signal processing viewpoint. In Proc. 13th Signal Processing Conf., EUSIPCO.

[48] Brcich, R. F., & Iskander, D. R. (2006, May). Testing for stationarity in the frequency domain using a sphericity statistic. In Acoustics, Speech and Signal Processing, 2006. ICASSP 2006 Proceedings. 2006 IEEE International Conference on (Vol. 3, pp. III-III). IEEE.

[49] Kipiński, L., König, R., Sielużycki, C., & Kordecki, W. (2011). Application of modern tests for stationarity to single-trial MEG data. Biological cybernetics, 1-13.

[50] Bendat, J. S., & Piersol, A. G. (2011). Random data: analysis and measurement procedures (Vol. 729). Wiley.

[51] Corder, G. W., & Foreman, D. I. (2009). Nonparametric statistics for non-statisticians: a step-by-step approach. Wiley.

[52] Bhoje, S. B. (1996). Status of fast reactor development in India. In 29th Annual Meeting of the International Working Group on Fast Reactors, Aktau, Kazakhstan.

[53] Sematech, N. (2006). Engineering statistics handbook, pp. 1858.

[54] http://www.igcar.ernet.in/lis/nl41/ta1.html

[55] Tenchine, D. (2010). Some thermal hydraulic challenges in sodium cooled fast reactors. Nuclear Engineering and Design, 240(5), 1195-1217.

[56] Hoppé, P., & Mitzel, F. (1977). Noise analysis performed at the sodium cooled power reactor KNK I for malfunction diagnosis and plant surveillance. Progress in Nuclear Energy, 1(2), 427-436.

[57] Manuca, R., & Savit, R. (1996). Stationarity and nonstationarity in time series analysis. Physica D: Nonlinear Phenomena, 99(2), 134-161.

[58] Pincus, S. M., & Goldberger, A. L. (1994). Physiological time-series analysis: what does regularity quantify?. American Journal of Physiology-Heart and Circulatory Physiology, 266(4), H1643-H1656.

[59] Yan, R., & Gao, R. X. (2007). Approximate entropy as a diagnostic tool for machine health monitoring. Mechanical Systems and Signal Processing, 21(2), 824-839.

[60] Fusheng, Y., Bo, H., & Qingyu, T. (2001). Approximate entropy and its application to biosignal analysis. Nonlinear Biomedical Signal Processing: Dynamic Analysis and Modeling, Volume 2, 72-91.

[61] Eckner, A. (2012). Algorithms for Unevenly-Spaced Time Series: Moving Averages and Other Rolling Operators. Working Paper.

[62] Biserna, T., Cavallini, F., Taglienti, S., & Tosi, V. (1977). Results of acoustic and temperature noise measurements on sodium cooled electrically heated 7 rod bundle. Progress in Nuclear Energy, 1(2), 517-526.

[63] Bobkov, V., et al., 2008. Thermophysical properties of materials for nuclear engineering: A tutorial and collection of data. IAEA, Vienna.

[64] http://www.lbl.gov/CS/html/exascale4energy/reactor.html

[65] Moriya, S., & Ohshima, I. (1990). Hydraulic similarity in the temperature fluctuation phenomena of non-isothermal coaxial jets. Nuclear engineering and design, 120(2), 385-393.

[66] Lillington, J. N. (1981). A vector upstream differencing scheme for problems in fluid flow involving significant source terms in steady-state linear systems. International Journal for Numerical Methods in Fluids, 1(1), 3-16.

[67] Meyder, R. (1975). Turbulent velocity and temperature distribution in the central subchannel of rod bundles. Nuclear Engineering and Design, 35(2), 181-189.

[68] Bergman, T. L., Incropera, F. P., Lavine, A. S., & DeWitt, D. P. (2011). Fundamentals of heat and mass transfer. John Wiley & Sons.

[69] Chen, C. J., & Todreas, N. E. (1975). Prediction of the coolant temperature field in a breeder reactor including interassembly heat transfer. Nuclear Engineering and Design, 35(3), 423-440.

[70] Swaminathan, P. (2008). Modelling of Instrumentation and Control System of Prototype Fast Breeder Reactor. PhD. Thesis.

[71] Roychowdhury, D. G., Govindarajan, S., Chetal, S. C., & Bhoje, S. B. (1991). Design approach to local blockages. Indira Gandhi Center for Atomic Research. http://www.iaea.org/OurWork/ST/NE/inisnkm/nkm/aws/fnss/fulltext/1157_23.pdf

[72] Trimberger, S. (1994). Field-programmable gate array technology. Springer.

[73] Tamura, S., Otani, H., Taniyama, H., Sanda, T., Sano, K., & Ikegami, T. (1982). Reactor noise analysis of the experimental fast reactor JOYO. Progress in Nuclear Energy, 9, 399-410.

[74] Miyaguchi, K. (1980). Analytical studies on local flow blockages in LMFBR subassemblies, using the UZU code. Nuclear Engineering and Design, 62(1), 25-38.

[75] Donaldson, A. B., Lucero, R. E., Gill, W., & Yilmaz, N. (2008). Problems encountered in fluctuating flame temperature measurements by thermocouple (No. SAND2008-7384J). Sandia National Laboratories.

[76] ASTM Committee E-20 on Temperature Measurement. (1993). Manual on the use of thermocouples in temperature measurement, Fourth Edition, pp. 170. ASTM International.

[77] Bentley, R. E. (Ed.). (1998). Handbook of Temperature Measurement Vol. 3: The Theory and Practice of Thermoelectric Thermometry (Vol. 3). Springer.

[78] Hung, P., McLoone, S., Irwin, G. W., & Kee, R. J. (2010, June). A total least squares approach to sensor characterisation. In System Identification (SYSID'03): A Proceedings Volume from the 13th IFAC Symposium on System Identification, Rotterdam, the Netherlands, 27-29 August 2003 (p. 321). Elsevier Science.

[79] Tagawa, M., & Ohta, Y. (1997). Two-thermocouple probe for fluctuating temperature measurement in combustion—Rational estimation of mean and fluctuating time constants. Combustion and flame, 109(4), 549-560.

[80] Thermocouple - NIST ITS-90 Thermocouple Database. http://srdata.nist.gov/its90/download/type_k.tab

[81] Random number generator(s), SCILAB. http://help.scilab.org/docs/5.3.0/en_US/grand.html

[82] Picard, H. C. (1951). A note on the maximum value of kurtosis. The Annals of Mathematical Statistics, 22(3), 480-482.

[83] Samanta, B., & Al-Balushi, K. R. (2003). Artificial neural network based fault diagnostics of rolling element bearings using time-domain features. Mechanical systems and signal processing, 17(2), 317-328.

[84] Liu, W., & Mandic, D. P. (2006). A normalised kurtosis-based algorithm for blind source extraction from noisy measurements. Signal Processing, 86(7), 1580-1585.

[85] S. Ramachandran. (2007). Digital VLSI Systems Design: A Design Manual for Implementation of Projects on FPGAs and ASICs Using Verilog. Springer publishers.